

# Elastic And Inelastic Stability Of Two-Panel Tiered Concentrically Braced Frames

Michael Bloom  
*Marquette University*

---

## Recommended Citation

Bloom, Michael, "Elastic And Inelastic Stability Of Two-Panel Tiered Concentrically Braced Frames" (2013). *Master's Theses (2009 -)*. Paper 184.  
[http://epublications.marquette.edu/theses\\_open/184](http://epublications.marquette.edu/theses_open/184)

ELASTIC AND INELASTIC STABILITY OF TWO-PANEL TIERED  
CONCENTRICALLY BRACED FRAMES

by

Michael H. Bloom, B.S.

A Thesis submitted to the Faculty of the Graduate School,  
Marquette University,  
in Partial Fulfillment of the Requirements for  
the Degree of Master of Science

Milwaukee, Wisconsin

May 2013

ABSTRACT  
ELASTIC AND INELASTIC STABILITY OF TWO-PANEL TIERED  
CONCENTRICALLY BRACED FRAMES

Michael H. Bloom, B.S.

Marquette University, 2013

Multi-panel, tiered concentrically braced frames are commonly used in the lateral resisting systems of industrial facilities for loads resulting from wind and earthquake. To date, minimal investigation has been performed on the effect of gravity and lateral loads on the local and global (system) stability of these framing systems.

Recent research has evaluated the effects of in-plane and out-of-plane bending moments induced by inelastic brace deformation and transverse notional loads on the stability of columns in a two-panel concentrically braced frame with an x-bracing arrangement. Other recent research efforts have studied the effect that differential tier drifts resulting in weak-axis flexural yielding have on the strong-axis buckling strength of columns in a four-tier concentrically braced frame. A three-dimensional finite element analysis was used to impart varying levels of weak-axis flexural yielding onto various wide flange sections and the strong-axis buckling strength was analyzed. That study, however, consisted of analyzing columns isolated from the rest of the frame.

This research effort utilizes the structural analysis program MASTAN2 to conduct multiple elastic and inelastic critical load analyses and nonlinear inelastic analyses on a two-panel, tiered concentrically braced frame. Multiple lateral loading conditions, frame height, frame slenderness, and column orientation scenarios are considered to determine the effects of these variables on the stability behavior of the frame. The results of this research effort indicate that the ratio of applied lateral load to applied gravity load and the frame aspect ratio have a profound effect on whether frame stability behavior is controlled by local member behavior or global (system) behavior.

## ACKNOWLEDGMENTS

Michael H. Bloom, B.S.

I would like to thank my family for their continued support throughout the process of writing this Thesis. I would also like to thank Dr. Ronald Ziemian for sharing his knowledge of the MASTAN2 structural analysis program. Finally, I would like to thank my committee, Dr. Stephen Heinrich and Dr. Baolin Wan, and especially my advisor, Dr. Christopher Foley, for their time, input, and support throughout the thesis writing process and my entire time at Marquette University.

## TABLE OF CONTENTS

ACKNOWLEDGMENTS .....	i
CHAPTER	
1. INTRODUCTION .....	1
2. FRAME DESIGN .....	6
3. CRITICAL LOAD ANALYSES .....	21
3.1. Methodology .....	21
3.2. Effect of Applied Lateral Load .....	25
3.3. Effect of Overall Frame Geometry .....	31
3.4. Effect of Column Orientation .....	35
3.5. Inelastic Critical Load Analysis .....	45
3.6. Initial Geometric Imperfections .....	48
3.7. Conclusions .....	56
4. INELASTIC ANALYSIS OF SYSTEMS .....	59
4.1. Methodology .....	59
4.2. Inelastic Analysis Results .....	65
4.3. Conclusions .....	104
5. CONCLUSIONS AND RECOMMENDATIONS FOR FUTURE RESEARCH .....	107
6. BIBLIOGRAPHY .....	111

## 1. Introduction

Industrial buildings, convention centers, and warehouse facilities are usually tall single-story steel structures. In these buildings, lateral loads are commonly resisted by multi-panel concentrically braced frames built with two or more bracing panels, or tiers stacked between the ground and roof level (Imanpour and Tremblay 2012). This arrangement reduces the brace length as opposed to having a single bracing element extending from the base of the frame to its top. The bracing elements present in each panel of the frame are commonly arranged in either an x-configuration or chevron configuration. Figure 1 and Figure 2 illustrate various multi-panel concentrically braced frames with chevron and x-bracing brace configurations.

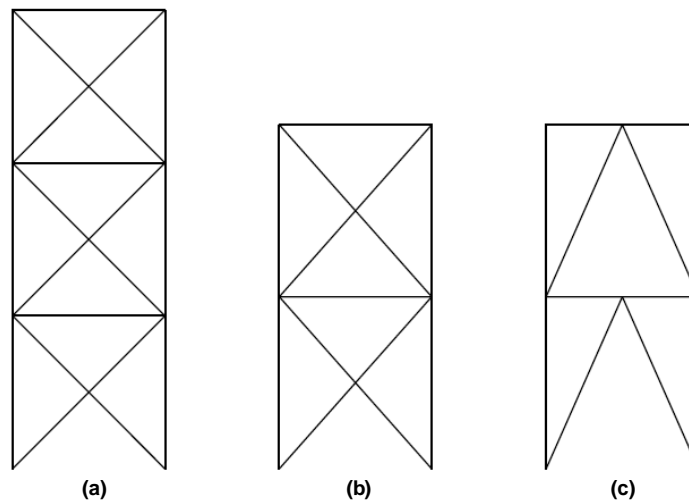


**Figure 1. Multi-panel concentrically braced frames with (a) three panels with an x-bracing configuration, (b) two panels with an x-bracing configuration, and (c) two panels with a chevron bracing configuration**

Beams are located at the boundary between each panel. The columns of the frame are braced in the plane of the frame by these beams at every panel point thereby reducing the column's in-plane buckling length and increasing their axial capacity. Figure 3 shows

the geometry of a two-panel concentrically braced frame with a chevron brace configuration.

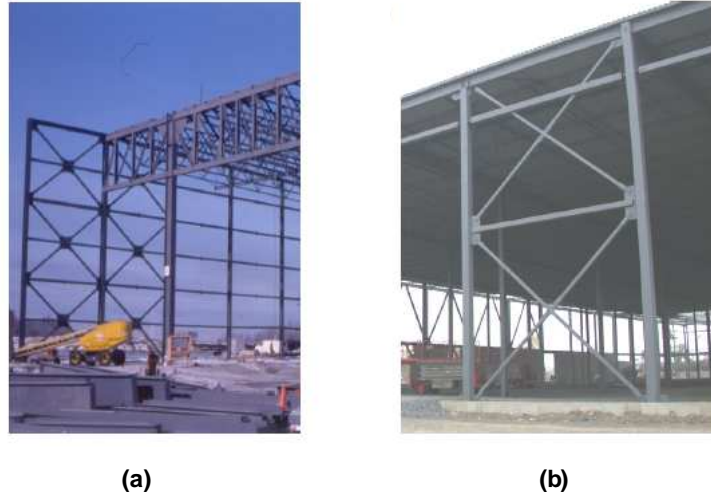


**Figure 2. Multi-panel concentrically braced frames over the height of (a) a tall single-story building and (b) a low-rise single-story building (Imanpour and Tremblay 2012)**

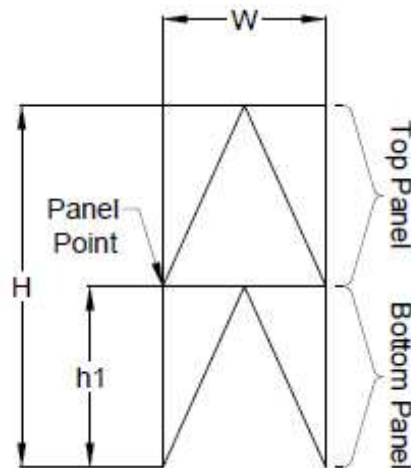


**Figure 3. Geometry of two-panel concentrically braced frame with chevron bracing configuration**

Wide-flange elements are typically used as the column members of the frame.

The columns are often oriented with their webs perpendicular to the plane of the frame so

that weak axis bending of the columns is associated with a smaller effective length due to the bracing provided at each panel point. Lateral loading is transferred from the roof diaphragm to the top of the frame. Despite the presence of beams at the tier levels of the frame, lateral load is transferred from the roof diaphragm and applied only at the top of the frame. This lateral load is transferred to the foundation through the frame's tension and compression acting bracing elements. Due to their high compressive strength, hollow structural section (HSS) elements are often used as braces, but double angle and wide flange sections are also common (Imanpour 2012). Figure 4 shows a typical loading scenario for a two-panel concentrically braced frame with lateral loading applied only at the top of the frame.

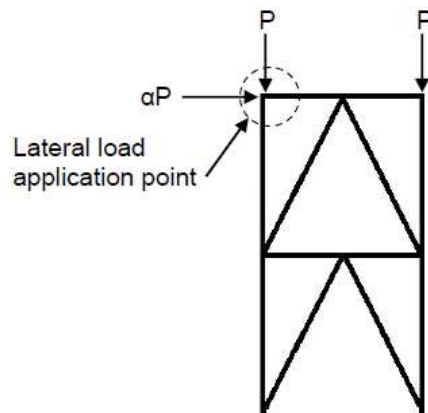


**Figure 4. Typical loading scenario for a two-panel concentrically braced frame**

The objectives and purpose of this thesis are to evaluate local and global instability phenomena in multiple-tier braced frame systems. The study will also evaluate the ductility in the collapse behavior of these systems including identifying frame aspect ratios and frame gravity to lateral load ratios that create force-controlled

(non-ductile) and displacement-controlled (ductile) behavior, which is important for seismic engineering design of these systems.

This thesis investigates the behavior of a two-panel concentrically braced frame with a chevron bracing configuration and equal panel heights designed to have a width of 15 feet and a height of 45 feet and to be subjected to the loads specified in Chapter 2 of the thesis. Selection and design of members for a frame in a typical industrial building application is examined. Then, the effect of frame slenderness and lateral loading level on the two-panel concentrically braced frame's stability is assessed by conducting elastic and inelastic critical load analyses on two-panel concentrically braced frames with height-to-width ratios varying from 2.0 to 3.5 and the ratio of applied lateral load to gravity load varying from 0.0 to 1.0. These analyses are also conducted on frames with initial geometric imperfections both in the plane and out of the plane of the frame. Second-order, inelastic, distributed plasticity analysis (distributed plasticity and plastic hinge) is also conducted on the two-panel concentrically braced frames with height-to-width ratios of 2.0, 2.5, 3.0, and 3.5 and lateral load ratios of 0.25, 0.5, and 1.0 with initial sinusoidal member out-of-straightness to assess the inelastic response of the frame to gravity and lateral loads.

The results of these analyses are used to evaluate the impact of aspect ratio and the applied lateral to gravity load ratio on the stability (local column or brace buckling or global system buckling) behavior of the frame. These results aid in the identification of aspect ratios and/or applied lateral to gravity load ratios that lead to behavior indicating whether global (system) stability or local member stability controls the tiered frame

behavior. These results also aid in the identification of frame and loading configurations that suggest elastic versus inelastic stability phenomena control the system behavior.

## 2. Frame Design

The frame under investigation is a two-panel concentrically braced frame composed of A992 wide-flange and A500 Grade C square HSS sections. Two wide-flange columns extend from ground level to a height of 45 feet to form the frame's exterior boundary. One wide-flange element spans between the two columns at the columns' top while another wide-flange element spans between the columns at the columns' mid-height. This intermediate element creates two equal height panels in the frame.

Square HSS sections are utilized for bracing elements. In the bottom panel, two square HSS bracing elements extend from the column-to-ground intersection to mid-span of the intermediate wide-flange element in a chevron configuration. This chevron bracing configuration is repeated in the top panel as two square HSS elements extend from the intersection of the intermediate wide-flange element and the columns to mid-span of the top wide-flange element. Figure 5 shows a schematic rendering of the two-panel concentrically braced frame. As shown in Figure 5, the webs of the top and intermediate beam are oriented parallel to the plane of the frame. The column webs can be oriented either perpendicular or parallel to the plane of the frame.

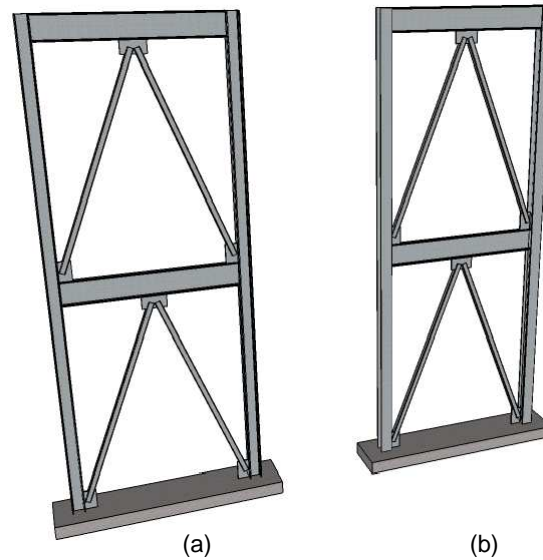


**Figure 5. Schematic rendering of two-panel concentrically braced frame with (a) column webs oriented parallel to the plane of the frame and (b) column webs oriented perpendicular to the plane of the frame**

These two-panel concentrically braced frames are designed to be part of the lateral force resisting system of a hypothetical industrial warehouse facility. The facility has a rectangular footprint with a length of 385 feet, width of 200 feet, and floor to roof height of 45 feet. The two-panel concentrically braced frames of the lateral force resisting system are all located along the exterior of the structure. In the north-south direction, the lateral force resisting system consists of two lines of three, two-panel concentrically braced frames while in the east-west direction, the lateral force resisting system consists of two lines of two, two-panel concentrically braced frames. Locations of the two-panel concentrically braced frames and the building's column layout are shown in Figure 6. Figure 7 shows a schematic representation of the two-panel concentrically braced frames and the gravity load columns.

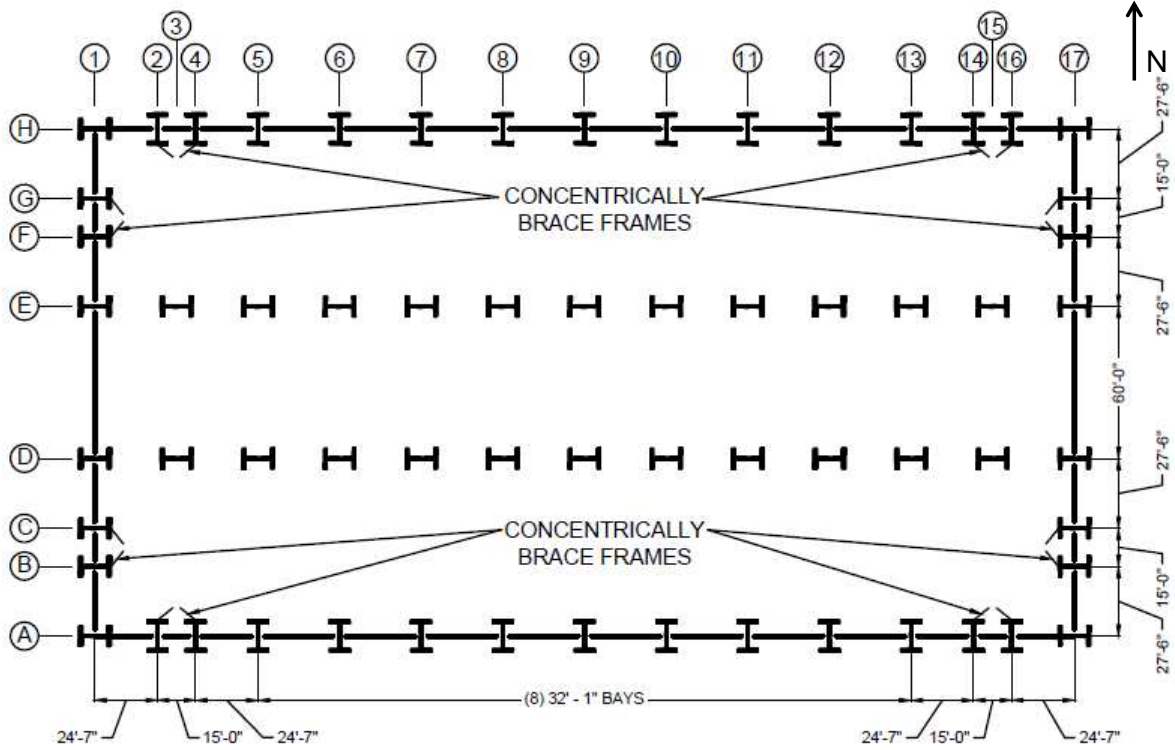


Figure 6. Column layout showing locations of two-panel concentrically braced frames of lateral force resisting system

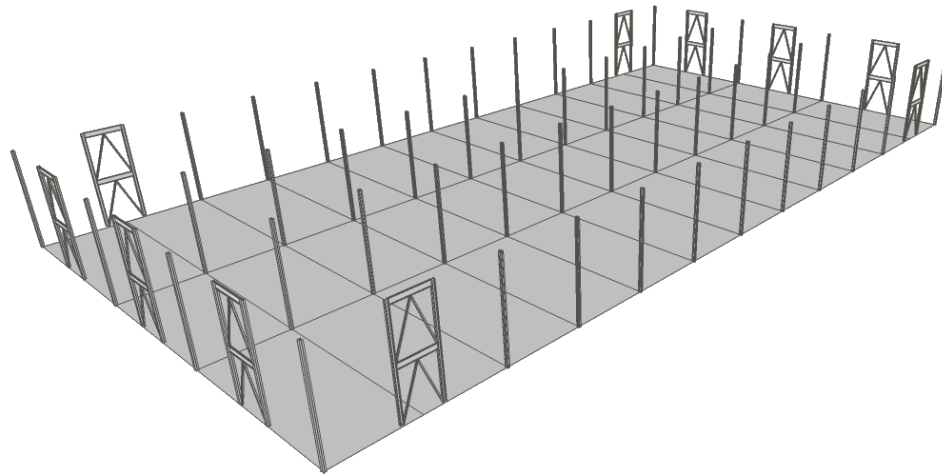


Figure 7. Schematic representation of two-panel concentrically braced frames with gravity load columns

Each element of the frame is designed to resist the effects induced by the loads acting on the industrial facility. These loads were determined using the provisions of *ASCE 7-05 Minimum Design Loads for Buildings and other Structures* (ASCE 2006). The gravity loads acting on the structure result from roof dead load, roof live load, and roof snow load. Table 1 summarizes the intensities of the roof dead loads assumed to act on the structure. Table 2 summarizes the intensities of the total dead load, roof live load, and flat roof snow load acting on the structure. The roof live load was determined using *ASCE 7-05 Minimum Design Loads for Buildings and other Structures* assuming the roof is an ordinary, flat roof. Snow load was calculated using the provisions of *ASCE 7-05 Minimum Design Loads for Buildings and other Structures* assuming a ground snow load of 30 psf and a flat roof.

**Table 1. Roof dead loading intensities**

<b>Dead Loading</b>	<b>Load Intensity</b>
Metal Roof Deck (18 gage)	3 psf
Roofing System	6 psf
Mechanical Duct Allowance	4 psf
Structural Steel Self-Weight	5 psf

**Table 2. Total gravity loading intensities**

<b>Gravity Load Type</b>	<b>Load Intensity</b>
Dead Load	18 psf
Roof Live Load	20 psf
Snow Load	21 psf

Wind pressures were calculated using the simplified procedure of *ASCE 7-05 Minimum Design Loads for Buildings and other Structures*. Two separate wind pressures corresponding to an interior zone and corner zone were calculated for each side of the structure. The width of the corner zone is 18 feet which is equal to 40% of the building

height. Figure 8 shows the locations of the corner and interior wind pressure zones as well as the corresponding wind pressure intensities for each zone.

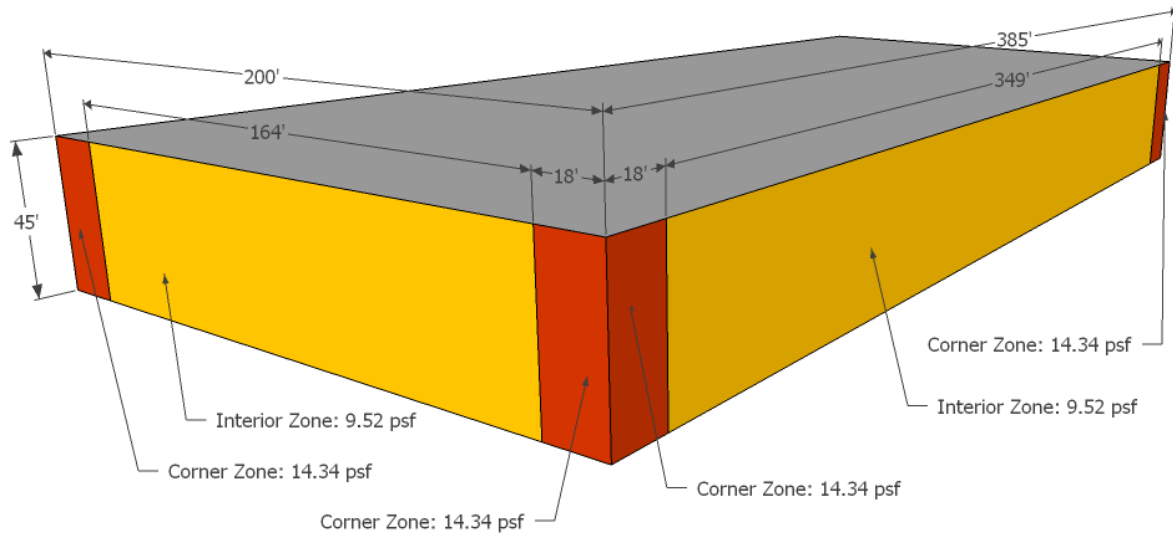


**Figure 8. Wind load diagram showing location of interior and corner wind pressure zones as well as interior and corner zone wind pressures**

Figure 9 shows the roof framing plan which consists of open-web steel joists spanning in the north-south direction between girders on column lines A and D and E and H. The joists are spaced at approximately 10'-9" between column lines 5 and 13. Between column lines 1 and 2, 4 and 5, 13 and 14, and 16 and 17, the joists are spaced at approximately 12'-4". The joists in the bays with the two-panel concentrically braced frames are spaced at 15 feet so that the joists frame directly into the columns of the two-panel concentrically braced frames.

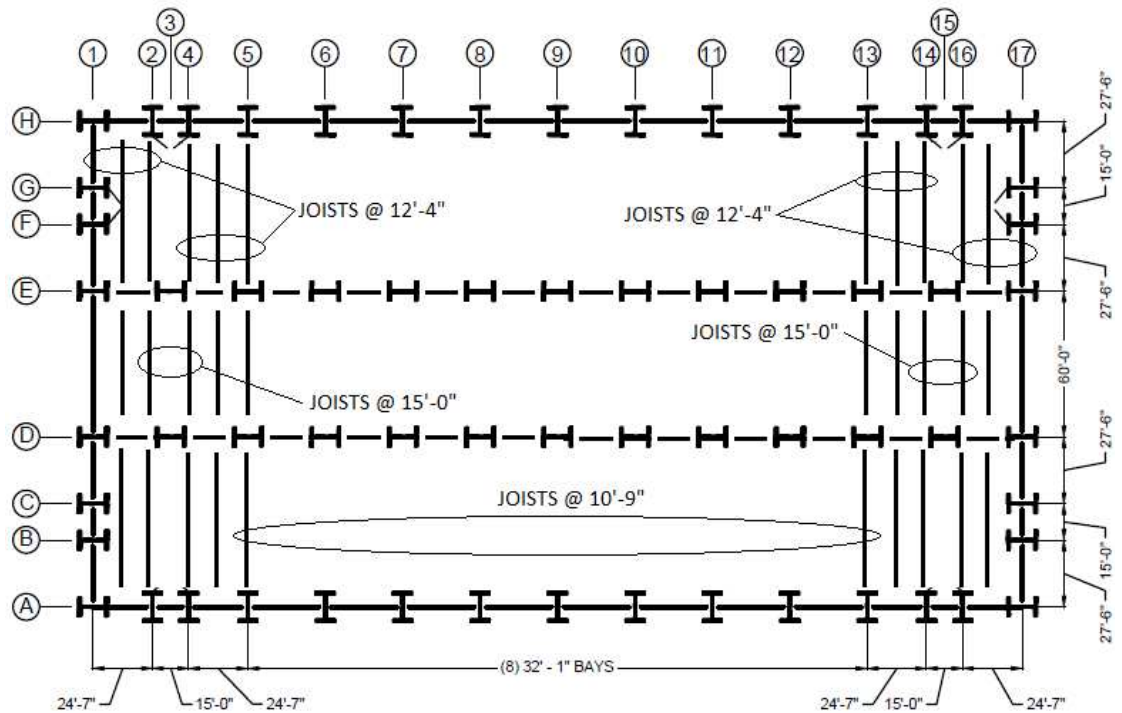


**Figure 9. Roof framing plan**

Loads acting on the frame were determined based on the framing plan for the building. Gravity loading on the two-panel concentrically braced frames on the north and south faces of the structure is assumed to act on the frame as concentrated forces at the columns' top. The forces acting on the columns emanate from the roof gravity loads acting on the metal roof deck being distributed to the steel joists and then being distributed along the joists to the columns. Gravity loading on the two-panel concentrically braced frames on the east and west faces of the structure is assumed to act as a uniformly distributed load applied transversely to the top beam and a concentrated force at the top of each column. This distributed force acting on the beam emanates from the roof gravity loads acting on the metal roof deck being distributed directly to the top beam of the frame at the exterior of the structure. The concentrated forces emanate from the roof gravity loads acting on the metal deck being distributed to the edge roof beams

and then being distributed to the columns of the two-panel concentrically braced frames. Figure 10 shows the load path for the gravity loads tributary to the two-panel concentrically braced frames located in the structure. Figure 11 shows the resulting forces on the two-panel concentrically braced frame due to gravity loading. Table 3 summarizes the unfactored gravity loads that act on the two-panel concentrically braced frames.

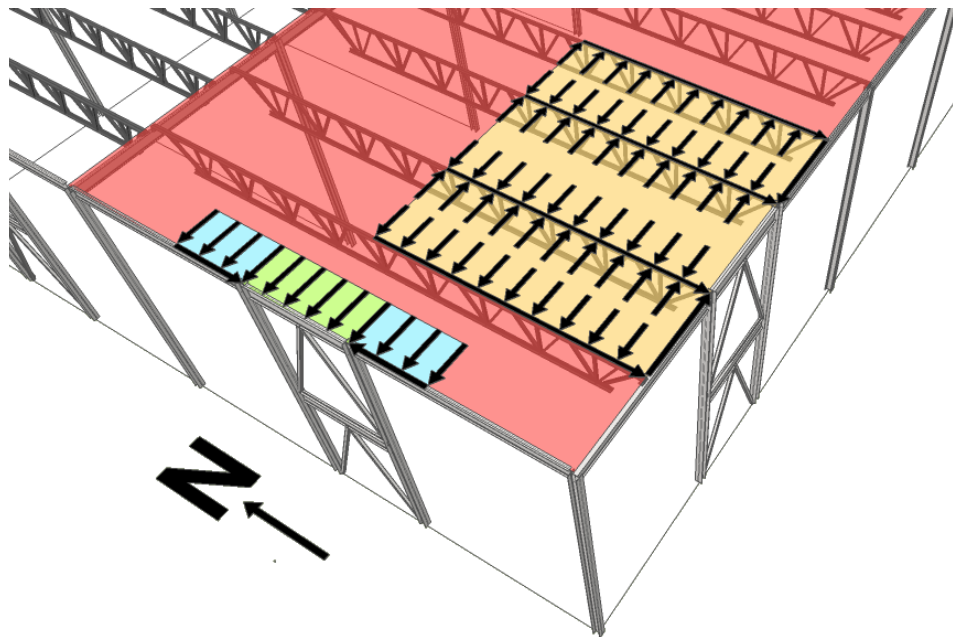


**Figure 10. Load paths for gravity loads tributary to two-panel concentrically braced frames**

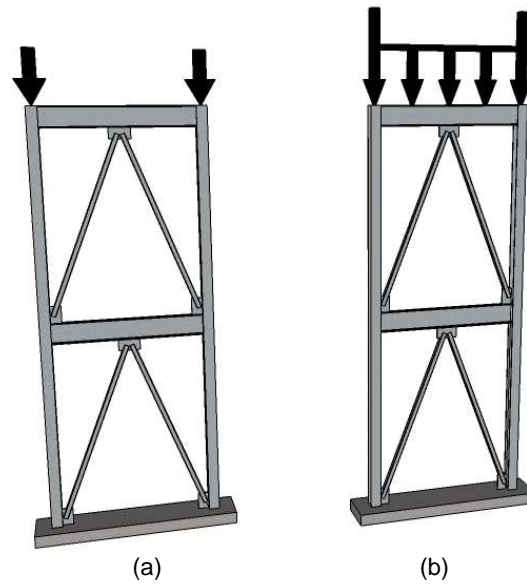


**Figure 11. Forces resulting from gravity loads acting on the two-panel concentrically braced frames on (a) the north/south structure faces and (b) the east/west structure faces**

**Table 3. Unfactored gravity loads acting on two-panel concentrically braced frames**

	Frames on North/South Building Face	Frames on East/West Building Face
Load Type	Load Intensity (kip)	Load Intensity (kip/ft)
Dead Load	12.5	0.22
Roof Live Load	13.9	0.25
Snow Load	14.6	0.26

Lateral load acting on the frames emanates from the wind pressures acting on the exterior walls of the structure. Wind pressure acting on the top half of the exterior walls is assumed to be distributed to the roof diaphragm whereas the wind pressure acting on the bottom half of the exterior walls is assumed to be distributed directly to the foundation. The wind pressure distributed to the roof diaphragm is evenly distributed to each line of two-panel concentrically braced frames and then distributed evenly as a concentrated force to each frame. Tributary loading areas on the building walls for each frame are illustrated in Figure 12.

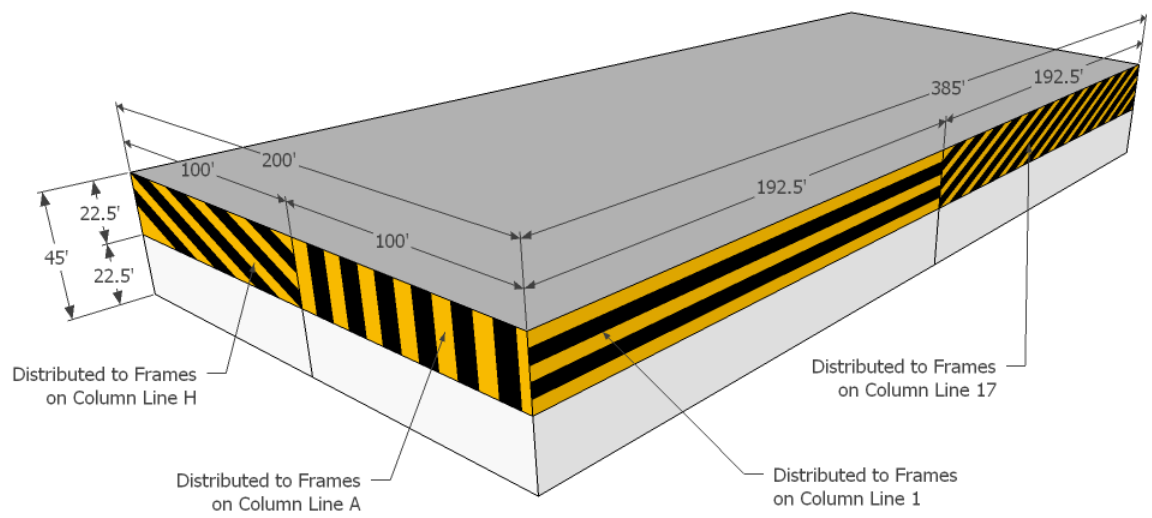


**Figure 12. Tributary areas for lateral wind loads**

The concentrated wind force is assumed to be applied laterally to the frame at its top. Figure 13 shows the resulting forces on the two-panel concentrically braced frame due to lateral wind loading. Table 4 summarizes the unfactored lateral wind loads that act on the two-panel concentrically braced frames.

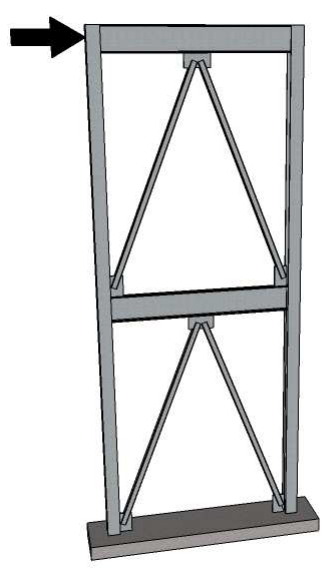


**Figure 13. Force resulting from lateral wind loads acting on the two-panel concentrically braced frames**

**Table 4. Unfactored concentrated lateral loads acting on two-panel concentrically braced frames**

	<b>Frames on North/South Building Face</b>	<b>Frames on East/West Building Face</b>
<b>Load Type</b>	<b>Load Intensity (kip)</b>	<b>Load Intensity (kip)</b>
Wind Load	11.7	14.3

Each column member is designed for the effects of the concentrated force applied to the tops of the columns of the two-panel concentrically braced frames on the north and south faces of the building. The concentrated force magnitude is obtained from LRFD load combinations given in *ASCE 7-05 Minimum Design Loads for Buildings and other Structures* which is shown in Equation 1.

$$1.2D + 1.6S \quad \text{Equation 1}$$

where,

$D$  = roof dead load

$S$  = roof snow load

This concentrated force results in a constant axial force of 38.3 kips throughout the height of the member. The column is conservatively assumed to have its web oriented parallel to the plane of the frame. The column is assumed to be braced in the plane of the frame at mid-height due to the intermediate beam resulting in an effective length about the column's strong axis of 22.5 feet. Out of the plane of the frame, the column is assumed to be braced only at its ends resulting in an effective length about the column's weak axis of 45 feet. Figure 14 shows the column assumed for design with its loading and bracing conditions.

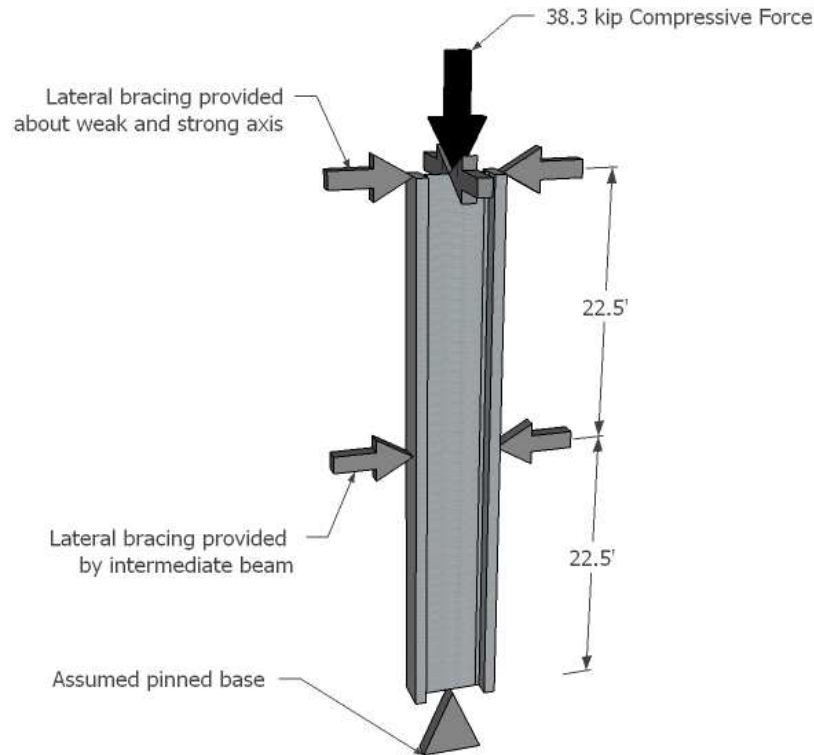


**Figure 14. Column assumed for design purposes with loads and bracing conditions**

Each beam member is designed for the combined effects of the concentrated lateral force applied to the top of the column and the uniform distributed load applied to the top beam of the two-panel concentrically braced frames on the east and west faces of the building. The controlling force magnitudes are obtained from the LRFD load combinations given in *ASCE 7-05 Minimum Design Loads for Buildings and other Structures* which is shown in Equation 2.

$$0.9D + 1.6W \quad \text{Equation 2}$$

where,

$$W = \text{wind load}$$

This load combination results in a concentrated axial compressive force of 22.88 kips from wind loading and a uniform distributed transverse force of intensity 0.20 kip/ft from roof dead loading. The member was assumed to have an effective length for flexural buckling of 7.5 feet about its major axis and 15 feet about its minor axis. These effective

lengths were conservatively determined for the time period when the metal roof deck is not yet installed. Figure 15 shows the member assumed for design with its loading and bracing conditions.

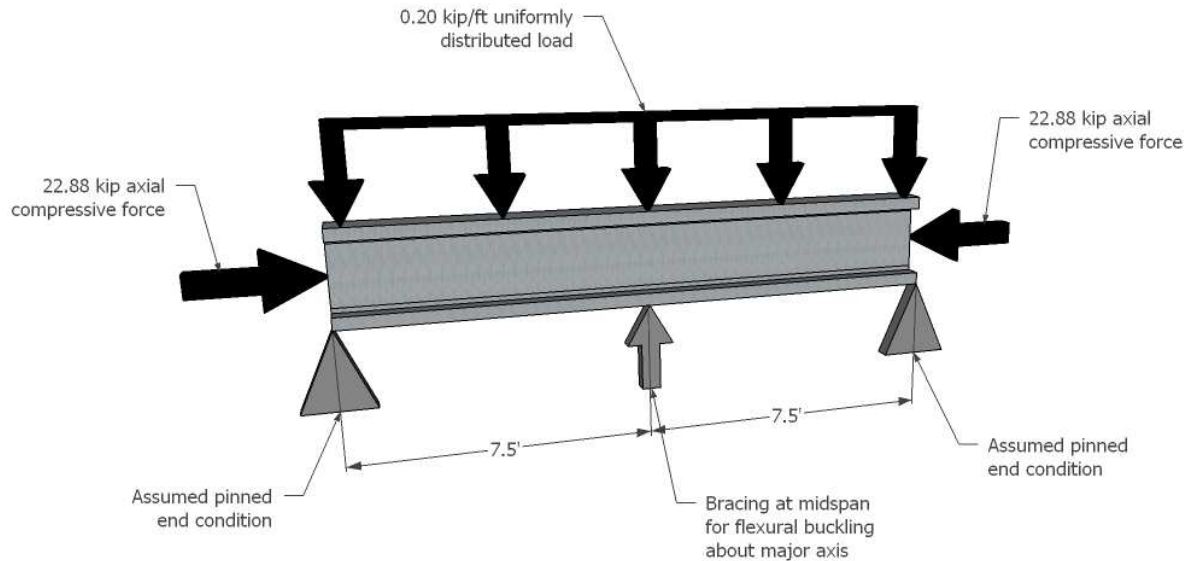


**Figure 15. Beam assumed for design purposes with loads and bracing conditions**

Each bracing member is designed for the effects of the concentrated lateral force applied to the top of the two-panel concentrically braced frames on the east and west faces of the building. The concentrated force magnitude is obtained from LRFD load combinations given in *ASCE 7-05 Minimum Design Loads for Buildings and other Structures* which is shown in Equation 3.

$$1.6W$$

**Equation 3**

This concentrated force results in a constant axial tensile or compressive force directed along the member longitudinal axis of 72.1 kips throughout the length of the member. The member was conservatively assumed to have an effective length equal to its actual length of 23.7 feet. Figure 16 shows the member assumed for design with its loading and bracing conditions.

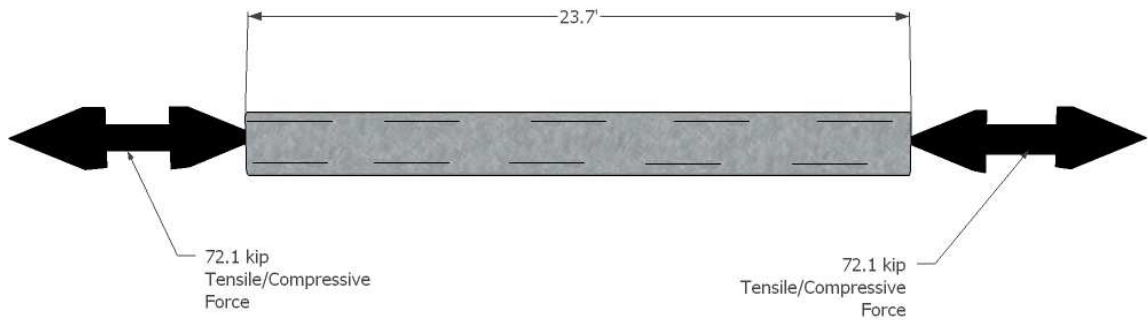


**Figure 16. Brace axial member assumed for design purposes with loads**

A W12x65 section of A992 steel was selected for the column members of each two-panel concentrically braced frame. Using the provisions of AISC (2010a), the axial capacity of the W12x65 was determined for the controlling limit state of flexural buckling about the member's weak axis. Assuming an effective length of 45.0 feet, the axial capacity of the W12x65 was calculated to be 135 kip using Equation 4.

$$P_d = \phi_c [0.877] F_e A_g \quad \text{Equation 4}$$

where,

$P_d$  = design compressive strength (kip)

$\phi_c$  = strength reduction factor (0.9)

$F_e$  = elastic buckling stress

$A_g$  = gross cross-sectional area of member (in<sup>2</sup>)

A W18x35 section of A992 steel was selected for the beam members of each two-panel concentrically braced frame. Using the provisions of AISC (2010a), the axial capacity of the W18x35 was determined for the controlling limit state of flexural buckling about the member's weak axis. Assuming an effective length equal to 15 feet and a net reduction factor equal to 0.84, the axial capacity of the W18x35 was calculated to be 106.9 kip using Equation 5.

$$P_d = \phi_c Q \leq 0.877 F_e A_g \quad \text{Equation 5}$$

where,

$Q$  = net reduction factor accounting for all slender elements

Since the top beam member of the two-panel concentrically braced frames on the east and west building faces are loaded transversely by a uniformly distributed load, the W18x35 is also subjected to an internal bending moment. As a result, the flexural capacity of the W18x35 was determined using the provisions of AISC (2010a) for the controlling limit state of yielding. Yielding controls the flexural capacity of the W18x35 because it is assumed to be continuously laterally braced along its length once the metal roof deck is installed. With  $F_y = 50$  ksi, the flexural capacity of the W18x35 was calculated to be 249 kip-ft using Equation 6.

$$M_d = \phi_b F_y Z_x \quad \text{Equation 6}$$

where,

$M_d$  = design flexural (kip-in)

$\phi_b$  = strength reduction factor (0.9)

$F_y$  = specified minimum yield stress of material (ksi)

$Z_x$  = plastic section modulus about the x-axis (in<sup>3</sup>)

Since the top beam member was subject to combined axial force and flexure, the provisions of AISC (2010a) were used to assess the interaction of the combined forces on the W18x35. The effect of this interaction was determined using Equation 7.

$$\frac{P_r}{P_c} + \frac{8}{9} \left( \frac{M_r}{M_x} \right) \leq 1.0 \quad \text{Equation 7}$$

where,

$P_r$  = required axial strength (22.9 kip)

$P_c$  = available axial strength (106.9 kip)

$M_{rx}$  = required flexural strength about major axis (67.2 kip-in)

$M_{cx}$  = available flexural strength about major axis (2988.0 kip-in)

The interaction equation result for the W18x35 was 0.23.

A HSS 5-1/2x5-1/2x5/16 section of A500 Grade C steel was selected for the bracing members of each two-panel concentrically braced frame. Using the provisions of AISC (2010a), the axial capacity of the HSS 5-1/2x5-1/2x5/16 was determined for the controlling limit state of flexural buckling. Since a square HSS section was selected, the capacity of the member about its strong and weak axis is equal. Assuming an effective length equal to 23.7 feet, the axial capacity of the HSS 5-1/2x5-1/2x5/16 was calculated to be 72.6 kip using Equation 8.

$$P_d = \phi_c [0.877] F_e A_g \quad \text{Equation 8}$$

Table 5 summarizes the actual and required member capacities for the elements of the two-panel concentrically braced frame.

**Table 5. Member demand and capacity summary**

Element	Required Axial Capacity	Required Flexural Capacity	Actual Axial Capacity	Actual Flexural Capacity	Interaction Equation Result
Column (W12x65)	38.3 kip	-	135 kip	-	-
Brace (HSS 5-1/2x5-1/2x5/16)	72.1 kip	-	72.6 kip	-	-
Beam (W18x35)	22.88 kip	5.6 kip-ft	106.9 kip	249 kip-ft	0.23 < 1.0

### **3. Critical Load Analyses**

The present chapter outlines elastic and inelastic critical load analysis carried out on the two-panel concentrically braced frame. A summary of how the critical load analyses are performed as well as the frame configurations that are analyzed is discussed first. The effects of applied lateral load on the frame elastic critical loads are then discussed. The effects of overall frame geometry (frame aspect ratio) are then evaluated. A comparison of frame elastic critical loads for frames with column webs oriented parallel to the plane of the frame and perpendicular to the plane of the frame is then made. Inelastic critical load analyses are then carried out and a summary of frame inelastic critical loads and a comparison of the frame inelastic critical loads to frame elastic critical loads for corresponding frame aspect ratios and applied lateral to gravity load ratios are provided. The effects of initial geometric imperfections on frame elastic critical loads are then discussed. Finally, conclusions of the important findings of the critical load analyses are given.

#### **3.1. Methodology**

To assess the elastic stability response of the two-panel concentrically braced frame, a series of critical load analyses were conducted with varying frame height-to-width ratios and lateral loading levels. A reference gravity load of 10 kips is applied at the top of each column and a lateral load varying from 0 to 1.0 times the intensity of the reference gravity load is applied at the top of the left column to assess the effect of lateral load on the stability response of the frame. Figure 17 illustrates the loading scenarios analyzed with the loads denoted by P symbolizing the 10 kip concentrated gravity loads

and the  $\alpha P$  load symbolizing the varying concentrated lateral load applied to the frame. The loads are proportionally applied through the use of an applied load ratio multiplier (ALR) ranging from 0 to a value corresponding to the critical load of the system.

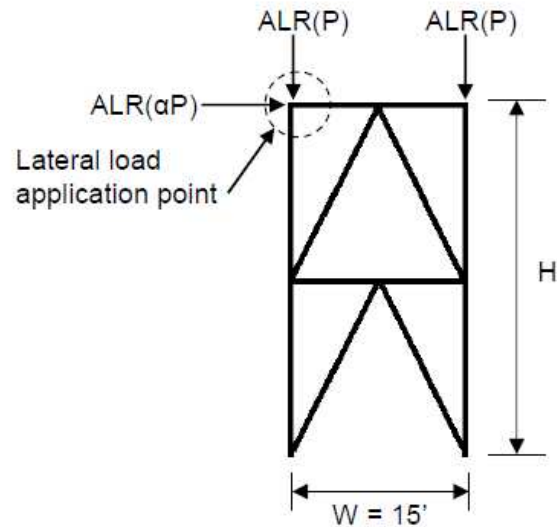
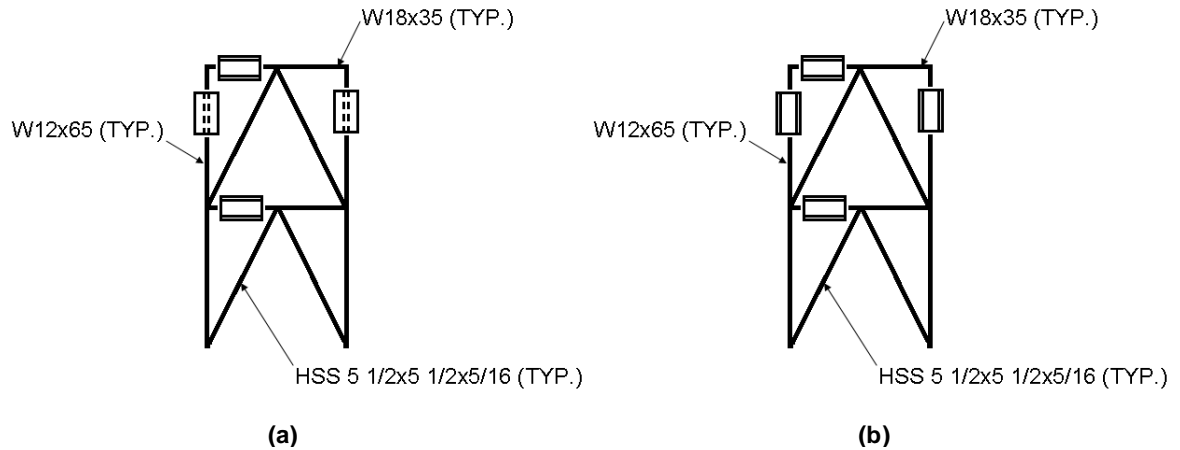


**Figure 17. Loading scenario for elastic critical load analyses**

These analyses were performed on frames with height-to-width ratios ( $H/W$ ) of 2.0, 2.5, 3.0, and 3.5 to assess the effect of frame slenderness on the stability of the frame. Frame width was held constant at a distance of 15 feet while the total height of the frame was adjusted to 30 feet, 37.5 feet, 45 feet, and 52.5 feet to achieve the height-to-width ratios of 2.0, 2.5, 3.0, and 3.5, respectively. Two different column orientation scenarios were also analyzed; one scenario with column webs oriented perpendicular to the plane of the frame and one scenario with column webs oriented parallel to the plane of the frame. When the column webs are oriented perpendicular to the plane of the frame, weak axis column buckling corresponds to buckling in the plane of the frame. When the column webs are oriented parallel to the plane of the frame, weak axis column buckling corresponds to buckling out of the plane of the frame. The W12x65 columns

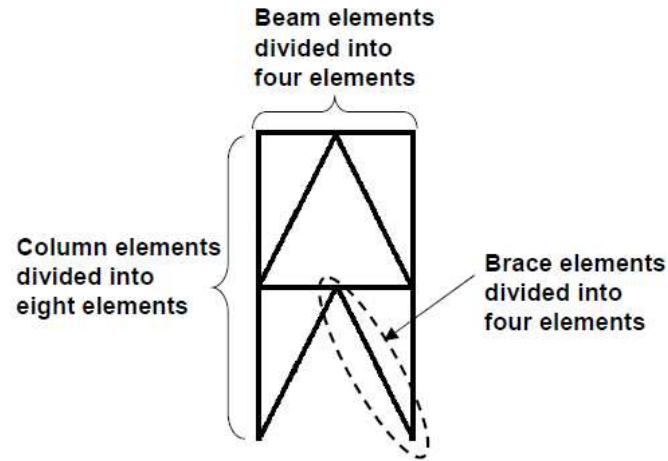
were sized assuming the column webs were oriented parallel to the plane of the frame.

Figure 18 shows the two column orientation scenarios considered.



**Figure 18. Frame scenarios analyzed with (a) column webs oriented perpendicular to the plane of the frame and (b) column webs oriented parallel to the plane of the frame**

In the MASTAN2 (MASTAN2 2010) analytical model, each structural member is divided into multiple discrete elements to better capture behavior along the length of the member. Each brace member and beam member is discretized into 4 equal length elements and each column member is discretized into 8 equal length elements from the base of the frame to its top. Figure 19 illustrates the member discretization scheme used in the MASTAN2 analytical model for the elastic and inelastic critical load analyses.



**Figure 19. Member discretization used in MASTAN2 analytical model**

For the elastic and inelastic critical load analyses, the connection of the columns to the foundation is idealized as a pin connection with zero rotational stiffness about both the columns' major and minor axes and zero warping restraint. The end connections of the brace elements are also idealized as pin connections with zero rotational stiffness about both the major and minor axis of the member and zero warping restraint. Beam-to-column connections are modeled as semi-rigid with a rotational stiffness of 164,322 kip-in/rad about the beams' local z-axes (bending in the plane of the frame) and infinite stiffness about the beams' local y-axes (bending out of the plane of the frame). The rotational stiffness about the z-axis is equal to  $2EI/L$  of the beam members which is the upper limit on the secant stiffness of a connection that can be considered as a simple connection (AISC 2010a). Global support conditions remain the same as introduced in the previous frame design section. Figure 20 shows the locations of the pin and semi-rigid connections in the MASTAN2 analytical model.

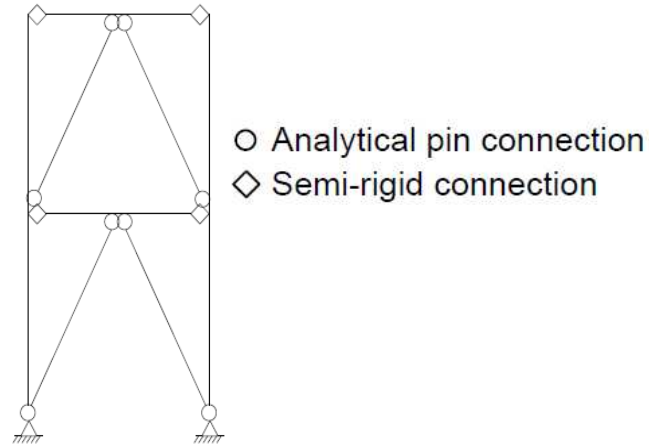


**Figure 20. Connection summary for MASTAN2 analytical model used in elastic and inelastic critical load analyses**

### **3.2. Effect of Applied Lateral Load**

Figure 21 illustrates the first mode elastic critical load capacity of the frames with column webs oriented perpendicular to the plane of the frame as illustrated in Figure 18a for all lateral load levels and all height-to-width ratios considered. The addition of lateral load at the top of the frame reduces the elastic critical load capacity of the frame. As the level of lateral load on the frame increases, the first mode elastic critical load capacity of the frame decreases. This is apparent in the downward sloping nature of each of the elastic critical load versus lateral load ratio ( $\alpha$ ) curves in Figure 21. Figure 21 also shows the buckled shapes for each frame configuration and lateral loading scenario considered.

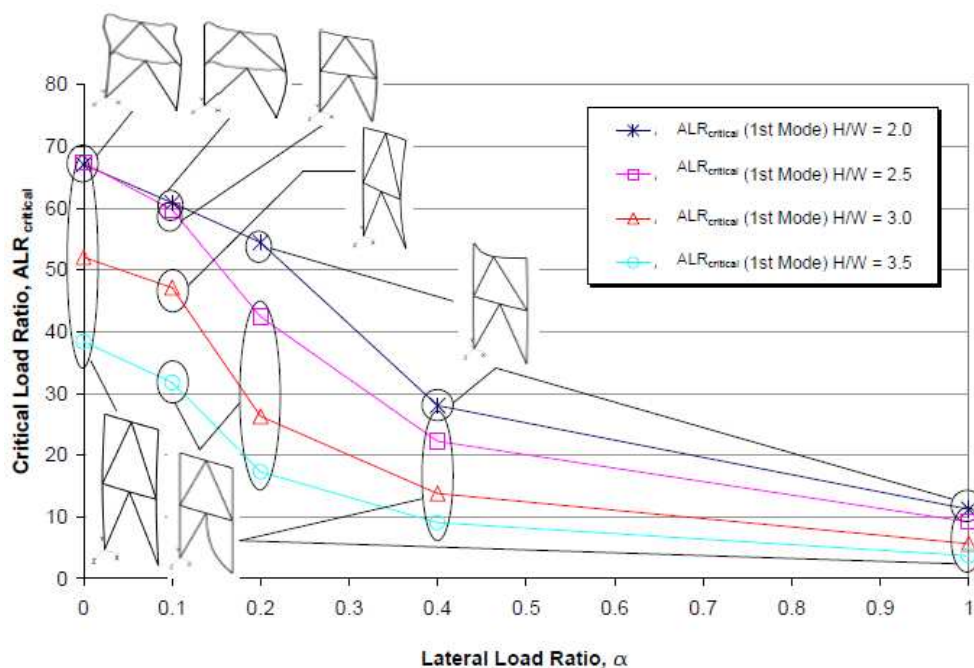


**Figure 21. Elastic critical load vs. lateral load ratio curves and buckled shapes for frame with column webs oriented perpendicular to the plane of the frame**

Table 6 illustrates numerically the decreasing elastic critical load trend in Figure 21 for the frames with column webs oriented perpendicular to the plane of the frame. The values in Table 6 are the percent changes in elastic critical load at each lateral load level measured with respect to the initial lateral load ratio of 0 (0 kip lateral load). First mode elastic critical load capacity of the frame at a lateral load ratio of 1.0 (10 kip lateral load) is between 83.24% and 90.29% less than the elastic critical load capacity of the frame at the initial lateral load level of 0 kips depending on the frame height-to-width ratio. As frame height-to-width ratio increases, the percent decrease in elastic critical load capacity at all lateral loading levels increases except for the lateral load ratio of 0.1 (1 kip lateral load). At the 1 kip lateral load level, the frame with a height-to-width ratio of 2.5 experiences an 11.27% decrease in elastic critical load capacity from the initial 0

kip lateral load level while the frame with a height-to-width ratio of 3.0 experiences only a 9.47% decrease in elastic critical load capacity from the initial 0 kip lateral load level.

**Table 6. Percent change in elastic critical load for varying lateral loads (Column webs perpendicular to plane of frame)**

$\alpha$	H/w = 2.0	H/w = 2.5	H/w = 3.0	H/w = 3.5
0.0	-	-	-	-
0.1	-9.18%	-11.27%	-9.47%	-17.24%
0.2	-18.80%	-37.02%	-49.49%	-54.92%
0.4	-58.21%	-66.94%	-73.53%	-76.40%
1.0	-83.24%	-86.37%	-89.10%	-90.29%

The elastic critical load for the frame with a height-to-width ratio of 2.0 decreases by approximately the same amount from the initial lateral load ratio of 0 to the lateral load ratio of 0.1 as it does between the lateral load ratios of 0.1 and 0.2. A larger decrease in elastic critical load between lateral load ratios of 0.1 and 0.2 as compared to the decrease in elastic critical load between lateral load ratios of 0 and 0.1 is observed for the frames with height-to-width ratios of 2.5, 3.0, and 3.5. This is due to differences in buckled geometry for the various height-to-width ratios

For the frame with a height-to-width ratio of 2.0, the first mode buckled shapes show in-plane buckling of the outer quarter of the top level and tier level beams and out-of-plane reverse curvature of both the left and right columns with an inflection point approximately halfway between the tier level and top level beam at a lateral load ratio of 0.0. When the lateral load ratio is increased to 0.10, in-plane buckling of the outer quarter of the top level and tier level beams is still present, but the right column is now buckling out of the plane of the frame in single curvature while the left column is nearly straight. The frame exhibits out-of-plane buckling of the top beam about its weak axis at a lateral load ratio of 0.20.

The frames with height-to-width ratios of 2.5 and 3.0 exhibit overall system buckling in the form of out-of-plane buckling of both columns at a lateral load ratio of 0.0 and out-of-plane buckling of the right column at a lateral load ratio of 0.10. At a lateral load ratio of 0.20, the frames exhibit local member buckling rather than system buckling in the form of out-of-plane buckling of the bottom panel compression brace. This results in the larger decrease in elastic critical load between lateral load ratios of 0.10 and 0.20 as compared to the decrease in elastic critical load between lateral load ratios of 0.0 and 0.10.

Similar to the frames with height-to-width ratios of 2.5 and 3.0, the frame with a height-to-width ratio of 3.5 exhibits overall system buckling in the form of out-of-plane buckling of both columns at a lateral load ratio of 0.0. Behavior transitions from system buckling to local member buckling at a lateral load ratio of 0.10. The frame exhibits local member buckling in the form of out-of-plane buckling of the bottom panel compression brace at lateral load ratios of 0.10 and 0.20. This early transition results in a percent decrease in elastic critical load between lateral load ratios of 0.0 and 0.10 nearly double that of the frames that do not transition from system buckling to local member buckling until the lateral load ratio reaches 0.20.

Figure 22 illustrates the elastic critical load capacity of the frames with column webs oriented parallel to the plane of the frame as shown in Figure 18b for all lateral load levels and all height-to-width ratios considered. The same downward sloping trend of each elastic critical load versus lateral load ratio curve present in Figure 21 is also present in Figure 22 for the frames with column webs oriented parallel to the plane of the frame. However, the decrease in elastic critical load as lateral load ratios increase is relatively

linear across the entire range of lateral load levels. This will be elaborated upon with further discussion.

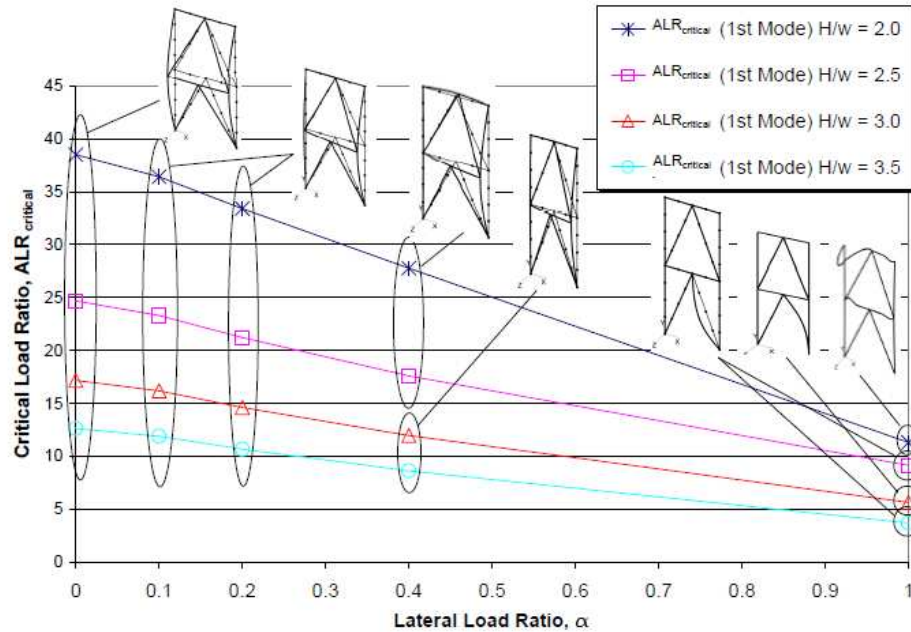


**Figure 22. Elastic critical load vs. lateral load ratio curves and buckled shapes for frame with column webs oriented parallel to the plane of the frame**

Table 7 illustrates numerically the decreasing elastic critical load trend in Figure 22 for the frames with column webs oriented parallel to the plane of the frame. The values in Table 7 represent the percent changes in elastic critical load at each lateral load level measured with respect to the initial lateral load ratio,  $\alpha = 0.0$ . First mode elastic critical load capacity of the frame with  $\alpha = 1.0$  is between 62.94% and 70.62% less than the elastic critical load capacity of the frame with  $\alpha = 0.0$  depending on the frame height-to-width ratio. As frame height-to-width ratio increases, the percent decrease in elastic critical load capacity at all lateral loading levels increases except for  $\alpha = 1.0$ . With  $\alpha = 1.0$ , the frame with a height-to-width ratio of 2.0 experiences a 70.62% decrease in elastic

critical load capacity compared to  $\alpha = 0.0$ . This is the largest percent decrease in elastic critical load while the frames with height-to-width ratios of 2.5, 3.0, and 3.5 experience a 62.94%, 67.04%, and 70.58% decrease in elastic critical load capacity from the  $\alpha = 0.0$  loading condition. This different trend seen for  $\alpha = 1.0$  occurs at the only lateral load ratio that has brace and beam buckling occur.

**Table 7. Percent change in elastic critical load for varying lateral loads (Column webs parallel to plane of frame)**

$\alpha$	H/w = 2.0	H/w = 2.5	H/w = 3.0	H/w = 3.5
0.0	-	-	-	-
0.1	-5.41%	-5.58%	-5.69%	-5.76%
0.2	-13.22%	-14.06%	-14.80%	-15.39%
0.4	-27.85%	-28.70%	-30.24%	-31.63%
1.0	-70.62%	-62.94%	-67.04%	-70.58%

The nearly linear nature of the elastic critical load versus lateral load ratio curves in Figure 22 is also expressed numerically in Table 7. The percent decrease in elastic critical load is proportional in an approximately linear relationship to the lateral load ratio across the range of lateral load ratios from  $0.0 \leq \alpha \leq 0.4$  for each respective frame height-to-width ratio. The percent decrease in elastic critical load between lateral load ratios  $0.4 \leq \alpha \leq 1.0$  is slightly larger than the percent decreases between the other lateral load ratios. This nearly linear relationship is due to frame buckled geometries exhibiting system buckling behavior for all lateral load ratios up to a lateral load ratio  $\alpha = 1.0$ .

The frame exhibits overall system buckling in the form of out-of-plane buckling of both columns at a lateral load ratio of 0 and out-of-plane buckling of the right column at lateral load ratios of 0.1, 0.2, and 0.4. At a lateral load ratio of 1.0, the frame with a height-to-width ratio of 2.0 transitions to local member buckling rather than system

buckling in the form of in-plane and out-of-plane buckling of the left half of the top level beam. The frames with height-to-width ratios of 2.5, 3.0, and 3.5 transition from system buckling to local member buckling in the form of out-of-plane buckling of the bottom panel compression brace for frames with height-to-width ratios of 2.5 and 3.5 and in-plane buckling of the bottom panel compression brace for frames with a height-to-width ratio of 3.0.

### 3.3. Effect of Overall Frame Geometry

As shown in Figure 21 and Figure 22, the first mode elastic critical load ratio for the frame, in general, decreases as the frame height-to-width ratio increases at each respective lateral load ratio. Table 8 shows the percent change in first mode elastic critical load ratio for frames with column webs oriented perpendicular to the plane of the frame as illustrated in Figure 18a as height-to-width ratio changes at each lateral load ratio. Each percent change value in Table 8 is measured with respect to the elastic critical load ratio at the next lowest height-to-width ratio.

**Table 8. Percent change in elastic critical load for varying height-to-width ratios (Web perpendicular to plane of frame)**

$\alpha$	H/w = 2.0	H/w = 2.5	H/w = 3.0	H/w = 3.5
0	-	0.43%	-22.69%	-26.27%
0.1	-	-1.88%	-21.13%	-32.60%
0.2	-	-22.10%	-38.01%	-34.19%
0.4	-	-20.55%	-38.10%	-34.28%
1	-	-18.32%	-38.16%	-34.34%

At lateral load ratios of 0.0 and 0.1, the percent change in elastic critical load ratio between frames with height-to-width ratios of 2.0 and 2.5 remains essentially unchanged. Between frames with height-to-width ratios of 2.5 and 3.0 and 3.0 and 3.5, the percent

change in elastic critical load ratio is -22.69% and -26.27%, respectively, for  $\alpha = 0.0$ . As seen in Figure 21, for a lateral load ratio of 0.0, the frame with a height-to-width ratio of 2.0 exhibits in-plane buckling of the outer quarters of the top level and tier level beam and reverse curvature out-of-plane buckling of both columns while frames with height-to-width ratios of 2.5, 3.0, and 3.5 exhibit out-of-plane buckling of both columns. As a result, the percent change in elastic critical load ratio between frames with height-to-width ratios of 2.0 and 2.5 is a function of frame slenderness and buckled geometry whereas the percent change in elastic critical load ratio between frames with the remaining height-to-width ratios is a function of only frame slenderness and consequently increases in column length.

At a lateral load ratio of 0.10, the frame with a height-to-width ratio of 2.0 exhibits out-of-plane buckling of the outer quarters of the top level and tier level beams and out-of-plane single curvature buckling of the right column while frames with height-to-width ratios of 2.5 and 3.0 exhibit only out-of-plane buckling of the right column. The frame with a height-to-width ratio of 3.5 exhibits local member buckling in the form of out-of-plane buckling of the bottom panel compression brace. As a result, the percent change in elastic critical load ratio between frames with height-to-width ratios of 2.0 and 2.5 is a function of changes in frame slenderness and buckled geometry whereas the percent change in elastic critical load between frames with height-to-width ratios of 2.5 and 3.0 is simply a function of frame slenderness and consequently increases in column length. The larger percent change in elastic critical load between frames with height-to-width ratios of 3.0 and 3.5 is a function of both frame slenderness and the transition from system buckling to local member buckling behavior.

At lateral load ratios of 0.2, 0.4, and 1.0 the percent change in elastic critical load ratio between frames with height-to-width ratios of 2.0 and 2.5 ranges between -18.32% and -22.10%. Between frames with height-to-width ratios of 2.5 and 3.0 and 3.0 and 3.5, the percent change in elastic critical load ratio ranges between -38.01% and -38.16% and -34.19% and -34.34% respectively. The larger percent changes between frames with height-to-width ratios of 2.5 and 3.0 and 3.0 and 3.5 can be attributed to changes in frame buckled configurations. As seen in Figure 21, frames with a height-to-width ratio of 2.0 exhibit local out-of-plane buckling of the top beam while frames with height-to-width ratios of 2.5, 3.0, and 3.5 exhibit local out-of-plane buckling of the bottom panel compression brace. As a result, the percent change in elastic critical load ratio between frames with height-to-width ratios of 2.0 and 2.5 is a function of changes in frame slenderness and buckled geometry whereas the percent change in elastic critical load ratio between frames with the remaining height-to-width ratios is a function of frame slenderness and consequently increases in brace length.

Table 9 shows the percent change in first mode elastic critical load ratio for frames with column webs oriented parallel to the plane of the frame as illustrated in Figure 18b as height-to-width ratio changes at each lateral loading level. Each percent change value in Table 9 is measured with respect to the elastic critical load ratio at the next lowest height-to-width ratio.

**Table 9. Percent change in elastic critical load for varying height-to-width ratios measured with respect to next lowest height-to-width ratio (Web parallel to plane of frame)**

$\alpha$	H/w = 2.0	H/w = 2.5	H/w = 3.0	H/w = 3.5
0	-	-35.86%	-30.45%	-26.44%
0.1	-	-35.98%	-30.53%	-26.50%
0.2	-	-36.49%	-31.04%	-26.95%
0.4	-	-36.63%	-31.95%	-27.91%
1	-	-19.11%	-38.15%	-34.33%

As seen in Table 9, the percent changes in elastic critical load between frames with varying height-to-width ratios follows a similar trend when  $0.0 \leq \alpha \leq 0.4$ . When frame height-to-width ratio changes from 2.0 to 2.5, elastic critical load ratio decreases between 35.86% and 36.63%. As frame height-to-width ratio changes from 2.5 to 3.0, elastic critical load ratios decrease between 30.45% and 31.95%. As frame height-to-width ratio changes from 3.0 to 3.5, elastic critical load ratios decrease between 26.44% and 27.91%.

As seen in Figure 22, the frame buckled shapes at each respective lateral load ratio exhibit the same behavior as height-to-width ratio changes. At a lateral load ratio of 0.0, frames at each height-to-width ratio exhibit system buckling in the form of out-of-plane buckling of both columns. At lateral load ratios of 0.10, 0.20, and 0.40, frames at each height-to-width ratio exhibit system buckling in the form of out-of-plane buckling of the right column. When  $\alpha \geq 0.10$ , the left column undergoes tension loading as the lateral loading is increased. This is why the right column controls behavior. Since overall system buckling dominates the buckling behavior over the entire range of height-to-width ratios, the changes in elastic critical load ratio can be attributed to changes in frame slenderness and the associated change in column length.

The percent change in elastic critical load ratio between frames with varying height-to-width ratios with  $\alpha = 1.0$  does not follow the trend exhibited by the frames with  $0.0 \leq \alpha \leq 0.40$ . When frame height-to-width ratio changes from 2.0 to 2.5, elastic critical load ratio decreases only 19.11%. As frame height-to-width ratio changes from 2.5 to 3.0 and 3.0 to 3.5, elastic critical load ratio decreases 38.15% and 34.33% respectively.

When  $\alpha = 1.0$ , the buckled shapes of the frame at a height-to-width ratio of 2.0 exhibits local member buckling in the form of both in-plane and out-of-plane buckling of the left half of the top level beam. At height-to-width ratios of 2.5, 3.0, and 3.5, the buckled shape of the frame transitions to local buckling of the bottom panel compression brace. Buckling is out of the plane of the frame for height-to-width ratios of 2.5 and 3.5 and in the plane of the frame for a height-to-width ratio of 3.0. The change in buckled shape behavior between height-to-width ratios of 2.0 and 2.5 appears to decrease the percent change in elastic critical load ratio between the two height-to-width ratios. The 19.11% decrease in elastic critical load is approximately 52% of the same percent decrease when lateral load ratios range between 0 and 0.4. Since the buckled shape behavior remains of the same form for height-to-width ratios of 2.5, 3.0, and 3.5, only frame slenderness affects the frame elastic critical load ratio as the percent decreases are only 20% to 23% greater than the same percent decreases for the frame with lateral load ratios of 0 to 0.4.

### **3.4. Effect of Column Orientation**

Figure 23 shows a comparison of the elastic stability response for frames with a height-to-width ratio of 2.0 and column webs oriented both parallel and perpendicular to

the plane of the frame. Out-of-plane buckling of the columns is the predominant behavior driving the frame buckled shape when column webs are oriented parallel to the plane of the frame. For frames with column webs oriented perpendicular to the plane of the frame, out-of-plane buckling of the top beam dominates behavior. As seen in Figure 23, the elastic critical load ratio is larger when column webs are oriented perpendicular to the plane of the frame when  $0.0 \leq \alpha \leq 0.2$ , but is nearly identical to the elastic critical load ratio for the frames with column webs oriented parallel to the plane of the frame when  $\alpha > 0.4$ .

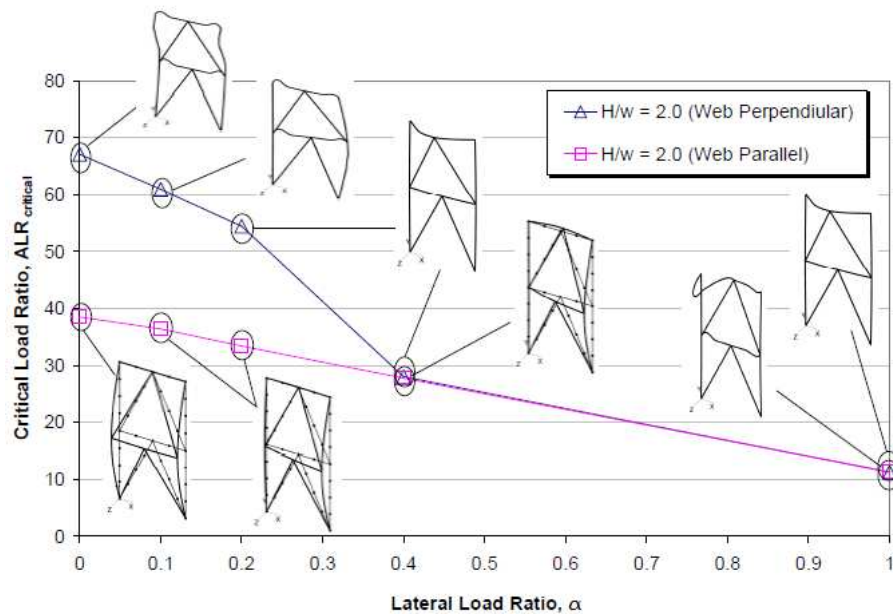


**Figure 23. Comparison of elastic critical loads for strong-axis and weak-axis column orientations for a frame with a height-to-width ratio of 2.0**

For the frame with a height-to-width ratio of 2.0 and column webs oriented perpendicular to the plane of the frame, in-plane buckling of the outer quarter of the top level and tier level beams and out-of-plane reverse curvature of both the left and right columns with an inflection point approximately halfway between the tier level and top

level beam at a lateral load ratio of 0.0. When the lateral load ratio is increased to 0.10, in-plane buckling of the outer quarter of the top level and tier level beams is still present, but the right column is now buckling out of the plane of the frame in single curvature while the left column is nearly straight. When column webs are oriented parallel to the plane of the frame, however, only the columns buckle about their weak axis which is laterally unsupported along its entire length.

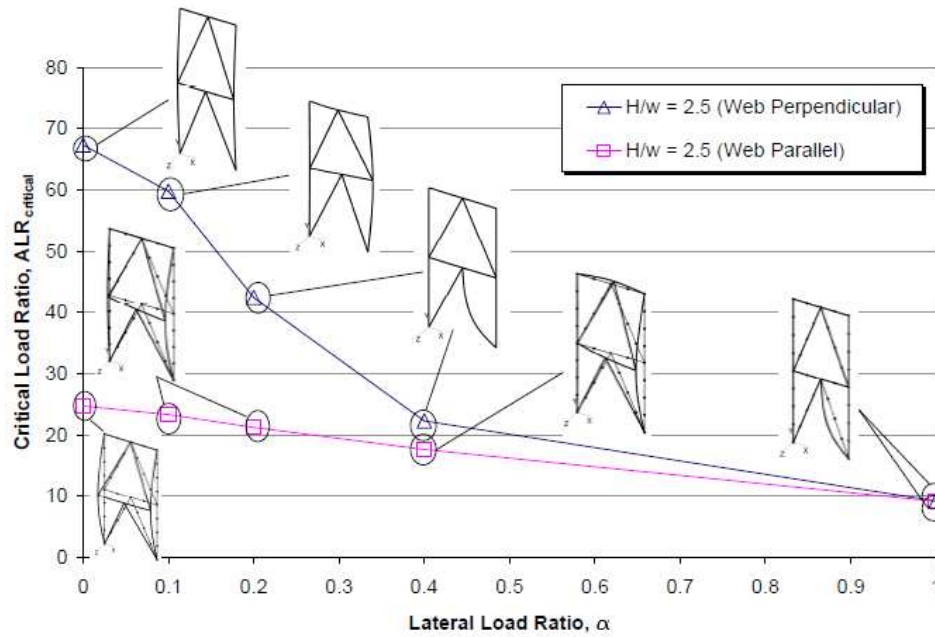
At  $\alpha = 0.2$ , out-of-plane buckling of the frame's top beam is the predominant feature of the elastic buckled shape for the frame with column webs oriented perpendicular to the plane of the frame. As the applied lateral load increases, the axial force in the beam increases causing the top beam to buckle. The top beam buckles before the columns in this arrangement as the columns' strong axes are laterally unsupported along their entire length, but the weak axes are laterally supported at mid-height. Out-of-plane buckling of the columns is still the dominant behavior exhibited by the frame with column webs oriented parallel to the plane of the frame since the columns' weak axes are laterally unsupported along their entire length.

At a lateral load ratio of 0.4, out-of-plane buckling of the frame's top beam is again the predominant feature of the elastic buckled shape for the frame with column webs oriented perpendicular to the plane of the frame. Out-of-plane buckling of the columns is still the dominant behavior exhibited by the frame with column webs oriented parallel to the plane of the frame, but slight buckling of the top beam is also present due to the increased axial force in the top beam.

At a lateral load ratio of 1.0, out-of-plane buckling of the frame's top beam is still the predominant feature of the elastic buckled shape for the frame with column webs

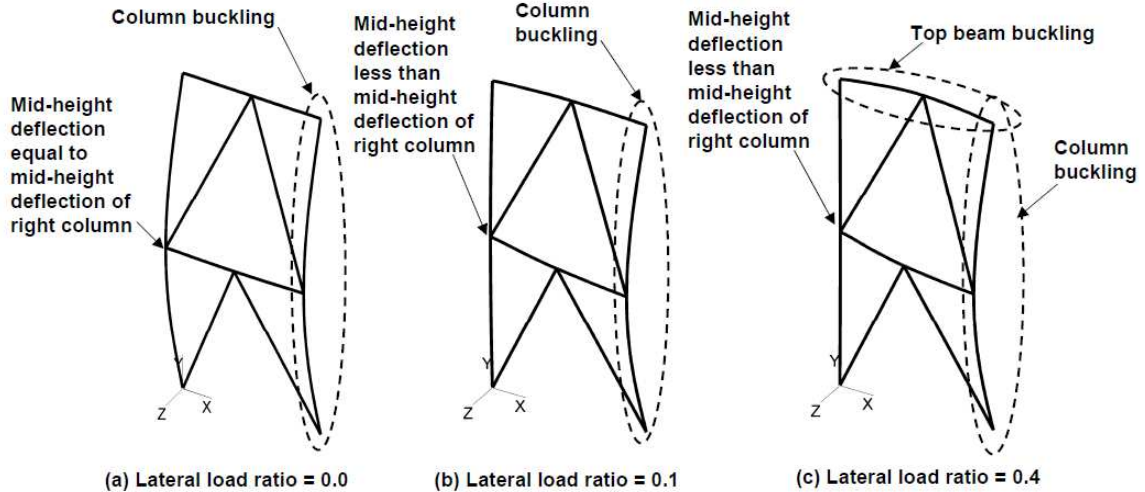
oriented perpendicular to the plane of the frame. In-plane and out-of-plane buckling of the left half of the top level beam is exhibited by the frame with column webs oriented parallel to the plane of the frame.

Figure 24 shows a comparison of the elastic stability response of both the frame with column webs oriented parallel and the frame with column webs oriented perpendicular to the plane of the frame for a frame with a height-to-width ratio of 2.5. Out-of-plane buckling about the columns' weak axes is the predominant behavior exhibited by the frames with column webs oriented parallel to the plane of the frame for  $0.0 \leq \alpha \leq 0.40$ . For frames with column webs oriented perpendicular to the plane of the frame, small out-of-plane buckling of the columns is exhibited for  $0.0 \leq \alpha \leq 0.10$  and out-of-plane buckling of the bottom panel bracing element is the predominant buckled behavior for  $0.20 \leq \alpha \leq 1.0$ . As seen in Figure 24, the elastic critical load ratio is larger when column webs are oriented perpendicular to the plane of the frame with  $0.0 \leq \alpha \leq 0.40$ , but is nearly identical to the elastic critical load for the frames with column webs oriented parallel to the plane of the frame when  $\alpha = 1.0$ .



**Figure 24. Comparison of elastic critical loads for strong-axis and weak-axis column orientations for a frame with a height-to-width ratio of 2.5**

For frames with column webs oriented parallel to the plane of the frame, the mid-height deflection of both columns is equal when no lateral load is applied, but as lateral load increases up to a lateral load ratio of 0.4, the deflection of the column closest to the applied lateral load decreases resulting from tensile forces due to lateral loads while the deflection of the other column remains the same. Small out-of-plane buckling of the top beam is also exhibited in the frame with a height-to-width ratio of 0.4. Figure 25 shows a comparison of the buckled shapes for the frame with a height-to-width ratio of 2.5 and column webs oriented parallel to the plane of the frame at lateral load ratios of 0, 0.1, and 0.2. Figure 25 also illustrates the interaction of beam and column buckling behavior with  $\alpha \geq 0.1$ . When lateral load is present, the windward column is subjected to tension loading resulting in an out-of-plane warping-type buckled shape of the tiered braced frame.



**Figure 25. Buckled shape comparison for frame with height-to-width ratio of 2.5 at lateral load ratios of 0, 0.1, 0.2, and 0.4**

When the lateral load ratio is increased to 1.0, the axial compressive force in the bottom panel brace increases to the point where out-of-plane buckling of that single element is the predominant behavior of the frame. Buckling of the bracing element is not seen in the frame with a height-to-width ratio of 2.0 and column webs oriented parallel to the plane of the frame since the length of the brace is short enough to allow buckling of the top level beam to control the frame's behavior.

With the column webs oriented perpendicular to the plane of the frame small out-of-plane buckling of the columns is seen for a frame with a height-to-width ratio of 2.5 and lateral load ratios of 0.0 and 0.10. As the height-to-width ratio increases from 2.0 to 2.5, the laterally unsupported length of the columns increases and the column buckling strength decreases. This decrease in column buckling strength results in column buckling controlling the behavior of the frame with a height-to-width ratio of 2.5 whereas the same lateral load ratios applied to the frame with a height-to-width ratio of 2.0 exhibited in-plane buckling of the top level beam about its major axis.

For lateral load ratios of 0.20, 0.40, and 1.0 and a height-to-width ratio of 2.5, out-of-plane buckling of the bottom panel bracing element dominates the behavior of the frame. The increase in the height-to-width-ratio from 2.0 to 2.5 increases the length of the brace, but does not change the length of the top beam. As a result, the buckling capacity of the bracing element decreases and it becomes the element which drives the buckled shape of the frame. The lateral load ratio of 1.0 applied to the frame with a height-to-width ratio of 2.5 results in both the frame with column webs oriented parallel and perpendicular to the plane of the frame to have the same first mode buckled geometry.

Figure 26 shows a comparison of the elastic stability response of both the frame with column webs oriented parallel and the frame with column webs oriented perpendicular to the plane of the frame for a frame with a height-to-width ratio of 3.0. Similarly to the frames with a height-to-width ratio of 2.5, out-of-plane buckling about the columns' weak axes is the predominant behavior exhibited by the frames with column webs oriented parallel to the plane of the frame for lateral load ratios from 0.0 to 0.40. For frames with column webs oriented perpendicular to the plane of the frame, small out-of-plane buckling of the columns is exhibited at lateral load ratios of 0.0 and 0.10 and out-of-plane buckling of the bottom panel bracing element is the predominant buckled behavior at lateral load ratios of 0.20, 0.40, and 1.0. This behavior is also identical to the behavior seen in frames with a height-to-width ratio of 2.5. As seen in Figure 26, the elastic critical load is larger when column webs are oriented perpendicular to the plane of the frame at lateral load ratios of 0.0, 0.10, and 0.20, but is nearly identical to the elastic

critical load for the frames with column webs oriented parallel to the plane of the frame at lateral load ratios of 0.40, and 1.0.

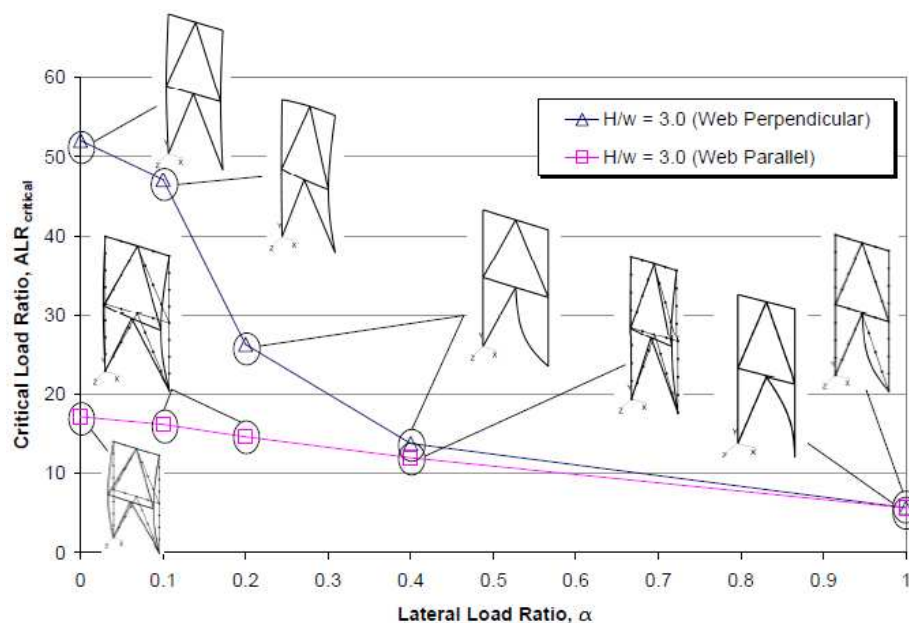


**Figure 26. Comparison of elastic critical loads for strong-axis and weak-axis column orientations for a frame with a height-to-width ratio of 3.0**

Consistent with the behavior seen for the frames with column webs oriented parallel to the plane of the frame and a height-to-width ratio of 2.5, the mid-height deflection of both columns is equal when no lateral load is applied, but as lateral load increases up to a lateral load ratio of 0.40, the deflection of the column closest to the applied lateral load decreases while the deflection of the other column remains the same. When the lateral load ratio is increased to 1.0, the axial compressive force in the bottom panel brace again increases to the point where out-of-plane buckling of that single element is the predominant buckled behavior of the frame.

With the column webs oriented perpendicular to the plane of the frame small out-of-plane buckling of the columns is again seen for lateral load ratios of 0.0 and 0.10.

This behavior is consistent with the behavior observed for the frame with a height-to-width ratio of 2.5 and column webs oriented perpendicular to the plane of the frame. As the height-to-width ratio increases, the laterally unsupported length of the columns increases and the column buckling strength decreases. This decrease in column buckling strength results in column buckling controlling the behavior of the frame with a height-to-width ratio of 3.0 as it did for the frame with a height-to-width ratio of 2.5.

For lateral load ratios of 0.20 and 0.40 out-of-plane buckling of the bottom panel compression brace is the dominant behavior of the frame. In-plane buckling of the bottom panel compression brace is the dominant behavior of the frame for a lateral load ratio of 1.0. As seen in the frame with a height-to-width ratio of 2.5, the increase in the height-to-width-ratio increases the length of the brace, but does not change the length of the top beam. As a result, the buckling capacity of the bracing element decreases and it becomes the element which controls the buckled behavior of the frame. The lateral load ratio of 1.0 applied to the frame with a height-to-width ratio of 3.0 again results in both the frame with column webs oriented parallel and perpendicular to the plane of the frame to have the bottom panel compression brace buckling dominate behavior.

Figure 27 shows a comparison of the elastic stability response of both the frame with column webs oriented parallel and the frame with column webs oriented perpendicular to the plane of the frame for a frame with a height-to-width ratio of 3.5. Out-of-plane buckling about the columns' weak axes is the predominant behavior exhibited by the frames with column webs oriented parallel to the plane of the frame for lateral load ratios from 0.0 to 0.40. For frames with column webs oriented perpendicular to the plane of the frame, small out-of-plane buckling of the columns is exhibited at a

lateral load ratio of 0.0 and out-of-plane buckling of the bottom panel compression bracing element is the predominant buckled behavior at lateral load ratios of 0.10, 0.20, 0.40, and 1.0. As seen in Figure 27, the elastic critical load ratio is larger when column webs are oriented perpendicular to the plane of the frame at lateral load ratios of 0.0, 0.10, and 0.20, but is nearly identical to the elastic critical load for the frames with column webs oriented parallel to the plane of the frame at lateral load ratios of 0.40, and 1.0.

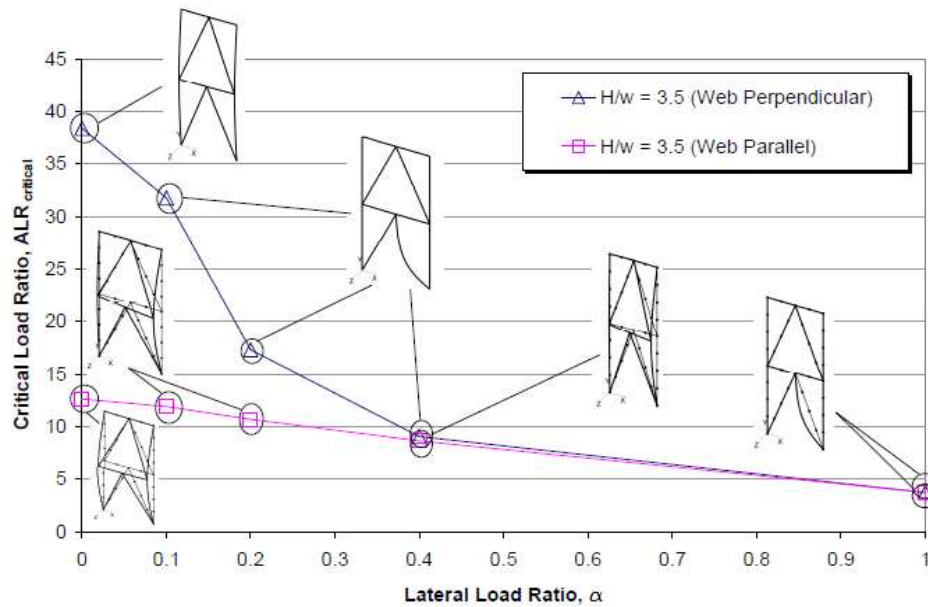


**Figure 27. Comparison of elastic critical loads for strong-axis and weak-axis column orientations for a frame with a height-to-width ratio of 3.5**

The deflected shapes at the elastic critical load ratio for the frames with column webs oriented parallel to the plane of the frame are identical to the deflected shapes for the frames with a height-to-width ratio of 3.0 and the same column orientation. With the column webs oriented perpendicular to the plane of the frame, small out-of-plane buckling of the columns is again seen at a lateral load ratio of 0.0. At lateral load ratios

of 0.1, 0.2, 0.4, and 1.0 out-of-plane buckling of the bottom panel bracing element is the dominant buckled behavior of the frame. As opposed to the frames with height-to-width ratios of 2.5 and 3.0, buckling of the bottom panel bracing element occurs at a lateral load ratio of 0.10 due to the increase in the brace length that accompanies the increase in height-to-width ratio. As a result, the buckling capacity of the bracing element decreases and it becomes the element which controls the buckled behavior of the frame. The lateral load ratio of 1.0 applied to the frame with a height-to-width ratio of 3.5 again results in both the frame with column webs oriented parallel and perpendicular to the plane of the frame to have the same first mode buckled geometry.

### **3.5. Inelastic Critical Load Analysis**

To include the effect of material nonlinear behavior, inelastic critical load analyses were also conducted on the suite of frames previously analyzed. Recognizing that material stiffness is not completely elastic above some proportional limit, MASTAN2 applies a modified tangent modulus to the material in the model to obtain agreement with complex plastic zone analyses when initial geometric imperfections are present. Equation 9 gives the modified tangent modulus equation.

$$E_{tm} = \tau E \text{ with } \tau = \min \left( \frac{1.0}{(1+2p)[1-(p+\alpha m_y)]} \right)$$

**Equation 9**

where,

$E_{tm}$  = modified tangent modulus

$E$  = full elastic modulus of elasticity

$p = \frac{P}{P_y}$  = ratio of axial force to squash load

$m_y = \frac{M_y}{M_{py}}$  = ratio of internal minor axis bending moment

to minor axis plastic moment capacity

The factor  $\alpha$  is equal to 0.65 based on the work of Ziemian et al (2002) calibrating plastic hinge analysis results to those of the plastic zone for a moment-thrust-curvature response of a W8x31 with a nominal yield stress of 36 ksi subjected to minor-axis bending and an axial force of  $P/P_y = 0.4$ . In the inelastic critical load analyses executed on the suite of frames considered, the steel was assumed to have a yield stress equal to 50 ksi and a full elastic modulus of elasticity equal to 29,000 ksi.

In MASTAN2, an eigenvalue approach is used to solve the eigenvalue problem in Equation 10 to determine the frame inelastic critical loads.

$$[[K_{I,ff}(\beta P)] + \lambda[K_{G,ff}(\beta P)]]\{\Delta_f\} = \{0\}$$

**Equation 10**

where,

$K_{I,ff}$  = inelastic stiffness matrix for the  
structure's unsupported degrees of freedom

$K_{G,ff}$  = geometric stiffness matrix for the  
structure's unsupported degrees of freedom

$\beta$  = applied load ratio

$P$  = applied load vector

$\{\Delta_f\}$  = eigenvector corresponding to eigenvalue  $\lambda$

The minimum value of  $\beta$  that satisfies Equation 10 with an eigenvalue of  $\lambda = 1$  is the inelastic critical load ratio and when multiplied by the applied load vector  $P$  gives the frame inelastic critical load. The algorithm used to solve the eigenvalue problem in Equation 10 uses an iterative nonlinear analysis to determine the force distribution for calculating  $[K_{I,ff}]$  and  $[K_{G,ff}]$  and an interpolation scheme for predicting the inelastic critical load ratio” (Ziemian 1999).

Table 10 shows the elastic and inelastic critical load ratio magnitudes at varying height-to-width ratios and lateral load ratios for frames with column webs oriented perpendicular to the plane of the frame. The dashes in Table 10 represent frame height-to-width ratio and lateral load ratio combinations where the inelastic critical load ratio is equal to the elastic critical load ratio.

**Table 10. Elastic critical load ratio vs. inelastic critical load ratio comparison (Column webs oriented perpendicular to plane of frame)**

$\alpha$	Elastic Critical Load Ratio / Inelastic Critical Load Ratio			
	H/w = 2.0	H/w = 2.5	H/w = 3.0	H/w = 3.5
0	67.1 / 66.8	67.3 / 65.7	52.1 / 52.0	38.4 / -
0.1	60.9 / 60.7	59.8 / 59.5	47.1 / 46.9	31.8 / -
0.2	54.4 / 54.3	42.4 / 42.3	26.3 / -	17.3 / -
0.4	28.0 / -	22.3 / -	13.8 / -	9.0 / -
1	11.2 / -	9.2 / -	5.7 / -	3.7 / -

The inelastic critical load ratio magnitudes are very close to the elastic critical load ratio magnitudes at each respective height-to-width ratio/lateral load ratio combination. Inelastic critical load magnitudes range from 97.57% of the elastic critical load ratio magnitude at a height-to-width ratio of 2.5 and lateral load ratio of 0 to 99.85% of the elastic critical load ratio magnitude at a height-to-width ratio of 3.0 and lateral load

ratio of 0. It can be concluded that for the section sizes used in the frames analyzed the impact of inelastic behavior is very small.

At lateral load ratios of 0.4 and 1.0, the inelastic critical load ratio is equal to the elastic critical load ratio. As a result, elastic buckling controls frame stability behavior at all height-to-width ratios when the lateral load ratio is 0.4 and 1.0. Elastic buckling also controls frame stability behavior at a height-to-width ratio of 3.5 for all lateral load ratios and at a lateral load ratio of 0.2 and height-to-width ratio of 3.0. When column webs are oriented parallel to the plane of the frame resulting in weak axis bending of the column out of the plane of the frame being unsupported along the entire column length, elastic buckling controls frame stability behavior at all combinations of height-to-width ratio and lateral load ratio.

### **3.6. Initial Geometric Imperfections**

Initial geometric imperfections were added to the frame to assess their effect on the elastic stability response of the frame. The first imperfections considered were an in-plane out-of-plumb of the columns equal to  $H/500$  where  $H$  is the total height of the frame. This initial out-of-plumb magnitude represents the maximum tolerance on column out-of-plumb specified in the *AISC Code of Standard Practice* (AISC 2010b). A frame with the given imperfections was created and then an elastic critical load analysis was conducted on the initially deformed frame. The deformed frame configuration was created in the MASTAN2 model by moving the nodes at the top of each column and the nodes along the top beam a distance of  $H/500$  in the same direction in the plane of the frame and keeping the nodes at the base of each column in their original position. Nodes

at elevations between the base and top of the frame were moved by a distance equal to  $y/500$  where  $y$  is the elevation of the node measured from the base of the frame. Figure 28 represents the deformed frame geometry used in the elastic critical load analyses.

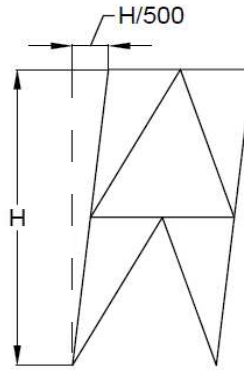


**Figure 28. Deformed geometry used in MASTAN2 model based on AISC Code of Standard Practice maximum tolerance on column plumb**

The presence of initial geometric imperfections had a negligible effect on the elastic critical load ratio of the frame as expected. Table 11 shows the percent change between the elastic critical load ratios for the frames with initial geometric imperfections versus the elastic critical load ratios for the frames with initially perfect geometry with column webs oriented perpendicular to the plane of the frame. The percent change in elastic critical load ranges from -0.03% to -3.10% with all but 4 scenarios exhibiting a percent decrease less than 1%. At all lateral load ratios and height-to-width ratios, the elastic critical load for the frames with initial imperfections is lower than the elastic critical load for the frames with initially perfect geometry. As lateral load ratio increases, the percent decrease in elastic critical load ratio increases to a maximum at a lateral load ratio of 0.2 and then decreases as lateral load ratio increases to 1.0. This is true for all height-to-width ratios except 3.5 where the percent decrease in elastic critical load ratio reaches a maximum value of -3.10% at a lateral load ratio of 0.1.

**Table 11. Percent change in elastic critical load between frames with column out-of-plumb vs. initially perfect geometry (Column webs oriented perpendicular to plane of frame)**

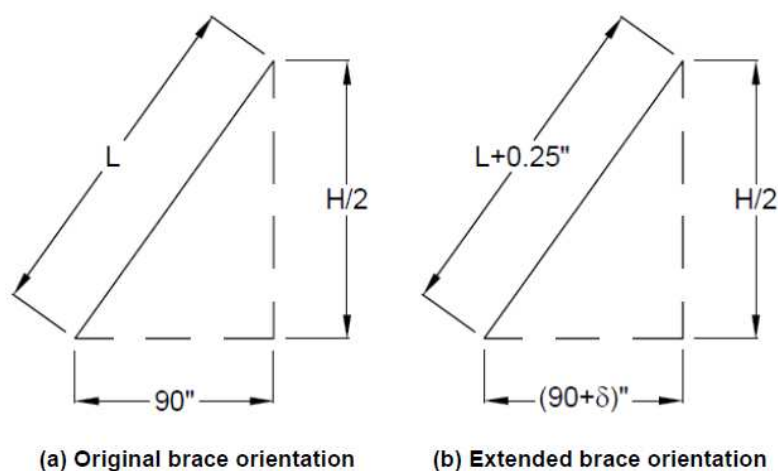
$\alpha$	H/w = 2.0	H/w = 2.5	H/w = 3.0	H/w = 3.5
0.0	-0.29%	-0.37%	-0.03%	-0.03%
0.1	-0.37%	-0.45%	-0.95%	-3.10%
0.2	-0.96%	-1.60%	-1.63%	-1.65%
0.4	-0.47%	-0.76%	-0.79%	-0.81%
1.0	-0.19%	-0.21%	-0.23%	-0.25%

Table 12 shows the percent change between the elastic critical load ratios for the frames with initial geometric imperfections versus the elastic critical load ratios for the frames with initially perfect geometry with column webs oriented parallel to the plane of the frame. The percent change in elastic critical load ratio ranges from -0.01% to -0.45%. At all lateral load ratios and height-to-width ratios, the elastic critical load for the frames with initial imperfections is lower than the elastic critical load for the frames with initially perfect geometry. As lateral load ratio increases, the percent decrease in elastic critical load increases to a maximum at a lateral load ratio of 0.2 and then decreases as lateral load ratio increases to 1.0. This is true for all height-to-width ratios except 2.0 where the percent decrease in elastic critical load ratio reaches a maximum value of -0.37% at a lateral load ratio of 0.4. Also, as height-to-width ratio increases, the percent decrease in elastic critical load ratio remains constant or increases at all lateral load ratios.

**Table 12. Percent change in elastic critical load between frames with column out-of-plumb vs. initially perfect geometry (Column webs oriented parallel to plane of frame)**

$\alpha$	H/w = 2.0	H/w = 2.5	H/w = 3.0	H/w = 3.5
0.0	-0.01%	-0.01%	-0.01%	-0.01%
0.1	-0.33%	-0.36%	-0.38%	-0.40%
0.2	-0.35%	-0.38%	-0.42%	-0.45%
0.4	-0.37%	-0.35%	-0.38%	-0.40%
1.0	-0.18%	-0.21%	-0.24%	-0.26%

In-plane initial geometric imperfections caused by bolt hole deformation at brace connections were also considered. Extension of the brace elements due to a  $\frac{1}{4}$ " bolt hole deformation was considered. A  $\frac{1}{4}$ " deformation magnitude is selected as it is the maximum deformation anticipated to occur when bolt hole bearing strength limits in Chapter J3.10 of the AISC Specification (AISC 2010a) are reached. The panel height was assumed to remain unchanged, so the horizontal displacement of the beams at the top and tier level was calculated. Figure 29 shows a comparison of the original and extended brace configurations.



**Figure 29. Brace in (a) original configuration before extension and (b) extended configuration after bolt hole deformation**

For height-to-width ratios of 2.0 and 2.5, the additive horizontal displacements caused by bolt hole deformation at the brace end connections to the tier level and top level beams cause a horizontal displacement at the top of the frame equal to 1.12 inches and 1.08 inches respectively. Both of these displacements exceed the displacement considered by a horizontal displacement equal to  $H/500$ . Figure 30 shows the horizontal

displacement resulting from brace extension at each level and its effect on overall frame geometry.

The presence of initial geometric imperfections caused by bolt hole deformation also had a negligible effect on the elastic critical load ratio of the frame. Table 13 shows the percent change between the elastic critical load ratios for the frames with initial geometric imperfections versus the elastic critical load ratios for the frames with initially perfect geometry with column webs oriented perpendicular to the plane of the frame. The percent change in elastic critical load ratio ranges from -0.25% to -1.90%.

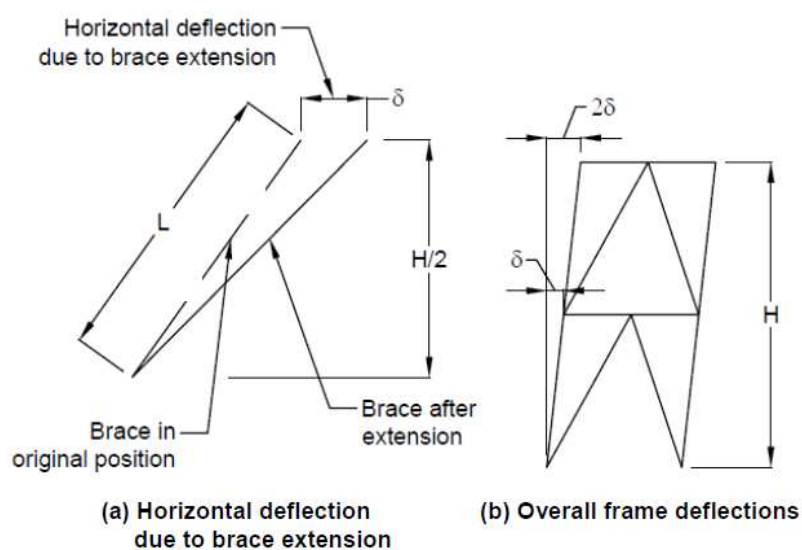


Figure 30. (a) Horizontal deflection at each level due to brace extension and (b) effect of brace extension on overall frame geometry

Table 13. Percent change in elastic critical load between frames with geometric imperfections due to bolt hole deformation vs. initially perfect geometry (Column webs oriented perpendicular to plane of frame)

$\alpha$	$H/w = 2.0$	$H/w = 2.5$
0.0	-0.51%	-0.47%
0.1	-0.57%	-0.54%
0.2	-1.34%	-1.90%
0.4	-0.73%	-0.90%
1.0	-0.29%	-0.25%

Table 14 shows the percent change between the elastic critical load ratios for the frames with initial geometric imperfections versus the elastic critical load ratios for the frames with initially perfect geometry with column webs oriented parallel to the plane of the frame. The percent change in elastic critical load ratio ranges from -0.02% to -0.54%.

**Table 14. Percent change in elastic critical load between frames with geometric imperfections due to bolt hole deformation vs. initially perfect geometry (Column webs oriented parallel to plane of frame)**

$\alpha$	H/w = 2.0	H/w = 2.5
0.0	-0.04%	-0.02%
0.1	-0.51%	-0.43%
0.2	-0.54%	-0.46%
0.4	-0.57%	-0.42%
1.0	-0.28%	-0.25%

As seen in the frames with geometric imperfections due to column out-of-plumb, the percent decrease in elastic critical load ratio for frames with geometric imperfections due to bolt hole deformation increases to a maximum at a lateral load ratio of 0.2 and then decreases as lateral load ratio increases to 1.0. Also, a comparison of the percent decreases in elastic critical load in Table 11 and Table 13 indicates that geometric imperfections due to bolt hole deformation has a greater influence on elastic critical load for frames with column webs oriented perpendicular to the plane of the frame. This same conclusion can be made for frames with column webs oriented parallel to the plane of the frame by comparing the percent decreases in elastic critical load in Table 12 and Table 14.

Elastic critical load analyses were also conducted on frames with initial out-of-plane geometric imperfections. An out-of-plane column out-of-plumb equal to H/500 where H is the total height of the frame was applied to each column in the frame. This initial out-of-plumb magnitude represents the maximum tolerance on column out-of-

plumb specified in the *AISC Code of Standard Practice* (AISC 2010b). The deformed frame configuration was created in the MASTAN2 model by moving the nodes at the top of each column a distance of  $H/500$  in opposite directions out of the plane of the frame and keeping the nodes at the base of each column in their original position. Columns were deformed in opposite directions to simulate deformations that will occur due to racking of the roof diaphragm. Column nodes at elevations between the base and top of the frame were moved by a distance equal to  $y/500$  out of the plane of the frame where  $y$  is the elevation of the node measured from the base of the frame. After the imperfections were applied, the top of each deformed column still remains braced out of the plane of the frame. Figure 31 shows the linearly sloped column geometry used in the MASTAN2 model.

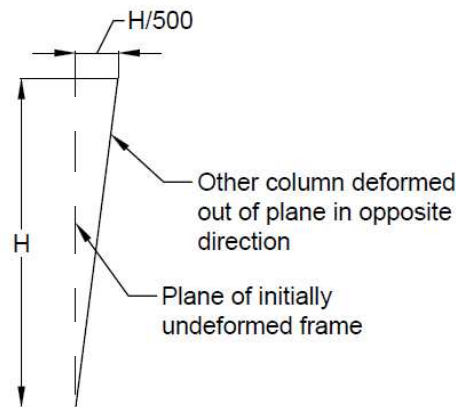


**Figure 31. Column geometry for frame model with out-of-plane geometric imperfections**

Nodes for both the top and tier level beams were moved specified distances out of the plane of the frame to form an element that spans between the columns in a linear fashion with the midpoint of each beam remaining in the plane of the original undeformed frame. Figure 32 shows the typical beam orientation.

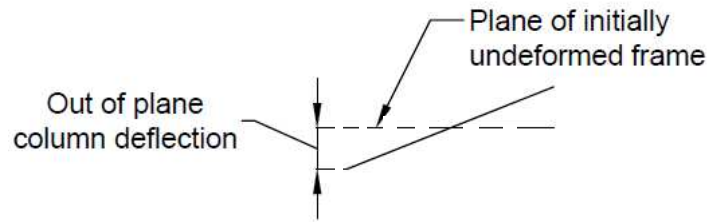


**Figure 32. Typical beam geometry in frame model with out-of-plane geometric imperfections**

Nodes for the top panel brace elements were moved specified distances out of the plane of the frame to form elements that span between the tier level beam column intersection and the midpoint of the top beam in a linear fashion. Nodes for the bottom panel brace elements remain in the plane of the original undeformed frame since the bottom panel braces span between the base of each column and the midpoint of the tier level beam which are all located in the plane of the original undeformed frame. Figure 33 shows the twisting nature of the initially imperfect frame geometry as viewed from the side of the frame.

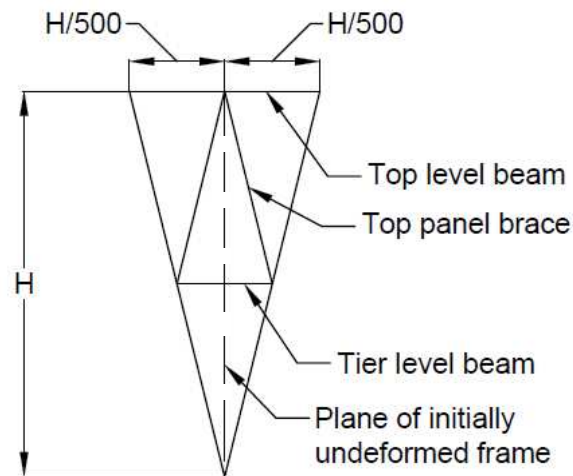


**Figure 33. Side view of frame with initial out-of-plane geometric imperfections**

Table 15 shows the percent change between the elastic critical load ratio for the frames with out-of-plane geometric imperfections and initially perfect geometry with column webs oriented perpendicular to the plane of the frame. Table 16 shows the same data for frames with column webs oriented parallel to the plane of the frame. Initial out-of-plane geometric imperfections have very little effect on elastic critical load ratio as all of the percent changes in elastic critical load are smaller than the corresponding percent changes for in plane geometric imperfections by one to two orders of magnitude.

**Table 15. Percent change in elastic critical load between frames with out-of-plane geometric imperfections vs. initially perfect geometry (Column webs oriented perpendicular to plane of frame)**

$\alpha$	H/w = 2.0	H/w = 2.5	H/w = 3.0	H/w = 3.5
0.0	-0.001%	-0.001%	-0.006%	-0.008%
0.1	-0.001%	-0.001%	-0.001%	-0.001%
0.2	-0.006%	-0.001%	-0.001%	-0.001%
0.4	-0.005%	-0.001%	-0.001%	-0.001%
1.0	-0.004%	-0.001%	-0.002%	-0.003%

**Table 16. Percent change in elastic critical load between frames with out-of-plane geometric imperfections vs. initially perfect geometry (Column webs oriented parallel to plane of frame)**

$\alpha$	H/w = 2.0	H/w = 2.5	H/w = 3.0	H/w = 3.5
0.0	0.002%	0.003%	0.005%	0.006%
0.1	0.006%	0.006%	0.009%	0.012%
0.2	0.008%	0.008%	0.012%	0.017%
0.4	0.005%	0.010%	0.015%	0.021%
1.0	-0.001%	-0.008%	-0.011%	-0.013%

### 3.7. Conclusions

In the critical load analysis section, elastic and inelastic critical load analyses were performed on a suite of two-panel tiered concentrically braced frames. To determine the effect of frame aspect ratio on frame critical load capacity, frames with height-to-width ratios of 2.0, 2.5, 3.0, and 3.5 were analyzed. To evaluate the effect of

lateral load on frame critical load capacity, each frame was analyzed with an applied lateral load to gravity load ratio of 0.0, 0.1, 0.2, 0.4, and 1.0. The effect of initial geometric imperfections on the critical load capacity of each frame was evaluated by performing elastic critical load analyses after both in-plane and out-of-plane initial geometric were applied to the frame. In addition all analyses were performed on frames with column webs oriented both parallel and perpendicular to the plane of the frame.

The results of the elastic and inelastic critical analyses yield the following conclusions:

- As applied lateral load ratio increases, the elastic critical load ratio decreases.
- As applied lateral load ratio increases, stability behavior of the frame tends to be driven by buckling of brace elements as opposed to global buckling of the entire frame system.
- As height-to-width ratio increases, the frame elastic critical load ratio decreases.
- When the columns' webs are oriented perpendicular to the plane of the frame, stability behavior tends to be driven by buckling of brace elements. When the columns' webs are oriented parallel to the plane of the frame, stability behavior tends to be driven by out-of-plane buckling of the columns.
- Inelastic critical load ratios are slightly smaller than elastic critical load ratios for all frames where elastic buckling does not control frame behavior. This is true only for the members used in the frame analyzed. As members with strengths closer to the required capacity are used, the impact of inelastic behavior may be greater.

- Initial in-plane and out-of-plane geometric imperfections have a negligible effect on frame elastic critical loads.

## **4. Inelastic Analysis of Systems**

In this chapter, the inelastic response of the suite of frames analyzed previously is evaluated. The results of these analyses are intended to determine the effect of aspect ratio and applied lateral load on the limit state response of the frame when material nonlinearity is considered. Section 4.1 – Methodology describes the distributed plasticity analysis scheme and the concentrated plasticity analysis scheme used to evaluate the inelastic response of the frames. Section 4.2 – Inelastic Analysis Results presents applied load ratio versus top of frame horizontal displacement response curves, deflected shape diagrams, and force point traces for each frame configuration analyzed. Section 4.3 – Conclusions summarizes the major findings and results of the inelastic analyses.

### **4.1. Methodology**

Inelastic analyses were performed using MASTAN2 to evaluate the inelastic response of the two-panel concentrically braced frame. The inelastic analysis conducted utilized a distributed plasticity analysis scheme within MASTAN2 with the ability to perform distributed plasticity analysis and post-limit state modeling (FE++ 2012; Alemdar 2001).

The FE++ analysis scheme uses a distributed plasticity model which explicitly models the gradual spread of yielding across the section and along the element (Alemdar 2001). Fiber-type discretization is applied to cross-sections in the FE++ analytical model which results in cross-sections being divided into many smaller sections which when put together constitute the entire cross-section (Alemdar 2001). Figure 34 shows a typical discretized beam element bent about its weak and strong axes. As seen in Figure 34, a

single fiber is also placed at each fillet location. To aid in computational efficiency during analysis, member cross-sections are divided into fibers only when yielding is observed at a point in the cross-section.

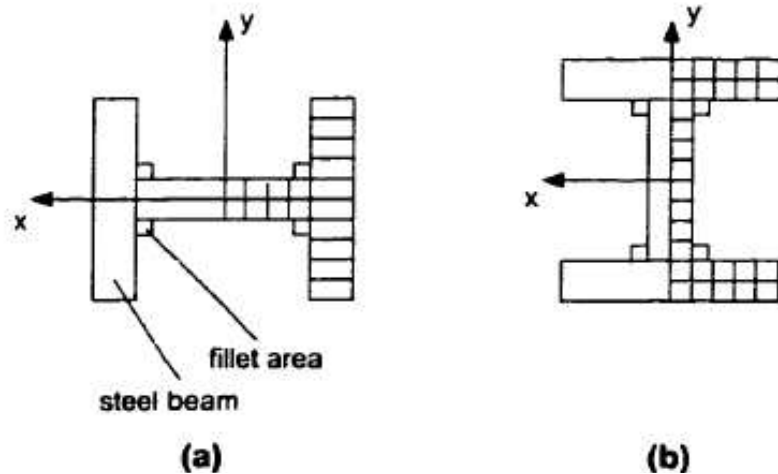


**Figure 34. Member discretization models used in the FE++ distributed plasticity analysis for wide flange sections bent about their (a) minor axis and (b) major axis (Alemdar 2001)**

To account for residual stresses, the FE++ analysis scheme uses the classic Ketter residual stress pattern for wide flange sections. Based on the fiber location in the cross-section and the residual stress pattern, residual stresses are calculated for each fiber in the cross-section (Alemdar 2001). Figure 35 shows the Ketter residual stress pattern.

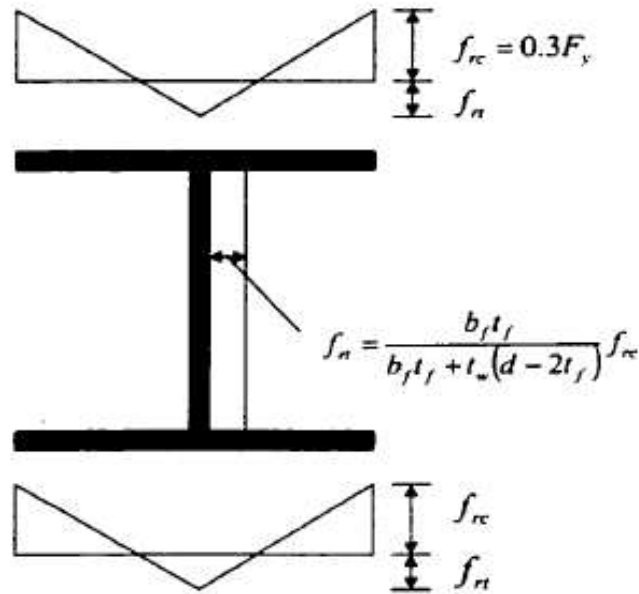


Figure 35. Ketter residual stress pattern (Alemdar 2001)

Throughout the presentation of the inelastic analysis results, force point traces are presented with the MASTAN2 concentrated plastic hinge yield surface model illustrated in Figure 36. This stress resultant yield surface accounts for axial force and both major- and minor-axis bending given by Equation 11.

$$\Phi = p^2 + m_z^2 + m_y^4 + 3.5p^2m_z^2 + 3p^6m_y^2 + 4.5m_z^4m_y^2 = 1$$

Equation 11

where,

$$p = \frac{P}{P_y} = \text{ratio of axial force to squash load}$$

$$m_z = \frac{M_z}{M_{pz}} = \text{ratio of internal major axis bending moment to major axis plastic moment capacity}$$

$$m_y = \frac{M_y}{M_{py}} = \text{ratio of internal minor axis bending moment to minor axis plastic moment capacity}$$

MASTAN2 uses this yield surface to develop nonlinear material behavior when calculating limit state responses for two- and three-dimensional steel frames under static loads (Ziemian and McGuire 2002). When the stress resulting from interaction of axial force and major- and minor-axis bending reaches the yield surface, a zero-length plastic hinge is inserted at the end of the element. As opposed to the distributed plasticity approach of FE++, the insertion of the zero-length plastic hinge results in an elastic-plastic model that accounts for complete yielding of the cross-section at the end of the element.

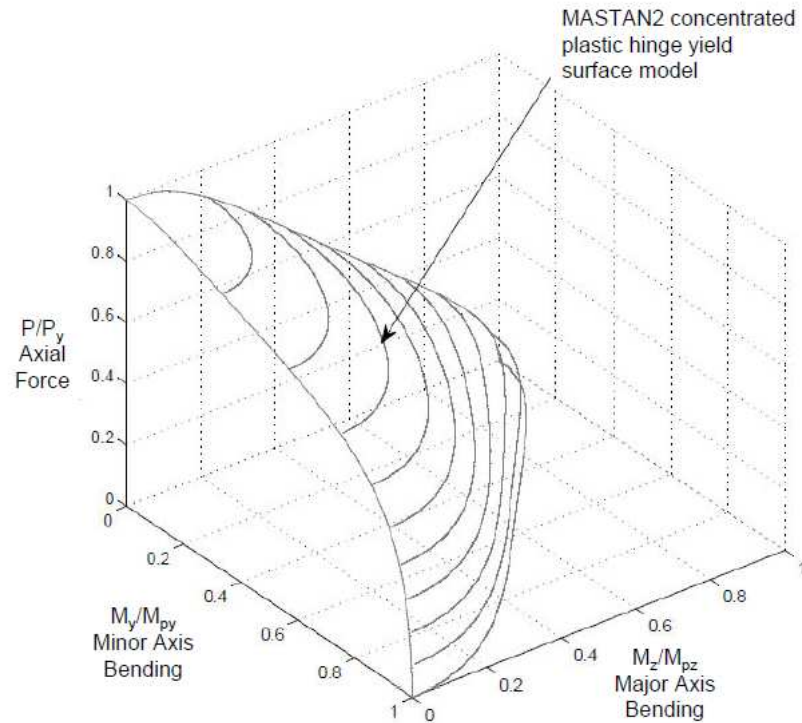


**Figure 36. MASTAN2 concentrated plastic hinge yield surface model**

To assess the inelastic response of the two-panel concentrically braced frame, a series of nonlinear inelastic analyses were conducted with varying frame geometry and lateral loading levels. A reference gravity load of 10 kips is applied at the top of each

column and a lateral load of 0.25, 0.5, and 1.0 times the intensity of the reference gravity load is applied at the top of the left column to assess the effect of lateral load on the inelastic response of the frame. Figure 37 illustrates the loading scenarios analyzed with the loads denoted by  $P$  symbolizing the 10 kip concentrated gravity loads and the  $\alpha P$  load symbolizing the varying concentrated lateral load applied to the frame.

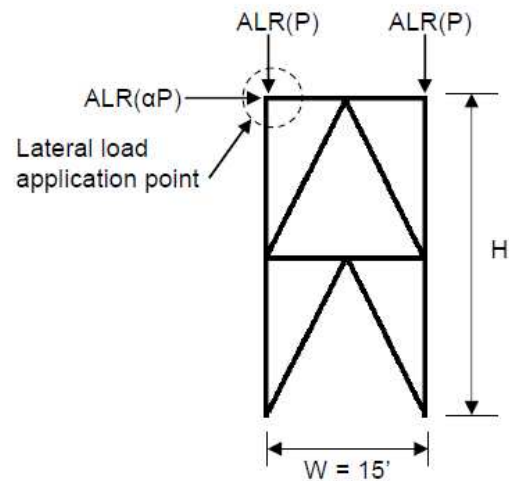


**Figure 37. Loading scenario for inelastic analyses**

These analyses were performed on frames with height-to-width ratios of 2.0, 2.5, 3.0, and 3.5 to assess the effect of frame slenderness on the inelastic response of the frame. Frame width was held constant at a distance of 15 feet while the total height of the frame was adjusted to 30 feet, 37.5 feet, 45 feet, and 52.5 feet to achieve the height-to-width ratios of 2.0, 2.5, 3.0, and 3.5 respectively. For all analyses, column webs were oriented perpendicular to the plane of the frame

In the MASTAN2 analytical model, each structural member is divided into multiple discrete elements to better capture behavior along the length of the member. Each brace member and beam member is discretized into 8 equal length elements and

each column member is discretized into 16 equal length elements from the base of the frame to its top. Figure 38 illustrates the member discretization scheme used in the MASTAN2 analytical model for the nonlinear inelastic analyses.

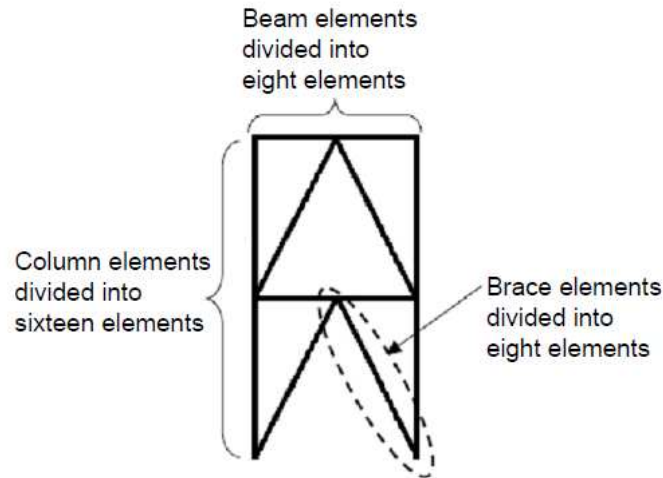


**Figure 38. Member discretization used in MASTAN2 analytical model**

Due to limitations in the distributed plasticity analysis scheme, all member connections are considered to have infinite flexural stiffness about the members' local minor and major axes and zero warping restraint. Also, the distributed plasticity analysis scheme is only programmed for wide-flange shapes, so all brace elements were taken as W8x28 members with webs oriented parallel to the plane of the frame. A W8x28 member was chosen because it had a minor axis moment of inertia of  $25.9 \text{ in}^4$  which is very similar to the minor axis moment of inertia of the HSS  $5\text{-}1/2 \times 5\text{-}1/2 \times 5/16$  which is  $21.7 \text{ in}^4$ . Globally, translation is restrained at the top of each column out of the plane of the frame with translation in the global x-, y-, and z-directions restrained at the bottom of each column. At the bottom of each column, rotation about the columns' longitudinal axis is restrained. Global support conditions are illustrated in Figure 39.

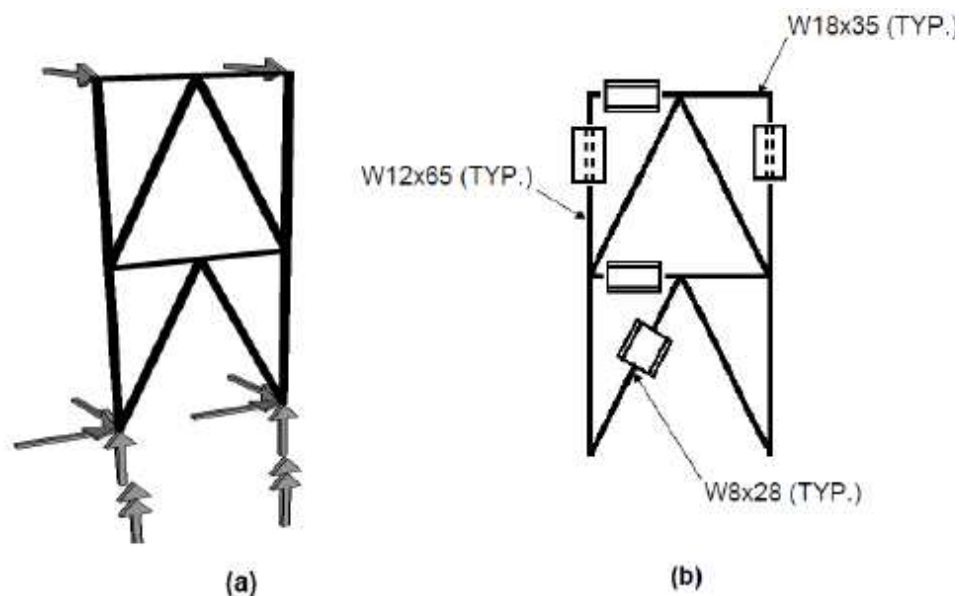


**Figure 39. (a) Global support conditions and (b) member sections in MASTAN2 nonlinear inelastic analysis analytical model**

Initial sinusoidal out-of-straightness with maximum amplitude of 1/1000 of the frame height was applied to both column members. An initial sinusoidal out-of-straightness with maximum amplitude of 1/1000 of the unsupported member length was applied to each bracing member. These are consistent with allowable out-of-straightness allowed in steel buildings (AISC 2011b). These out-of-straightness quantities were all applied in the same direction out of the plane of the frame causing members to deform in a half sine wave between their ends. All steel members in the model were given a yield strength of 50 ksi and a modulus of elasticity of 29,000 ksi.

#### **4.2. Inelastic Analysis Results**

Figure 40 shows applied load ratio versus top of frame horizontal displacement curves for frames with a height-to-width ratio of 3.5 and lateral load ratios of 0.25, 0.50,

and 1.00. The distributed plasticity analysis scheme of FE++ was used to analyze the frame with a height-to-width ratio of 3.5. Table 17 provides a summary of the distributed plasticity analysis peak applied load ratios and elastic critical load ratios for frames with height-to-width ratios of 3.5 and lateral load ratios of 0.25, 0.5, and 1.0. Figure 41 shows the typical deflected shape of the frame with a height-to-width ratio of 3.5 and lateral load ratios of 0.25, 0.5, and 1.0 at location L1 in Figure 40. Figure 42, Figure 43, and Figure 44 show both two-dimensional and three-dimensional force point traces for the right column and bottom panel compression brace of the frame with a height-to-width ratio of 3.5 at a lateral load ratio of 1.0, 0.5, and 0.25 respectively. These force point traces show the progression of internal major axis bending moment, minor axis bending moment, and axial force from the beginning of the analysis to the peak applied load ratio. Figure 45 shows both two-dimensional and three-dimensional force point traces for the right column and bottom panel compression brace of the frame with a height-to-width ratio of 3.5 and a lateral load ratio of 0.5. This force point trace shows the progression of internal major axis bending moment, minor axis bending moment, and axial force from the beginning of the analysis to a top of frame horizontal displacement of 8.2 inches.

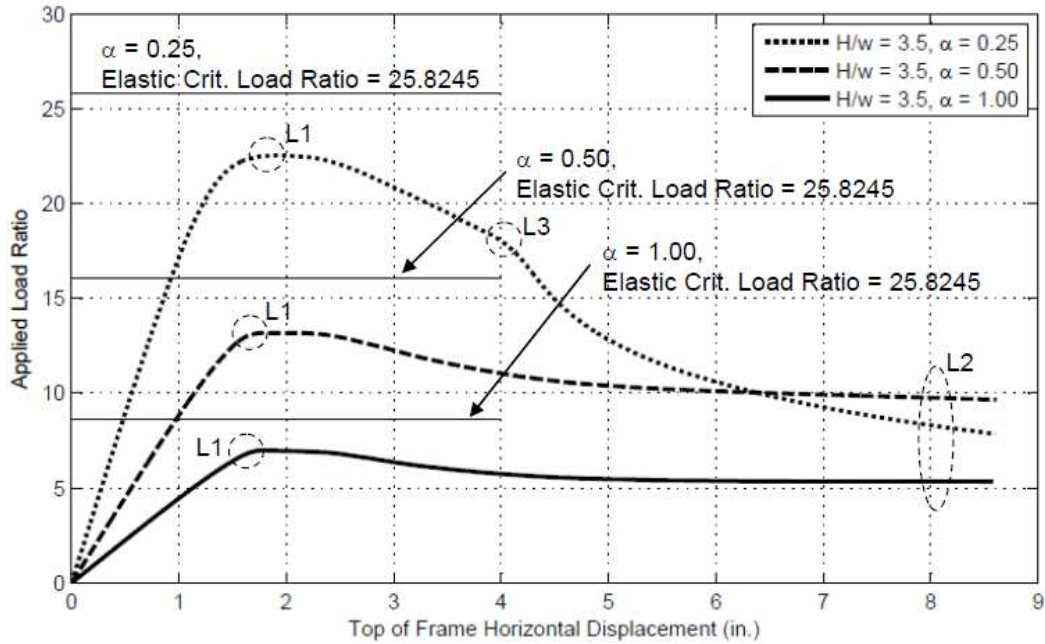


Figure 40. Applied load ratio versus top of frame horizontal displacement curves for frames with height-to-width ratios of  $H/W = 3.5$  and varying lateral load ratios

Table 17. Distributed plasticity analysis peak applied load ratio and elastic critical load ratio

Lateral Load Ratio	Top of Frame Horizontal Displacement at Peak Applied Load Ratio (in.)	Peak Applied Load Ratio	Elastic Critical Load Ratio
0.25	1.9752	22.5339	25.8245
0.50	1.7731	13.1765	16.0699
1.00	1.8219	6.9943	8.5914

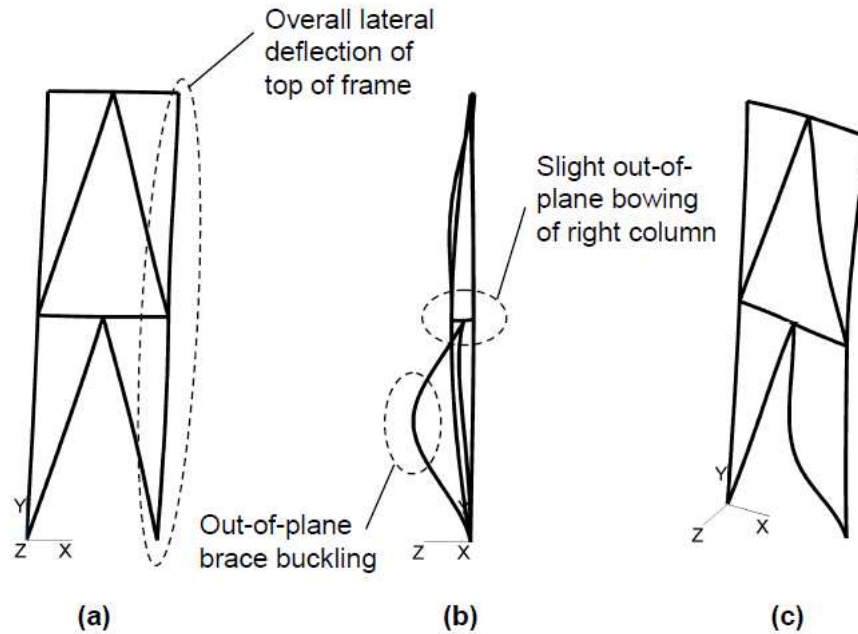


Figure 41. Typical displaced shape of frame with  $H/W = 3.5$  at the peak applied load ratio (Level L1) with lateral load ratios of 1.0, 0.5, and 0.25: (a) Front view, (b) side view, and (c) isometric view of deflected frame geometry

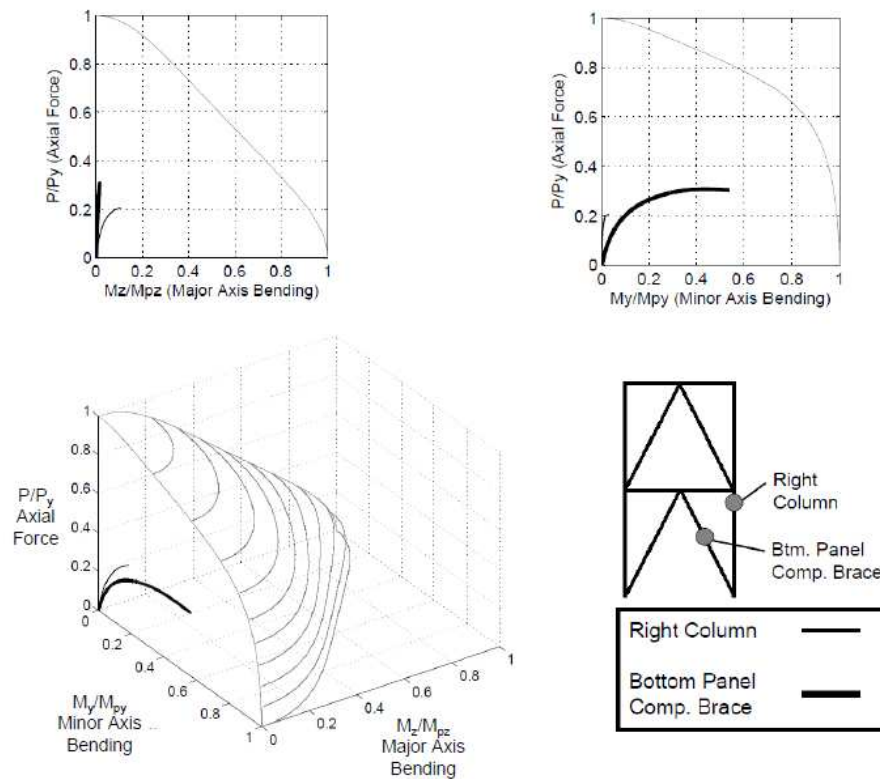
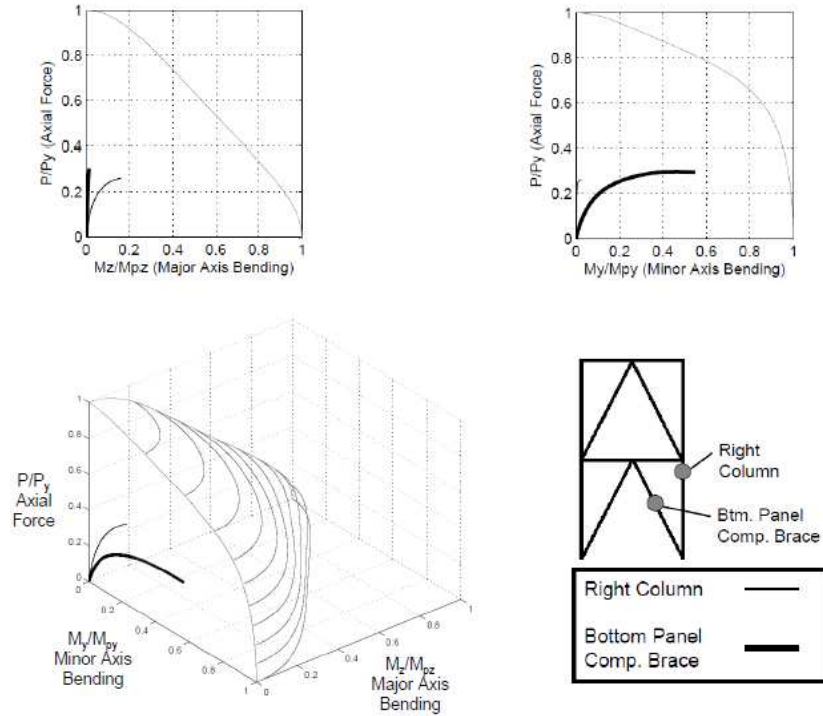
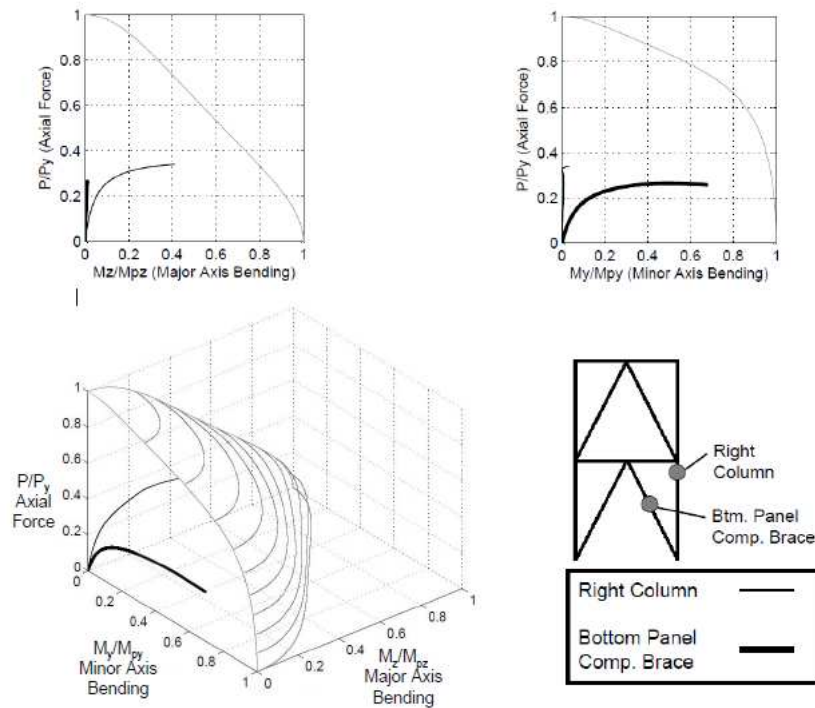


Figure 42. Axial, major axis bending, and minor axis bending force point traces for the right column and bottom panel compression brace at the peak applied load ratio for a frame with a height-to-width ratio of 3.5 and a lateral load ratio of 1.0



**Figure 43. Axial, major axis bending, and minor axis bending force point traces for the right column and bottom panel compression brace at the peak applied load ratio for a frame with a height-to-width ratio of 3.5 and a lateral load ratio of 0.5**



**Figure 44. Axial, major axis bending, and minor axis bending force point traces for the right column and bottom panel compression brace at the peak applied load ratio for a frame with a height-to-width ratio of 3.5 and a lateral load ratio of 0.25**

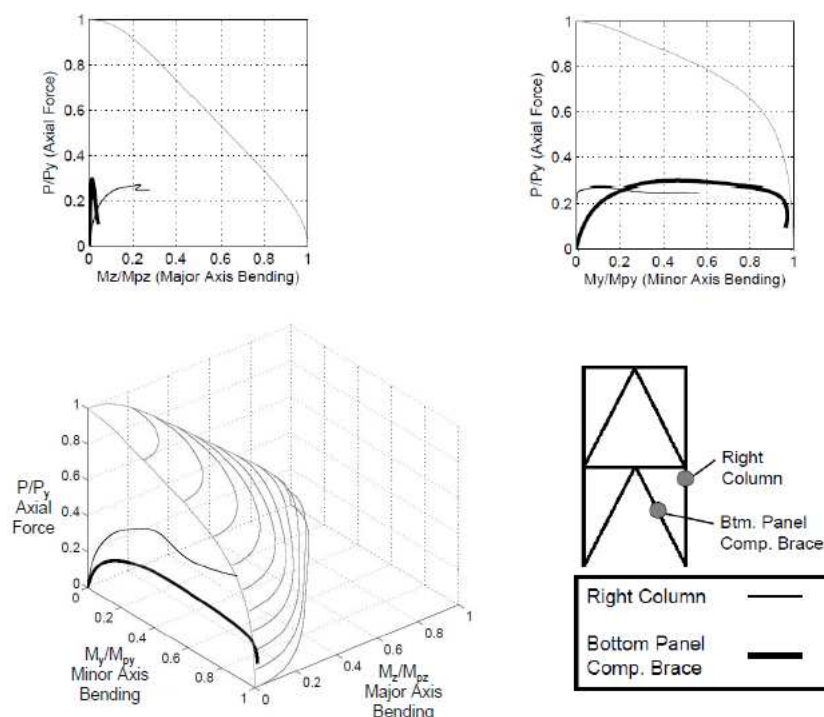


**Figure 45. Axial, major axis bending, and minor axis bending force point traces for the right column and bottom panel compression brace at a top of frame horizontal displacement of 8.2 inches for a frame with a height-to-width ratio of 3.5 and a lateral load ratio of 0.5**

The applied load ratio initially increases in a manner that is essentially linear to the limit loading. The rate of increase in the applied load ratio decreases with additional horizontal displacements until the applied load ratio reaches its peak value. The peak applied load ratio occurs at location L1 on each applied load ratio curve. The peak applied load ratio for all three lateral load ratio conditions occurs at essentially the same top of frame horizontal displacement which indicates a similar deformation demand resulting in the load limit for the frame.

When the lateral load ratio is equal to 1.0, the overall capacity of the frame is significantly lower than the capacity for the other two frames as the force in the brace is greater when the lateral load ratio increases. After the peak applied load ratio is reached, the applied load ratio plateaus and then gradually decreases as top of frame horizontal

displacement increases. A significant change in system stiffness occurs for the frame subjected to a lateral load ratio of 0.25 at location L3 in Figure 40 caused by significant deformations out of the plane of the frame. Applied load ratio decreases more for equivalent increases in top of frame horizontal displacement for displacements larger than 4.0 inches as compared to displacements less than 4.0 inches. All three lateral load ratio conditions result in applied load ratio versus horizontal displacement response that is very ductile in behavior and can be classified as displacement-controlled response.

Table 17 illustrates that for all lateral load ratios, the distributed plasticity analysis peak applied load ratio is slightly less than the elastic critical load ratio. The second order inelastic analysis peak applied load ratio is 87.3%, 82.0%, and 81.4% of the elastic critical load ratio for frames with a lateral load ratio of 0.25, 0.5, and 1.0 respectively.

Figure 41 shows the typical deflected shape of the frame with a height-to-width ratio of 3.5 and lateral load ratio of 0.25, 0.5, and 1.0 at location L1 in Figure 40. The deflected shapes for all lateral load ratio conditions are essentially the same which supports the lateral sway-type instability (displacement-controlled) failure instigated by a brace out-of-plane buckling interacting with the compression column.

When Figure 41 is viewed with the front elevation of the frame in mind, there is overall lateral deflection at the top of the frame with little noticeable in-plane column curvature. When viewed from the side, out-of-plane buckling of the bottom panel compression brace about its minor axis is evident as well as slight out-of-plane, single curvature bowing of the right column about its major axis. It should be noted that these displaced shapes are scaled.

In Figure 42, the force point traces show the progression of internal axial force, internal major axis bending moment, and internal minor axis bending moment from the beginning of the analysis to location L1 on the applied load ratio curve in Figure 40. The right column force point trace shows internal member forces at a location 6.56 feet below the tier level beam and the bottom panel compression brace force point trace shows internal member forces at midspan of the brace element.

As illustrated in Figure 42, as the applied load ratio increases to its peak, the internal axial force in the right column increases and reaches a plateau at 0.205 times the yield load of the W12x65 member. The internal axial force in the bottom panel compression brace also increases and reaches a plateau at 0.303 times the yield load of the W8x28 member. At the peak applied load ratio, the internal major axis bending moment in the right column is 0.107 times the plastic moment capacity of the W12x65 member while the internal minor axis bending moment in the right column is only 0.030 times the plastic moment capacity of the W12x65 member. The low level of minor axis bending moment in the right column is the result of lateral forces being carried to the frame's base by the bracing elements. As a result there is very little in-plane column curvature in the right column as illustrated in Figure 41. The slightly larger internal major axis bending moment in the right column can be attributed to P- $\delta$  effects resulting from the initial out-of-plane, sinusoidal geometric imperfections applied to the column. This internal major axis bending moment is seen in the deformed frame geometry of Figure 41 in the form of out-of-plane bowing of the right column.

The internal major axis bending moment in the bottom panel compression brace is very small as compared to its plastic moment capacity, whereas, the internal minor axis

bending moment is 0.541 times the plastic moment capacity of the W8x28 member. The high internal minor axis bending moment is caused by P- $\delta$  effects resulting from the initial out-of-plane, sinusoidal geometric imperfections applied to the brace. The effect of this large internal minor axis bending moment is seen in the deformed frame geometry of Figure 41 in the form of out-of-plane bowing of the bottom panel compression brace whereas there is very little in-plane bowing of the brace. While neither the right column or bottom panel compression brace force point trace comes close to reaching the MASTAN2 yield surface, the bottom panel compression brace force point trace extends farther from the origin which leads to the conclusion that the ductile instability behavior of the frame with a height-to-width ratio of 3.5 and a lateral load ratio of 1.0 is driven by out-of-plane buckling of the bottom panel compression brace.

In Figure 43, the force point traces show the progression of internal axial force, internal major axis bending moment, and internal minor axis bending moment from the beginning of the analysis to location L1 on the applied load ratio curve in Figure 40. The right column force point trace shows internal member forces at a location 6.56 feet below the tier level beam and the bottom panel compression brace force point trace shows internal member forces at midspan of the brace element.

As illustrated in Figure 43, as the applied load ratio increases to its peak, the internal axial force in the right column increases and reaches a plateau at 0.260 times the yield load of the W12x65 member. The internal axial force in the bottom panel compression brace also increases and reaches a plateau at 0.294 times the yield load of the W8x28 member. At the peak applied load ratio, the internal minor axis bending moment in the right column and the internal major axis bending moment in the bottom

panel compression brace are nearly equal to zero. The low level of minor axis bending moment in the right column is again the result of lateral forces being carried to the frame base by the bracing elements. As a result there is very little in-plane column curvature in the right column as illustrated in Figure 41.

At the peak applied load ratio, the internal major axis bending moment in the right column is 0.163 times the plastic moment capacity of the W12x65 member. The internal minor axis bending moment in the bottom panel compression brace is 0.548 times the plastic moment capacity of the W8x28 member. Both the internal major axis bending moment in the right column and the internal minor axis bending moment in the bottom panel compression brace can be attributed to  $P-\delta$  effects resulting from initial out-of-plane, sinusoidal geometric imperfections applied to the column and brace members. This internal major axis bending moment in the column is seen in the deformed frame geometry of Figure 41 in the form of out-of-plane bowing of the right column. The large internal minor axis bending moment in the bottom panel compression brace is seen in the deformed frame geometry of Figure 41 in the form of out-of-plane bowing of the bottom panel compression brace whereas there is very little in-plane bowing of the brace. While neither the right column or bottom panel compression brace force point trace comes close to reaching the MASTAN2 yield surface, the bottom panel compression brace force point trace extends farther from the origin which leads to the conclusion that the ductile instability behavior of the frame with a height-to-width ratio of 3.5 and a lateral load ratio of 0.5 is driven by out-of-plane buckling of the bottom panel compression brace.

In Figure 44, the force point traces show the progression of internal axial force, internal major axis bending moment, and internal minor axis bending moment from the

beginning of the analysis to location L1 on the applied load ratio curve in Figure 40. The right column force point trace shows internal member forces at a location 6.56 feet below the tier level beam and the bottom panel compression brace force point trace shows internal member forces at midspan of the brace element.

As illustrated in Figure 44, as the applied load ratio increases to its peak, the internal axial force in the right column increases and reaches a plateau at 0.340 times the yield load of the W12x65 member. The internal axial force in the bottom panel compression brace also increases and reaches a plateau at 0.258 times the yield load of the W8x28 member. The axial force in the right column is higher than the axial forces in the right column for frames with a height-to-width ratio of 3.5 and lateral load ratios of 1.0 and 0.5. This higher axial force is the result of a higher peak applied load ratio being reached when the lateral load ratio is equal to 0.25. At the peak applied load ratio, the internal minor axis bending moment in the right column and the internal major axis bending moment in the bottom panel compression brace are nearly equal to zero. The low level of minor axis bending moment in the right column is again the result of lateral forces being carried to the frame base by the bracing elements. As a result there is very little in-plane column curvature in the right column as illustrated in Figure 41.

At the peak applied load ratio, the internal major axis bending moment in the right column is 0.411 times the plastic moment capacity of the W12x65 member. The internal minor axis bending moment in the bottom panel compression brace is 0.681 times the plastic moment capacity of the W8x28 member. Both the internal major axis bending moment in the right column and the internal minor axis bending moment in the bottom

panel compression brace can be attributed to  $P-\delta$  effects resulting from initial out-of-plane, sinusoidal geometric imperfections applied to the column and brace members.

The internal major axis bending moment in the right column is nearly three times the level of the internal major axis bending moment in the right column of the frame with a height-to-width ratio of 3.5 and a lateral load ratio of 0.5. This larger internal major axis bending moment in the column results from the  $P-\delta$  effects of the larger axial force and slightly larger out-of-plane bowing of the right column. The large internal minor axis bending moment in the bottom panel compression brace is seen in the deformed frame geometry of Figure 41 in the form of out-of-plane bowing of the bottom panel compression brace whereas there is very little in-plane bowing of the brace. In contrast to the frames with a height-to-width ratio of 3.5 and lateral load ratios of 1.0 and 0.5, the bottom panel compression brace force point trace and right column force point trace extend approximately the same distance from the origin which leads to the conclusion that the ductile instability behavior of the frame, while still driven by local buckling at a lateral load ratio of 0.25, moves toward global system buckling as the lateral load ratio decreases.

In Figure 45, the force point traces show the progression of internal axial force, internal major axis bending moment, and internal minor axis bending moment from the beginning of the analysis to location L2 on the applied load ratio curve in Figure 40. This force point trace illustrates the post limit state strength of the frame. The right column force point trace shows internal member forces at a location 6.56 feet below the tier level beam and the bottom panel compression brace force point trace shows internal member forces at midspan of the brace element.

As illustrated in Figure 45, as deformation demand increases from location L1 to location L2, the internal axial force in the bottom panel compression brace gradually decreases as from its plateau seen in Figure 43 as internal minor axis bending moment continues to increase. When the internal minor axis bending moment reaches approximately 0.97 times the plastic moment capacity of the W8x28 member, the axial force in the bottom panel compression brace decreases suddenly. This sudden decrease occurs just inside the MASTAN2 yield surface. The increase in internal minor axis bending moment is caused by P- $\delta$  effects resulting from the continually increasing out-of-plane bowing of the bottom panel compression brace. Despite the gradual decrease in axial force in the bottom panel compression brace, internal major axis bending moment increases slightly in the bottom panel compression brace. When the brace starts to exhibit in-plane bowing, P- $\delta$  effects from the member midspan displacement and the remaining axial force in the member cause the increase in internal major axis bending moment in the bottom panel compression brace.

As deformation demand is increased from location L1 to location L2 on the applied load ratio curve in Figure 40, the internal axial force in the right column remains nearly constant as illustrated by the force point traces in Figure 45. Internal minor axis bending moment, however, increases significantly to 0.558 times the plastic moment capacity of the W12x65 member. This significant increase can be attributed to load being diverted from the bottom panel compression brace to the right column. The horizontal component of this load formerly carried by the bottom panel compression brace is therefore being transferred to the frame base through internal bending moment about the minor axis of the right column. While the right column force point trace still

does not come close to reaching the MASTAN2 yield surface, the bottom panel compression brace's force point trace extends very close to the MASTAN2 yield surface where the internal axial force in the brace suddenly decreases. This sudden decrease in axial force very close to the assumed yield surface again leads to the conclusion that the ductile instability behavior for frames with a height-to-width ratio of 3.5 is driven by out-of-plane buckling of the bottom panel compression brace.

Figure 46 shows applied load ratio versus top of frame horizontal displacement curves for frames with a height-to-width ratio of 3.0 and lateral load ratios of 0.25, 0.50, and 1.00. The distributed plasticity analysis scheme of FE++ was used to analyze the frame with a height-to-width ratio of 3.0. Table 18 provides a summary of the distributed plasticity analysis peak applied load ratios and elastic critical load ratios for frames with height-to-width ratios of 3.0 and lateral load ratios of 0.25, 0.5, and 1.0. Figure 47, shows the typical deflected shape of the frame with a height-to-width ratio of 3.0 and lateral load ratios of 0.25, 0.5, and 1.0 at location L1 in Figure 46. Figure 48, Figure 49, and Figure 50 show both two-dimensional and three-dimensional force point traces for the right column and bottom panel compression brace of the frame with a height-to-width ratio of 3.0 at a lateral load ratio of 1.0, 0.5, and 0.25 respectively. These force point traces show the progression of internal major axis bending moment, minor axis bending moment, and axial force from the beginning of the analysis to the peak applied load ratio.

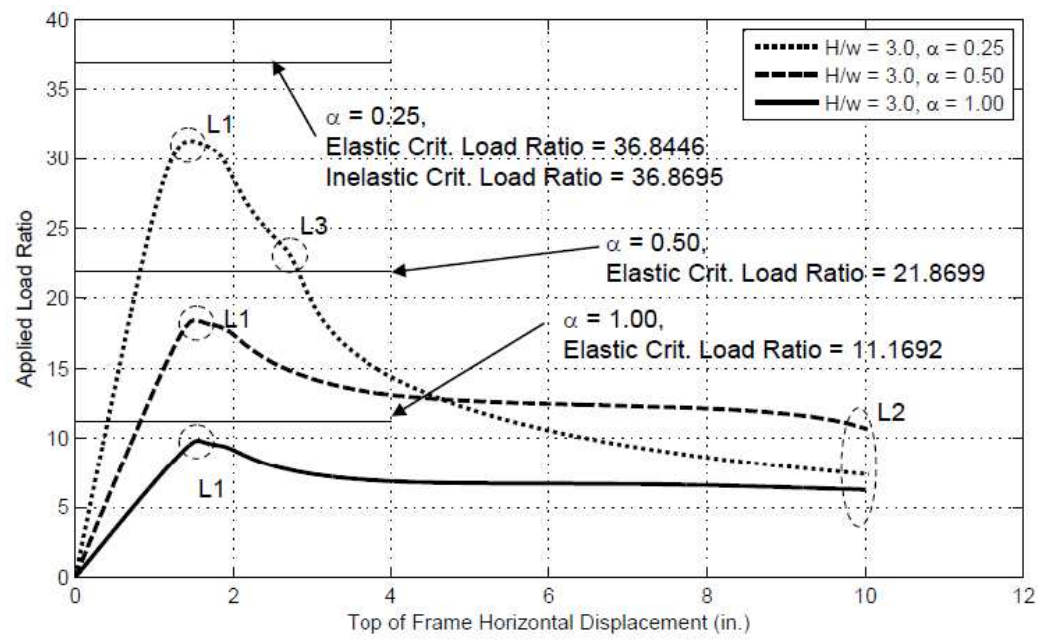


Figure 46. Applied load ratio versus top of frame horizontal displacement curves for frames with height-to-width ratios H/W = 3.0 and varying lateral load ratios

Table 18. Distributed plasticity analysis peak applied load ratio and elastic and inelastic critical load ratio comparison

Lateral Load Ratio	Top of Frame Horizontal Displacement at Peak Applied Load Ratio (in.)	Peak Applied Load Ratio	Elastic Critical Load Ratio	Inelastic Critical Load Ratio
0.25	1.4303	31.2813	36.8446	36.8695
0.50	1.4955	18.431	21.8699	-
1.00	1.5403	9.8039	11.1692	-

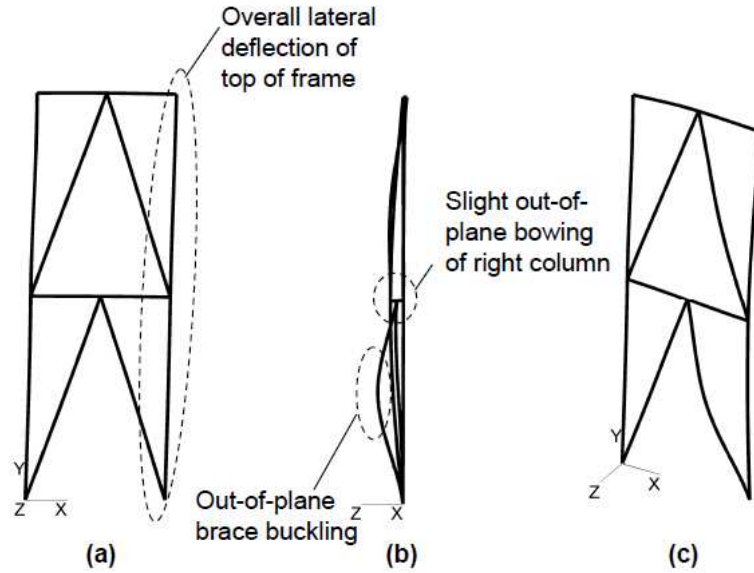


Figure 47. Typical displaced shape of frame with  $H/W = 3.0$  at the peak applied load ratio (Level L1) with lateral load ratios of 1.0, 0.5, and 0.25: (a) Front view, (b) side view, and (c) isometric view of deflected frame geometry

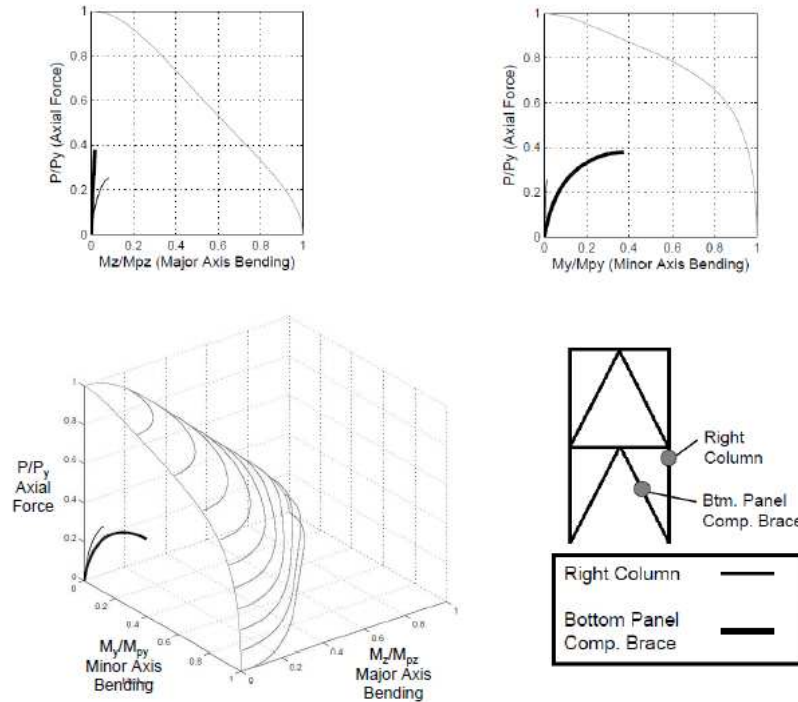
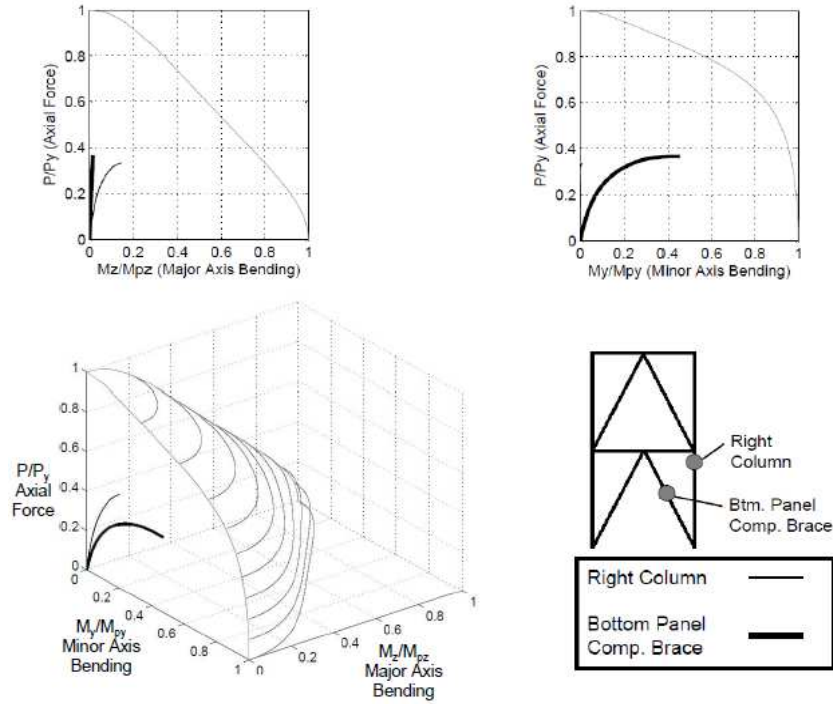
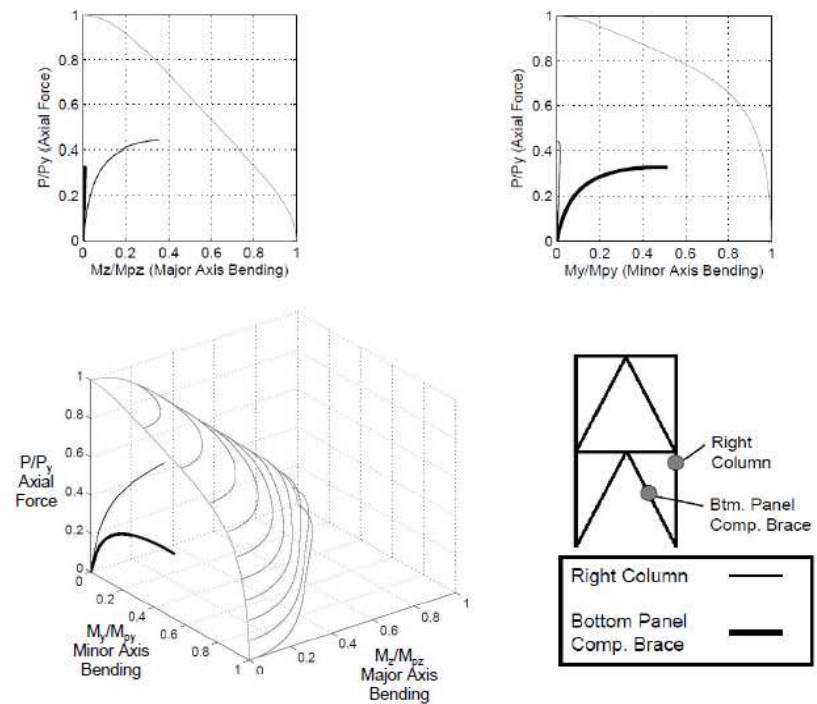


Figure 48. Axial, major axis bending, and minor axis bending force point traces for the right column and bottom panel compression brace at the peak applied load ratio for a frame with a height-to-width ratio of 3.0 and a lateral load ratio of 1.0



**Figure 49. Axial, major axis bending, and minor axis bending force point traces for the right column and bottom panel compression brace at the peak applied load ratio for a frame with a height-to-width ratio of 3.0 and a lateral load ratio of 0.5**



**Figure 50. Axial, major axis bending, and minor axis bending force point traces for the right column and bottom panel compression brace at the peak applied load ratio for a frame with a height-to-width ratio of 3.0 and a lateral load ratio of 0.25**

The applied load ratio initially increases in a manner that is essentially linear to the limit loading. The rate of increase in the applied load ratio decreases with additional horizontal displacements until the applied load ratio reaches its peak value. The peak applied load ratio occurs at location L1 on each applied load ratio curve. The peak applied load ratio for all three lateral load ratio conditions occurs at essentially the same top of frame horizontal displacement which indicates a similar deformation demand resulting in the load limit for the frame.

When the lateral load ratio is equal to 1.0, the overall capacity of the frame is significantly lower than the capacity for the other two frames as the force in the brace is greater when the lateral load ratio increases. At location L1 on the applied load ratio curves in Figure 46, there is slight pinching of the curve about the peak applied load ratio magnitude. After the applied load ratio reaches its peak, it decreases more suddenly as compared to the plateau and gradual decrease seen for frames with a height-to-width ratio of 3.5 in Figure 40. This behavior indicates that frame stability for this configuration is approaching force-controlled behavior driven by buckling within the frame. Also, a significant change in system stiffness occurs for the frame subjected to a lateral load ratio of 0.25 at location L3 in Figure 46. Applied load ratio decreases more for equivalent increases in top of frame horizontal displacement for displacements larger than 2.7 inches as compared to displacements less than 2.7 inches.

Table 18 illustrates that for all lateral load ratios, the distributed plasticity analysis peak applied load ratio is slightly less than the elastic critical load ratio. The distributed plasticity analysis peak applied load ratio is 84.9%, 84.3%, and 87.8% of the elastic critical load ratio for frames with a lateral load ratio of 0.25, 0.5, and 1.0 respectively.

Figure 47 shows the typical deflected shape of the frame with a height-to-width ratio of 3.0 and lateral load ratios of 0.25, 0.5, and 1.0 at location L1 in Figure 46. The deflected shapes for all lateral load ratio conditions are essentially the same which supports the force-controlled behavior instigated by out-of-plane buckling of the bottom panel compression brace and right column.

When Figure 47 is viewed with the front elevation of the frame in mind, there is overall lateral deflection at the top of the frame with little noticeable in plane column curvature. When viewed from the side, out-of-plane buckling of the bottom panel compression brace about its minor axis is evident as well as slight out-of-plane, single curvature bowing of the right column about its major axis. It should be noted that these displaced shapes are scaled.

In Figure 48, the force point traces show the progression of internal axial force, internal major axis bending moment, and internal minor axis bending moment from the beginning of the analysis to location L1 on the applied load ratio curve in Figure 46. The right column force point trace shows internal member forces at a location 6.56 feet below the tier level beam and the bottom panel compression brace force point trace shows internal member forces at midspan of the brace element.

As illustrated in Figure 48, as the applied load ratio increases to its peak, the internal axial force in the right column increases and reaches a plateau at 0.255 times the yield load of the W12x65 member. The internal axial force in the bottom panel compression brace also increases and reaches a plateau at 0.380 times the yield load of the W8x28 member. At the peak applied load ratio, the internal minor axis bending moment in the right column and the internal major axis bending moment in the bottom

panel compression brace are nearly equal to zero. The low level of minor axis bending moment in the right column is again the result of lateral forces being carried to the frame base by the bracing elements. As a result there is very little in-plane column curvature in the right column as illustrated in Figure 47.

At the peak applied load ratio, the internal major axis bending moment in the right column is 0.085 times the plastic moment capacity of the W12x65 member. The internal minor axis bending moment in the bottom panel compression brace is 0.377 times the plastic moment capacity of the W8x28 member. Both the internal major axis bending moment in the right column and the internal minor axis bending moment in the bottom panel compression brace can be attributed to  $P-\delta$  effects resulting from initial out-of-plane, sinusoidal geometric imperfections applied to the column and brace members. This internal major axis bending moment in the column is seen in the deformed frame geometry of Figure 47 in the form of out-of-plane bowing of the right column. The large internal minor axis bending moment in the bottom panel compression brace is seen in the deformed frame geometry of Figure 47 in the form of out-of-plane bowing of the bottom panel compression brace whereas there is very little in-plane bowing of the brace. While neither the right column or bottom panel compression brace force point trace comes close to reaching the MASTAN2 yield surface, the bottom panel compression brace force point trace extends farther from the origin which leads to the conclusion that the stability behavior of the frame with a height-to-width ratio of 3.0 and a lateral load ratio of 1.0 is driven by local member buckling of the bottom panel compression brace.

In Figure 49, the force point traces show the progression of internal axial force, internal major axis bending moment, and internal minor axis bending moment from the

beginning of the analysis to location L1 on the applied load ratio curve in Figure 46. The right column force point trace shows internal member forces at a location 6.56 feet below the tier level beam and the bottom panel compression brace force point trace shows internal member forces at midspan of the brace element.

As illustrated in Figure 49, as the applied load ratio increases to its peak, the internal axial force in the right column increases and reaches a plateau at 0.335 times the yield load of the W12x65 member. The internal axial force in the bottom panel compression brace also increases and reaches a plateau at 0.368 times the yield load of the W8x28 member. At the peak applied load ratio, the internal minor axis bending moment in the right column and the internal major axis bending moment in the bottom panel compression brace are nearly equal to zero. The low level of minor axis bending moment in the right column is again the result of lateral forces being carried to the frame base by the bracing elements. As a result there is very little in-plane column curvature in the right column as illustrated in Figure 47.

At the peak applied load ratio, the internal major axis bending moment in the right column is 0.148 times the plastic moment capacity of the W12x65 member. The internal minor axis bending moment in the bottom panel compression brace is 0.454 times the plastic moment capacity of the W8x28 member. Both the internal major axis bending moment in the right column and the internal minor axis bending moment in the bottom panel compression brace can be attributed to  $P-\delta$  effects resulting from initial out-of-plane, sinusoidal geometric imperfections applied to the column and brace members. This internal major axis bending moment in the column is seen in the deformed frame geometry of Figure 47 in the form of out-of-plane bowing of the right column. The large

internal minor axis bending moment in the bottom panel compression brace is seen in the deformed frame geometry of Figure 47 in the form of out-of-plane bowing of the bottom panel compression brace whereas there is very little in-plane bowing of the brace. While neither the right column or bottom panel compression brace force point trace comes close to reaching the MASTAN2 yield surface, the bottom panel compression brace force point trace extends farther from the origin which leads to the conclusion that the stability behavior of the frame with a height-to-width ratio of 3.0 and a lateral load ratio of 0.5 is driven by local member buckling of the bottom panel compression brace.

In Figure 50, the force point traces show the progression of internal axial force, internal major axis bending moment, and internal minor axis bending moment from the beginning of the analysis to location L1 on the applied load ratio curve in Figure 46. The right column force point trace shows internal member forces at a location 6.56 feet below the tier level beam and the bottom panel compression brace force point trace shows internal member forces at midspan of the brace element.

As illustrated in Figure 50, as the applied load ratio increases to its peak, the internal axial force in the right column increases and reaches a plateau at 0.444 times the yield load of the W12x65 member. The internal axial force in the bottom panel compression brace also increases and reaches a plateau at 0.328 times the yield load of the W8x28 member. The axial force in the right column is higher than the axial forces in the right column for frames with a height-to-width ratio of 3.0 and lateral load ratios of 1.0 and 0.5. This higher axial force is the result of a higher peak applied load ratio being reached when the lateral load ratio is equal to 0.25. At the peak applied load ratio, the internal minor axis bending moment in the right column and the internal major axis

bending moment in the bottom panel compression brace are nearly equal to zero. The low level of minor axis bending moment in the right column is again the result of lateral forces being carried to the frame base by the bracing elements. As a result there is very little in-plane column curvature in the right column as illustrated in Figure 47.

At the peak applied load ratio, the internal major axis bending moment in the right column is 0.353 times the plastic moment capacity of the W12x65 member. The internal minor axis bending moment in the bottom panel compression brace is 0.517 times the plastic moment capacity of the W8x28 member. Both the internal major axis bending moment in the right column and the internal minor axis bending moment in the bottom panel compression brace can be attributed to  $P-\delta$  effects resulting from initial out-of-plane, sinusoidal geometric imperfections applied to the column and brace members.

The internal major axis bending moment in the right column is nearly 2.4 times the level of the internal minor axis bending moment in the right column of the frame with a height-to-width ratio of 3.0 and a lateral load ratio of 0.5. This larger internal major axis bending moment in the column results from the  $P-\delta$  effects of the larger axial force in the right column. The large internal minor axis bending moment in the bottom panel compression brace is seen in the deformed frame geometry of Figure 47 in the form of out-of-plane bowing of the bottom panel compression brace whereas there is very little in-plane bowing of the brace. In contrast to the frames with a height-to-width ratio of 3.0 and lateral load ratios of 1.0 and 0.5, the bottom panel compression brace force point trace and right column force point trace extend approximately the same distance from the origin which leads to the conclusion that the stability behavior of the frame, while still

driven by local member buckling, moves toward global system buckling as the lateral load ratio decreases.

Figure 51 shows applied load ratio versus top of frame horizontal displacement curves for frames with a height-to-width ratio of 2.5 and lateral load ratios of 0.25, 0.50, and 1.00. The distributed plasticity analysis scheme of FE++ was used to analyze the frames with a height-to-width ratio of 2.5. Table 19 provides a summary of the distributed plasticity analysis peak applied load ratios and elastic critical load ratios for frames with a height-to-width ratio of 2.5 and lateral load ratios of 0.25, 0.5, and 1.0.

Figure 52 shows the typical deflected shape of the frame with a height-to-width ratio of 2.5 and lateral load ratios of 0.25, 0.5, and 1.0 at location L1 in Figure 51. Figure 53, Figure 54, and Figure 55 show both two-dimensional and three-dimensional force point traces for the right column and bottom panel compression brace of the frame with a height-to-width ratio of 2.5 at a lateral load ratio of 1.0, 0.5, and 0.25 respectively. These force point traces show the progression of internal major axis bending moment, minor axis bending moment, and axial force from the beginning of the analysis to the peak applied load ratio.

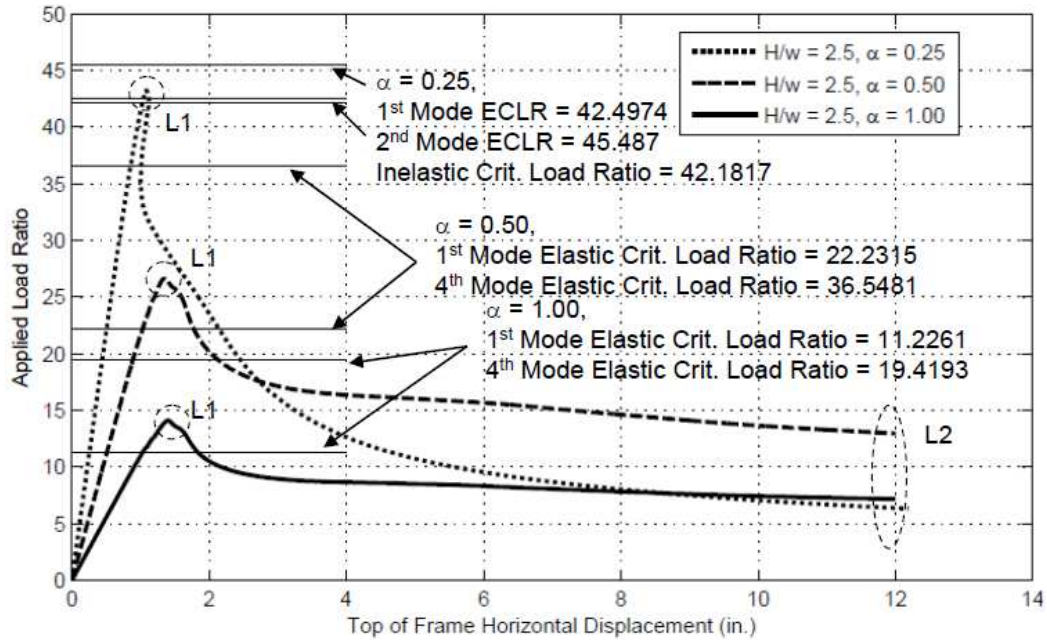


Figure 51. Applied load ratio versus top of frame horizontal displacement curves for frames with height-to-width ratios  $H/W = 2.5$  and varying lateral load ratios

Table 19. Distributed plasticity analysis peak applied load ratio and elastic and inelastic critical load ratio comparison

Lateral Load Ratio	Top of Frame Horizontal Displacement at Peak Applied Load Ratio (in.)	Peak Applied Load Ratio	1st Mode Elastic Critical Load Ratio	Higher Mode Elastic Critical Load Ratio	Inelastic Critical Load Ratio
0.25	1.0839	43.2319	42.4974	45.487 (4th Mode)	42.1817
0.50	1.3576	26.6152	22.2315	36.5481 (4th Mode)	-
1.00	1.3974	14.1224	11.2261	19.4193 (2nd Mode)	-

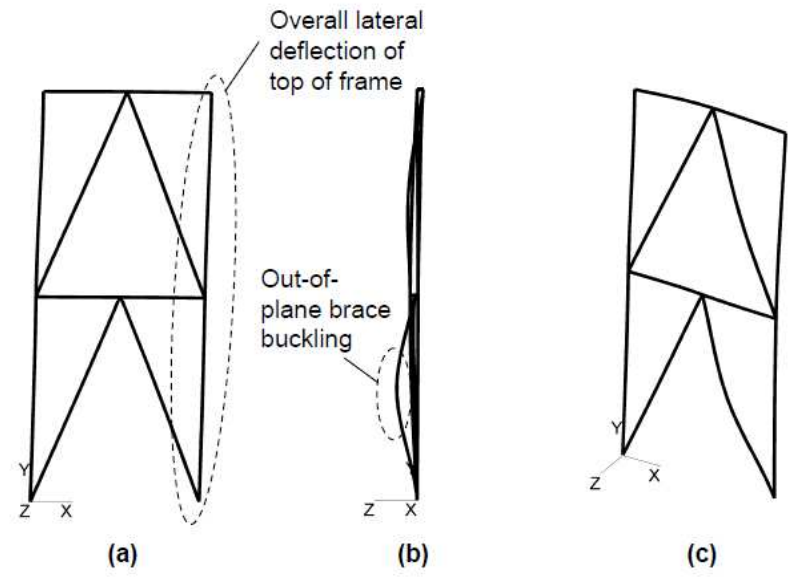


Figure 52. Typical displaced shape of frame with  $H/W = 2.5$  at the peak applied load ratio (Level L1) with lateral load ratios of 1.0, 0.5, and 0.25: (a) Front view, (b) side view, and (c) isometric view of deflected frame geometry

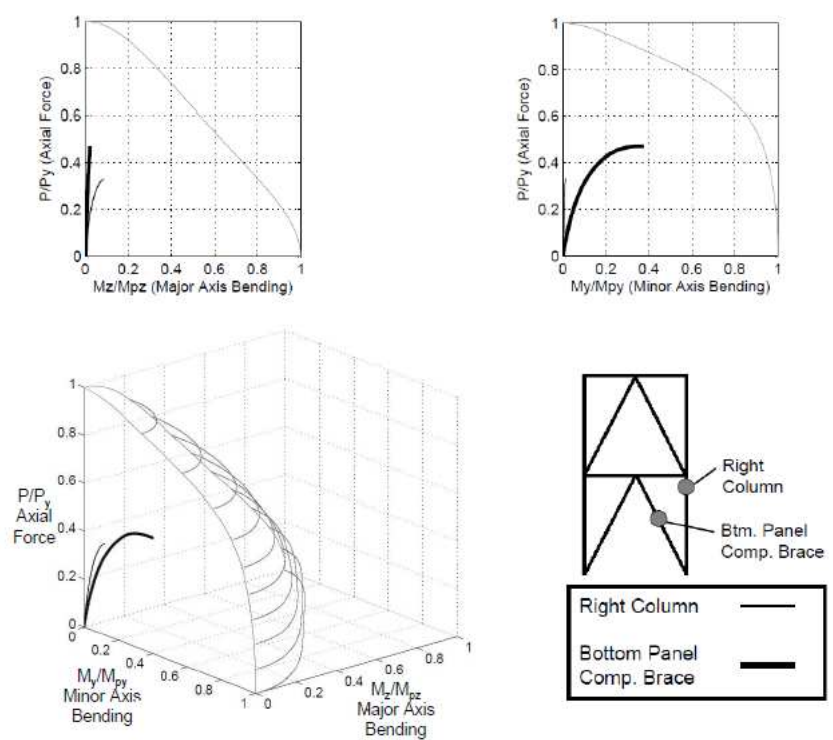
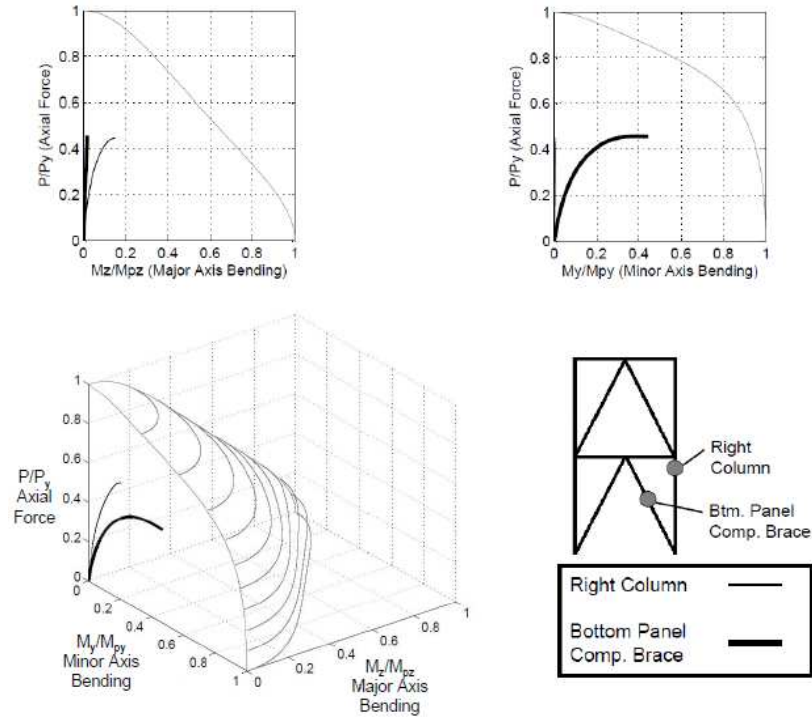
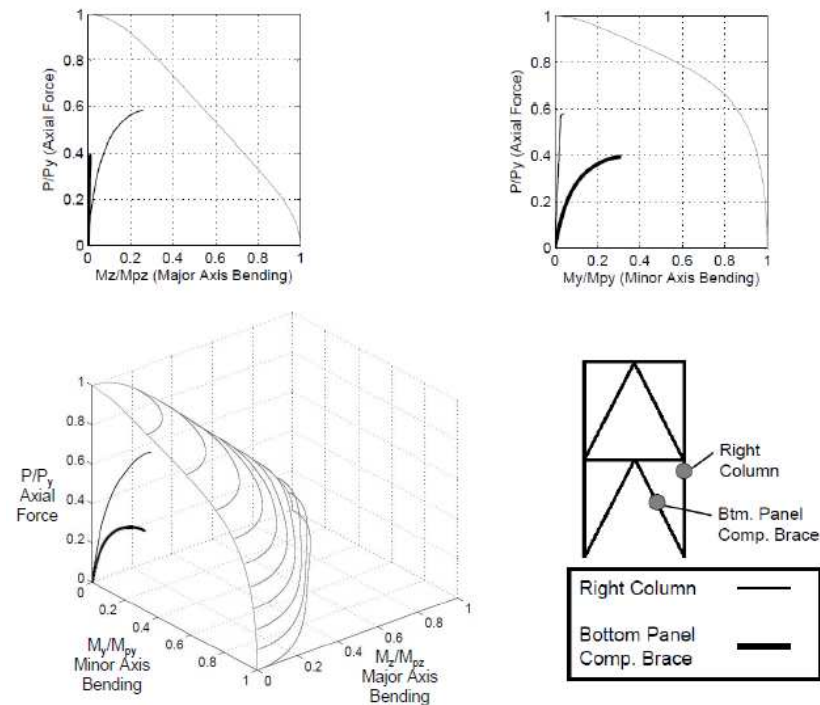


Figure 53. Axial, major axis bending, and minor axis bending force point traces for the right column and bottom panel compression brace at the peak applied load ratio for a frame with a height-to-width ratio of 2.5 and a lateral load ratio of 1.0



**Figure 54. Axial, major axis bending, and minor axis bending force point traces for the right column and bottom panel compression brace at the peak applied load ratio for a frame with a height-to-width ratio of 2.5 and a lateral load ratio of 0.5**



**Figure 55. Axial, major axis bending, and minor axis bending force point traces for the right column and bottom panel compression brace at the peak applied load ratio for a frame with a height-to-width ratio of 2.5 and a lateral load ratio of 0.25**

The applied load ratio initially increases in a manner that is essentially linear to the limit loading. The rate of increase in the applied load ratio decreases with additional horizontal displacements until the applied load ratio reaches its peak value. The peak applied load ratio occurs at location L1 on each applied load ratio curve. The peak applied load ratio for all three lateral load ratio conditions occurs at essentially the same top of frame horizontal displacement which indicates a similar deformation demand resulting in the load limit for the frame.

When the lateral load ratio is equal to 1.0, the overall capacity of the frame is significantly lower than the capacity for the other two frames as the force in the brace is greater when the lateral load ratio increases. At location L1 on the applied load ratio curves in Figure 51, there is significant pinching of the curve about the peak applied load ratio magnitude. After the applied load ratio reaches its peak, it decreases suddenly as compared to the plateau and gradual decrease seen for frames with a height-to-width ratio of 3.5 in Figure 40. This behavior indicates that frame stability for this configuration is a force-controlled behavior driven by local buckling within the frame.

Table 19 illustrates that for all lateral load ratios, the distributed plasticity analysis peak applied load ratio is slightly higher than the first mode elastic critical load ratio. The distributed plasticity analysis peak applied load ratio is 1.7%, 19.7%, and 25.8% greater than the first mode elastic critical load ratio for frames with a lateral load ratio of 0.25, 0.5, and 1.0 respectively. The first higher mode elastic critical load ratio that is larger than the distributed plasticity analysis peak applied load ratio is the fourth mode elastic critical load ratio for lateral load ratios of 0.25 and 0.5 and the second mode elastic critical load ratio for a lateral load ratio of 1.0.

Figure 52 shows the typical deflected shape of the frame with a height-to-width ratio of 2.5 and lateral load ratios of 0.25, 0.5, and 1.0 at location L1 in Figure 51. The typical frame deflected shape indicates a force-controlled type instability failure. The deflected shapes for all lateral load ratio conditions are essentially the same which supports the force-controlled behavior instigated by out-of-plane buckling of the bottom panel compression brace and right column.

When Figure 52 is viewed with the front elevation of the frame in mind, there is overall lateral deflection at the top of the frame with little noticeable in plane column curvature. When viewed from the side, out-of-plane buckling of the bottom panel compression brace about its minor axis is evident as well as slight out-of-plane, single curvature bowing of the right column about its major axis. It should be noted that these displaced shapes are scaled.

In Figure 53, the force point traces show the progression of internal axial force, internal major axis bending moment, and internal minor axis bending moment from the beginning of the analysis to location L1 on the applied load ratio curve in Figure 51. The right column force point trace shows internal member forces at a location 6.56 feet below the tier level beam and the bottom panel compression brace force point trace shows internal member forces at midspan of the brace element.

As illustrated in Figure 53, as the applied load ratio increases to its peak, the internal axial force in the right column increases and reaches a plateau at 0.331 times the yield load of the W12x65 member. The internal axial force in the bottom panel compression brace also increases and reaches a plateau at 0.471 times the yield load of the W8x28 member. At the peak applied load ratio, the internal minor axis bending

moment in the right column and the internal major axis bending moment in the bottom panel compression brace are nearly equal to zero. The low level of minor axis bending moment in the right column is again the result of lateral forces being carried to the frame base by the bracing elements. As a result there is very little in-plane column curvature in the right column as illustrated in Figure 52.

At the peak applied load ratio, the internal major axis bending moment in the right column is 0.088 times the plastic moment capacity of the W12x65 member. The internal minor axis bending moment in the bottom panel compression brace is 0.378 times the plastic moment capacity of the W8x28 member. Both the internal major axis bending moment in the right column and the internal minor axis bending moment in the bottom panel compression brace can be attributed to  $P-\delta$  effects resulting from initial out-of-plane, sinusoidal geometric imperfections applied to the column and brace members. This internal major axis bending moment in the column is seen in the deformed frame geometry of Figure 52 in the form of slight out-of-plane bowing of the right column. The large internal minor axis bending moment in the bottom panel compression brace is seen in the deformed frame geometry of Figure 52 in the form of out-of-plane bowing of the bottom panel compression brace whereas there is very little in-plane bowing of the brace. While neither the right column or bottom panel compression brace force point trace comes close to reaching the MASTAN2 yield surface, the bottom panel compression brace force point trace extends farther from the origin which leads to the conclusion that the stability behavior of the frame with a height-to-width ratio of 2.5 and a lateral load ratio of 1.0 is driven by member buckling of the bottom panel compression brace.

In Figure 54, the force point traces show the progression of internal axial force, internal major axis bending moment, and internal minor axis bending moment from the beginning of the analysis to location L1 on the applied load ratio curve in Figure 51. The right column force point trace shows internal member forces at a location 6.56 feet below the tier level beam and the bottom panel compression brace force point trace shows internal member forces at midspan of the brace element.

As illustrated in Figure 54, as the applied load ratio increases to its peak, the internal axial force in the right column increases and reaches a plateau at 0.448 times the yield load of the W12x65 member. The internal axial force in the bottom panel compression brace also increases and reaches a plateau at 0.457 times the yield load of the W8x28 member. At the peak applied load ratio, the internal minor axis bending moment in the right column and the internal major axis bending moment in the bottom panel compression brace are nearly equal to zero. The low level of minor axis bending moment in the right column is again the result of lateral forces being carried to the frame base by the bracing elements. As a result there is very little in-plane column curvature in the right column as illustrated in Figure 52.

At the peak applied load ratio, the internal major axis bending moment in the right column is 0.150 times the plastic moment capacity of the W12x65 member. The internal minor axis bending moment in the bottom panel compression brace is 0.445 times the plastic moment capacity of the W8x28 member. Both the internal major axis bending moment in the right column and the internal minor axis bending moment in the bottom panel compression brace can be attributed to  $P-\delta$  effects resulting from initial out-of-plane, sinusoidal geometric imperfections applied to the column and brace members.

This internal major axis bending moment in the column is seen in the deformed frame geometry of Figure 52 in the form of slight out-of-plane bowing of the right column. The large internal minor axis bending moment in the bottom panel compression brace is seen in the deformed frame geometry of Figure 52 in the form of out-of-plane bowing of the bottom panel compression brace whereas there is very little in-plane bowing of the brace. While neither the right column or bottom panel compression brace force point trace comes close to reaching the MASTAN2 yield surface, the bottom panel compression brace force point trace extends farther from the origin which leads to the conclusion that the stability behavior of the frame with a height-to-width ratio of 2.5 and a lateral load ratio of 0.5 is driven by local member buckling of the bottom panel compression brace.

In Figure 55, the force point traces show the progression of internal axial force, internal major axis bending moment, and internal minor axis bending moment from the beginning of the analysis to location L1 on the applied load ratio curve in Figure 51. The right column force point trace shows internal member forces at a location 6.56 feet below the tier level beam and the bottom panel compression brace force point trace shows internal member forces at midspan of the brace element.

As illustrated in Figure 55, as the applied load ratio increases to its peak, the internal axial force in the right column increases and reaches a plateau at 0.583 times the yield load of the W12x65 member. The internal axial force in the bottom panel compression brace also increases and reaches a plateau at 0.395 times the yield load of the W8x28 member. At the peak applied load ratio, the internal minor axis bending moment in the right column and the internal major axis bending moment in the bottom panel compression brace are nearly equal to zero. The low level of minor axis bending

moment in the right column is again the result of lateral forces being carried to the frame base by the bracing elements. As a result there is very little in-plane column curvature in the right column as illustrated in Figure 52.

At the peak applied load ratio, the internal major axis bending moment in the right column is 0.260 times the plastic moment capacity of the W12x65 member. The internal minor axis bending moment in the bottom panel compression brace is 0.312 times the plastic moment capacity of the W8x28 member. Both the internal major axis bending moment in the right column and the internal minor axis bending moment in the bottom panel compression brace can be attributed to  $P-\delta$  effects resulting from initial out-of-plane, sinusoidal geometric imperfections applied to the column and brace members. This internal major axis bending moment in the column is seen in the deformed frame geometry of Figure 52 in the form of out-of-plane bowing of the right column. The large internal minor axis bending moment in the bottom panel compression brace is seen in the deformed frame geometry of Figure 52 in the form of out-of-plane bowing of the bottom panel compression brace whereas there is very little in-plane bowing of the brace.

In contrast to the frames with a height-to-width ratio of 2.5 and lateral load ratios of 1.0 and 0.5, the bottom panel compression brace force point trace and right column force point trace extend approximately the same distance from the origin. In particular, the axial force in the right column is approximately 1.3 times higher than it is for frames with a height-to-width ratio of 2.5 and lateral load ratios of 1.0 and 0.5. This increase in internal axial force and distance traveled by the right column force point trace leads to the conclusion that the stability behavior of the frame is driven by local buckling for a lateral

load ratio of 0.25 and moves toward global system buckling as lateral load ratio decreases.

The frames with a height-to-width ratio of 2.0 were not analyzed using the FE++ distributed plasticity analysis scheme. When this analysis was executed, the applied load ratio versus top of frame horizontal displacement curves would reach a peak applied load ratio value and then immediately double back to the origin along their original path. As a result, the concentrated plasticity analysis scheme in MASTAN2 was used to evaluate the inelastic response of the frames with a height-to-width ratio of 2.0. As previously discussed, this analysis procedure uses a modified tangent modulus to model material nonlinear behavior and does not model post limit-state response.

Figure 56 shows applied load ratio versus top of frame horizontal displacement curves for frames with a height-to-width ratio of 2.0 and lateral load ratios of 0.25, 0.50, and 1.00. Table 20 provides a summary of the distributed plasticity analysis peak applied load ratios and elastic critical load ratios for frames with height-to-width ratio of 2.0 and lateral load ratios of 0.25, 0.50, and 1.0. Figure 57 shows the typical deflected shape of the frame with a height-to-width ratio of 2.0 and lateral load ratios of 0.25, 0.50, and 1.0 at location L1 in Figure 56. Figure 58, Figure 59, and Figure 60 show both two-dimensional and three-dimensional force point traces for the right column and bottom panel compression brace of the frame with a height-to-width ratio of 2.0 at a lateral load ratio 1.0, 0.5, and 0.25 respectively. These force point traces show the progression of internal major axis bending moment, minor axis bending moment, and axial force from the beginning of the analysis to the peak applied load ratio.

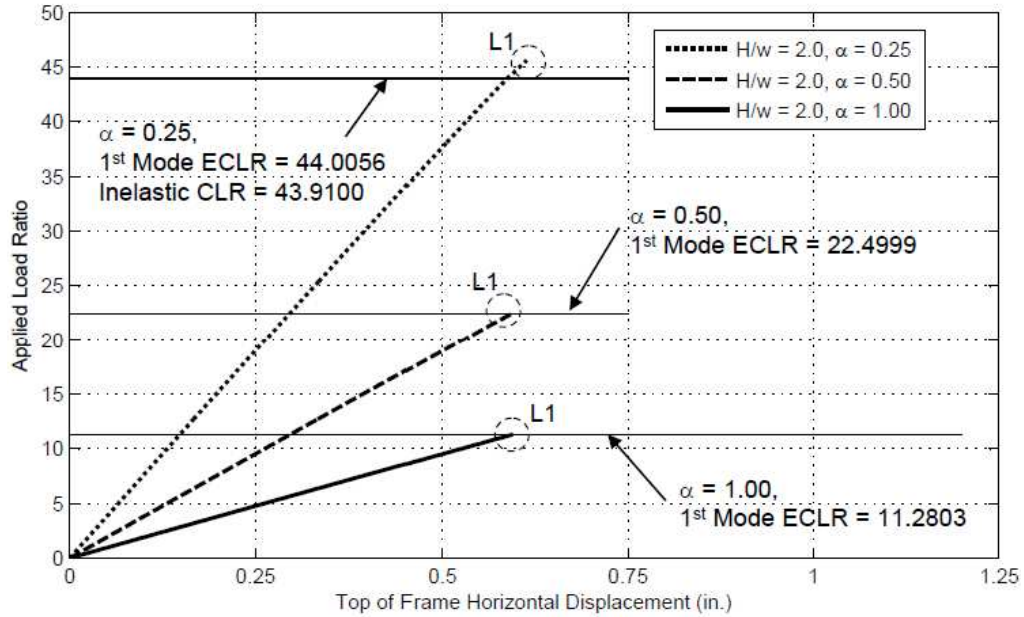


Figure 56. Applied load ratio versus top of frame horizontal displacement curves for frames with height-to-width ratios  $H/W = 2.0$  and varying lateral load ratios

Table 20. Second order inelastic analysis peak applied load ratio and elastic and inelastic critical load ratio comparison

Lateral Load Ratio	Top of Frame Horizontal Displacement at Peak Applied Load Ratio (in.)	Peak Applied Load Ratio	1st Mode Elastic Critical Load Ratio	Inelastic Critical Load Ratio
0.25	0.6137	45.6000	44.0056	43.9100
0.50	0.595	22.5000	22.4999	-
1.00	0.5953	11.3000	11.2803	-

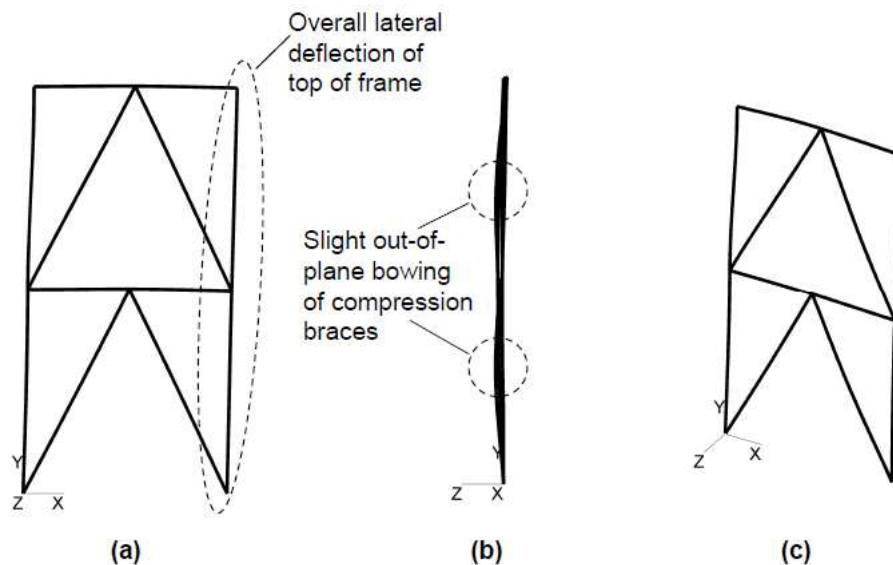


Figure 57. Typical displaced shape of frame with  $H/W = 2.0$  at the peak applied load ratio (Level L1) with lateral load ratios of 1.0, 0.5, and 0.25: (a) Front view, (b) side view, and (c) isometric view of deflected frame geometry

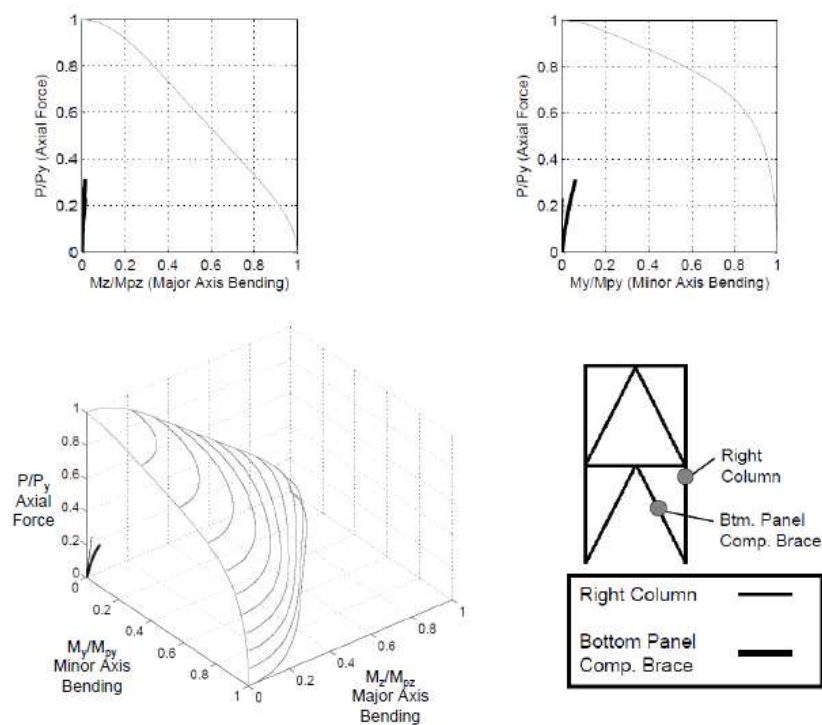
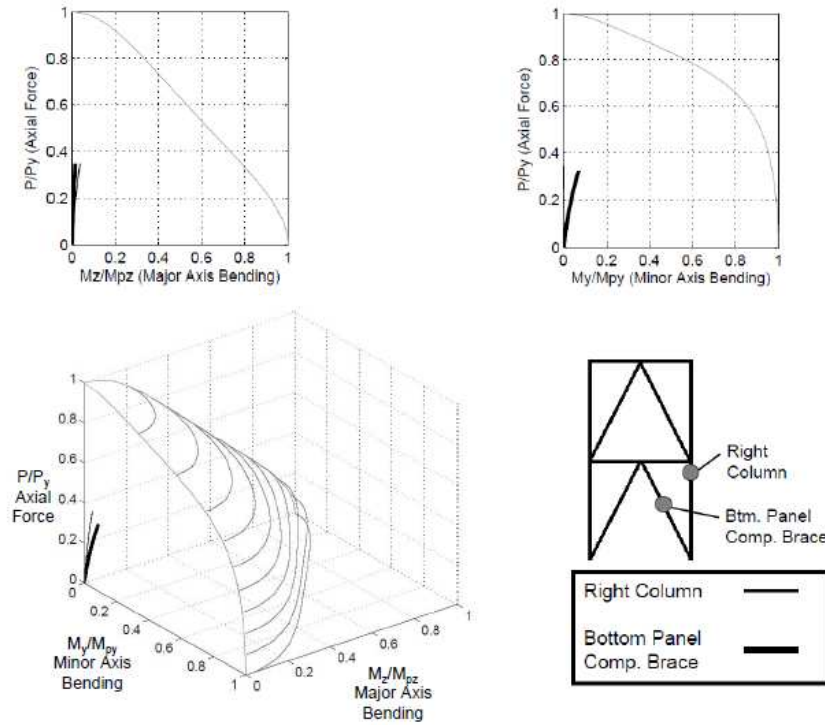
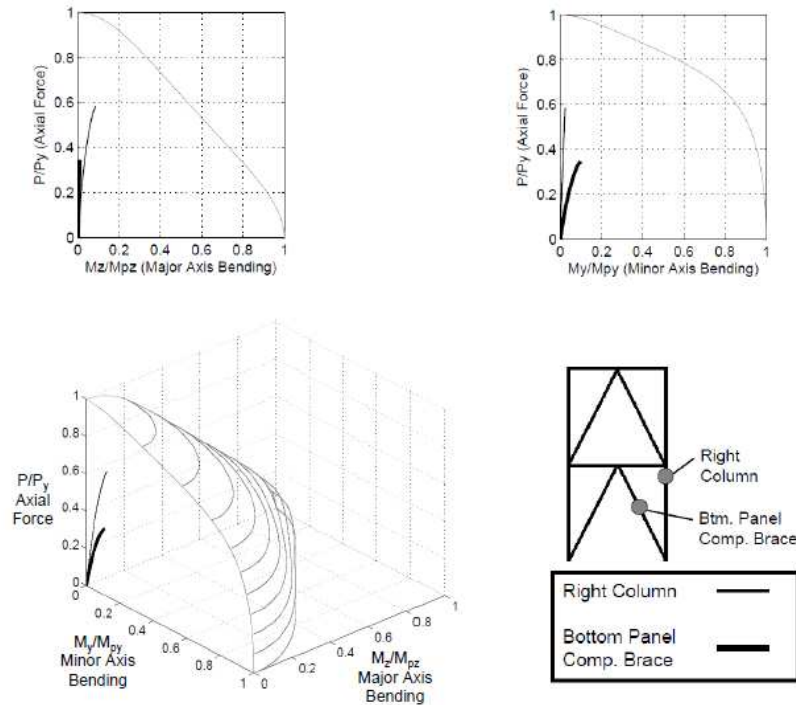


Figure 58. Axial, major axis bending, and minor axis bending force point traces for the right column and bottom panel compression brace at the peak applied load ratio for a frame with a height-to-width ratio of 2.0 and a lateral load ratio of 1.0



**Figure 59. Axial, major axis bending, and minor axis bending force point traces for the right column and bottom panel compression brace at the peak applied load ratio for a frame with a height-to-width ratio of 2.0 and a lateral load ratio of 0.5**



**Figure 60. Axial, major axis bending, and minor axis bending force point traces for the right column and bottom panel compression brace at the peak applied load ratio for a frame with a height-to-width ratio of 2.0 and a lateral load ratio of 0.25**

The applied load ratio increases in a linear manner until the applied load ratio reaches its peak value. The peak applied load ratio occurs at location L1 on each applied load ratio curve. The peak applied load ratio for all three lateral load ratio conditions occurs at essentially the same top of frame horizontal displacement which indicates a similar deformation demand resulting in the load limit for the frame. When the lateral load ratio is equal to 1.0, the overall capacity of the frame is significantly lower than the capacity for the other two frames as the force in the brace is greater when the lateral load ratio increases.

Table 20 illustrates that for all lateral load ratios, the second order inelastic analysis peak applied load ratio is nearly identical to the first mode elastic critical load ratio. This, as well as the linear nature of the applied load ratio response curves suggests that the stability behavior of the frame with a height-to-width ratio of 2.0 at all lateral load ratio levels is controlled by local member elastic buckling. The axial force in the bottom panel compression brace at the peak applied load ratio is 142.9 kip, 133.1 kip, and 129.6 kip for lateral load ratios of 0.25, 0.50, and 1.0 respectively. The Euler critical buckling load for a W8x28 bending about its minor axis with an unsupported length equal to 16.8 feet is 153.4 kip when the member is assumed to be pinned at both ends. In reality, at the intersection of the brace and tier level beam, the brace has rotation fixed and is free to translate while its opposite end is nearly fixed at the connection to the bottom of the right column. This results in an effective length factor slightly greater than 1.0 (AISC 2010a). As a result it can be concluded that out-of-plane buckling of the bottom panel compression brace controls the behavior of the frame with a height-to-width ratio of 2.0 at each lateral load ratio considered.

Figure 57 shows the typical deflected shape of the frame with a height-to-width ratio of 2.0 and lateral load ratios of 0.25, 0.5, and 1.0 at location L1 in Figure 56. The deflected shapes for all lateral load ratio conditions are essentially the same. When Figure 57 is viewed with the front elevation of the frame in mind, there is overall lateral deflection at the top of the frame with little noticeable in plane column curvature. When viewed from the side, slight out-of-plane buckling of both the top and bottom panel compression brace about their minor axes is evident with very little noticeable out-of-plane right column bowing. It should be noted that these displaced shapes are scaled.

In Figure 58, Figure 59, and Figure 60 the force point traces show the progression of internal axial force, internal major axis bending moment, and internal minor axis bending moment from the beginning of the analysis to location L1 on the applied load ratio curve in Figure 56. The right column force point trace shows internal member forces at a location 6.56 feet below the tier level beam and the bottom panel compression brace force point trace shows internal member forces at midspan of the brace element.

As illustrated in Figure 58, Figure 59, and Figure 60 as the applied load ratio increases to its peak, the internal axial force in the right column and bottom panel compression brace increases. At the peak applied load ratio, the internal minor axis bending moment in the right column and the internal major axis bending moment in the bottom panel compression brace are nearly equal to zero. The low level of minor axis bending moment in the right column is again the result of lateral forces being carried to the frame base by the bracing elements. As a result there is very little in-plane column curvature in the right column as illustrated in Figure 57.

At the peak applied load ratio, the internal major axis bending moment in the right column is less than 0.1 times the plastic moment capacity of the W12x65 member at each lateral load ratio level. The internal minor axis bending moment in the bottom panel compression brace is also less than 0.1 times the plastic moment capacity of the W8x28 member at each lateral load ratio level. These small internal major axis bending moments in the right column and internal minor axis bending moments in the bottom panel compression brace can be attributed to  $P-\delta$  effects resulting from initial out-of-plane, sinusoidal geometric imperfections applied to the column and brace members. The small internal major axis bending moment in the column is seen in the deformed frame geometry of Figure 57 in the form of very slight out-of-plane bowing of the right column. The internal minor axis bending moment in the bottom panel compression brace is seen in the deformed frame geometry of Figure 57 in the form of out-of-plane bowing of the bottom panel compression brace whereas there is very little in-plane bowing of the brace. Neither the right column nor bottom panel compression brace force point trace comes close to reaching the MASTAN2 yield surface which supports the conclusion that frame behavior at a height-to-width ratio of 2.0 is driven by elastic buckling of the bottom panel compression brace.

### **4.3. Conclusions**

A distributed plasticity analysis approach was used to evaluate the inelastic response of a suite of frames with height-to-width ratios of 2.0, 2.5, 3.0, and 3.5 and lateral load ratios of 0.25, 0.5, and 1.0. From this analysis, applied load ratio versus top of frame horizontal displacement response curves were plotted, deflected frame geometries were observed,

and force point traces showing the progression of internal axial force, internal major axis bending moment, and internal minor axis bending moment in the bottom panel compression brace and right column were developed. The results from these distributed plasticity analyses yield the following conclusions.

- For a frame with a given height-to-width ratio, the peak applied load ratio increases as lateral load ratio decreases.
- For a frame with a given height-to-width ratio, the top of frame horizontal displacement is essentially the same at each lateral load ratio condition indicating a similar deformation demand resulting in the load limit for the system.
- As frame height-to-width decreases, the applied load ratio versus top of frame horizontal displacement response curves exhibit a more defined peak when the peak applied load ratio is reached. After the applied load ratio reaches its peak for a frame with a height-to-width ratio of 3.0 and 2.5, it decreases suddenly as compared to the plateau and gradual decrease seen for frames with a height-to-width ratio of 3.5.
- At a height-to-width ratio of 3.5, behavior is generally a ductile instability, deformation-controlled failure. At height-to-width ratios of 3.0 and 2.5, behavior transitions to a more force-controlled failure which suggests local buckling within the frame leads to the limit capacity of the frame. At a height-to-width ratio of 2.0, out-of-plane elastic buckling of the bottom panel compression brace about its minor axis controls frame behavior.
- For a frame with a given height-to-width ratio, buckling of the compression column becomes more defined at lower lateral load ratios.

- For a given lateral load ratio, the peak applied load ratio increases as frame height-to-width ratio decreases from 3.5 to 2.5.
- For frames with height-to-width ratios of 3.5 and 3.0, the nonlinear inelastic peak applied load ratio is smaller than the first mode elastic critical load ratio. For frames with a height-to-width ratio of 2.5, the nonlinear inelastic peak applied load ratio is larger than the first mode elastic critical load ratio. For frames with a height-to-width ratio of 2.0, the nonlinear inelastic peak applied load ratio is nearly identical to the first mode elastic critical load ratio since behavior is controlled by elastic buckling of the bottom panel compression brace.

## 5. Conclusions and Recommendations for Future Research

The conclusions presented represent conclusions based only on the results of analyses performed on a two-panel concentrically braced frame with equal panel heights and the member sizes given. With this qualification in mind, the findings of this thesis can be used to as a starting point to begin to evaluate local and global instability behavior in multi-pane braced frame systems as well as ductility in the collapse behavior of these systems.

By performing elastic and inelastic critical load analyses, the effect of frame height-to-width ratio, applied lateral load to gravity load ratio, column orientation, and initial geometric imperfections on frame stability and critical load capacity was evaluated. The results of the elastic and inelastic critical analyses yield the following conclusions:

- As applied lateral load ratio increases, the elastic critical load ratio decreases.
- As applied lateral load ratio increases, stability behavior of the frame tends to be driven by buckling of brace elements as opposed to global buckling of the entire frame system.
- As height-to-width ratio increases, the elastic critical load ratio decreases.
- When the columns' webs are oriented perpendicular to the plane of the frame, stability behavior tends to be driven by buckling of brace elements. When the columns' webs are oriented parallel to the plane of the frame, stability behavior tends to be driven by global buckling of the entire frame system.
- Inelastic critical load ratios are slightly smaller than elastic critical load ratios for all frames where elastic buckling does not control frame behavior.

- Initial in-plane and out-of-plane geometric imperfections have a negligible effect on frame elastic critical loads.

By utilizing a distributed plasticity analysis approach, the inelastic response of the frame was analyzed. Specifically, the effect of frame height-to-width ratio and applied lateral load to gravity load ratio on frame inelastic response was evaluated. The results from these distributed plasticity analyses yield the following conclusions.

- For a frame with a given height-to-width ratio, the peak applied load ratio increases as lateral load ratio decreases.
- For a frame with a given height-to-width ratio, the top of frame horizontal displacement is essentially the same at each lateral load ratio condition indicating a similar deformation demand resulting in the load limit for the system.
- As frame height-to-width decreases, the applied load ratio versus top of frame horizontal displacement response curves exhibit a more defined peak when the peak applied load ratio is reached. After the applied load ratio reaches its peak for a frame with a height-to-width ratio of 3.0 and 2.5, it decreases suddenly as compared to the plateau and gradual decrease seen for frames with a height-to-width ratio of 3.5.
- At a height-to-width ratio of 3.5, behavior is generally a ductile instability, deformation-controlled failure. At height-to-width ratios of 3.0 and 2.5, behavior transitions to a more force-controlled failure which suggests buckling within the frame leads to the limit capacity of the frame. At a height-to-width ratio of 2.0, out-of-plane elastic buckling of the bottom panel compression brace about its minor axis controls frame behavior.

- For a frame with a given height-to-width ratio, buckling of the compression column becomes more defined at lower lateral load ratios.
- For a given lateral load ratio, the peak applied load ratio increases as frame height-to-width ratio decreases from 3.5 to 2.5.
- For frames with height-to-width ratios of 3.5 and 3.0, the nonlinear inelastic peak applied load ratio is smaller than the first mode elastic critical load ratio. For frames with a height-to-width ratio of 2.5, the nonlinear inelastic peak applied load ratio is larger than the first mode elastic critical load ratio. For frames with a height-to-width ratio of 2.0, the nonlinear inelastic peak applied load ratio is nearly identical to the first mode elastic critical load ratio since behavior is controlled by elastic buckling of the bottom panel compression brace.

The frames analyzed in this thesis contained members which were designed for the geometric characteristics of a frame with a height-to-width ratio of 3.0 and equal panel heights as well as the loads expected to act on a frame with a height-to-width ratio of 3.0. Designing the frame for other aspect ratios and panel heights may alter some results.

The results and knowledge generated through this thesis can be extended through future research by doing the following:

- Distributed plasticity analyses should be performed on frames with HSS and double-angle bracing members.
- Distributed plasticity analyses should be performed on frames with member-to-member connections with realistic semi-rigid flexural connections.

- Distributed plasticity analyses should be performed by initially applying gravity load on the frame and then applying lateral load without simultaneously increasing the gravity load to gain a better representation of frame response during ground motion.
- Evaluate the effect that changing individual member sizes has on the performance of the frame.

## BIBLIOGRAPHY

- AISC (2010a). *Specification for Structural Steel Buildings*, American Institute of Steel Construction, Inc., Chicago, IL.
- AISC (2010b). *Code of Standard Practice for Steel Buildings and Bridges*, American Institute of Steel Construction, Inc., Chicago, IL.
- Alemdar, Bulent Nedim. (2001). *Distributed Plasticity Analysis of Steel Building Structural Systems*. Thesis, Georgia Institute of Technology. Ann Arbor: ProQuest/UMI, (Publication No. 3032418.)
- ASCE (2006). *Minimum Design Loads for Buildings and Other Structures*, American Society of Civil Engineers.
- Dalal, S.T. (1969). Some non-conventional cases of column design. *Eng. J.*, AISC, 6(1): 28-39.
- FE++ (2012). developed by Bulent Alemdar.
- Galambos, T.V. and Ketter, R.L. (1958). *Columns Under Combined Bending and Thrust.*, Fritz Engineering Laboratory Report 205A.21, Bethlehem, Pennsylvania.
- Imanpour, A. and Tremblay, R.(2012) Analytical Assessment of Stability of Unbraced Column in Two-Panel Concentrically Braced Frames. 3rd International Structural Specialty Conference, June 6-9. Edmonton, Alberta, (CD-ROM).
- Imanpour, A., Tremblay, R., and Davaran, A. (2012). Seismic performance of steel concentrically braced frames with bracing members intersecting columns between floors. *Proc. 7th STESSA 2012*, Santiago, Chile: 447-453.
- MASTAN2 (2010). developed by R.D. Ziemian and W. McGuire, Version 3.3.1, [www.mastan2.com](http://www.mastan2.com).
- MASTAN2 (2012). developed by R.D. Ziemian and W. McGuire, Version 3.4, [www.mastan2.com](http://www.mastan2.com).
- Stoakes, C.D. and Fahnestock, L.A. (2012). "Cyclic flexural analysis and behavior of beam-column connections with gusset plates." *J. Const. St. Res.*, accepted for publication.
- Stoakes, C.D. and Fahnestock, L.A. (2012). Influence of weak-axis flexural yielding on strong-axis buckling strength of wide flange columns. Proc. of the Annual Stability Conference Structural Stability Research Council, April 18-21, Grapevine Texas (CD-ROM).

Ziemian, R.D. (1999). Inelastic Critical Loads by Eigenvalue Analysis. Proc. Of the 1999 Structures Congress, April 18-21, New Orleans Louisiana.

Ziemian, R.D. and McGuire, W. (2002). "Modified Tangent Modulus Approach, A Contribution to Plastic Hinge Analysis", *J Struct Eng.*, ASCE Vol. 128(10).